



Proceedings of the First Fields-MITACS Industrial Problems Workshop

The Fields Institute for Research in Mathematical Science
Toronto, Ontario

August 14–18, 2006

Editors:

Dhavide A. Aruliah

(University of Ontario Institute of Technology)

and

Gregory M. Lewis

(University of Ontario Institute of Technology)

Sponsored by:

The Fields Institute for Research in Mathematical Science
and

Mathematics of Information Technology and Complex Systems
(MITACS)

CONTENTS

Preface by the Director of the Fields Institute	v
Message from the Scientific Director of MITACS	vii
Acknowledgements	ix
Nonlinear Dimension Reduction for Microarray Data	1
S. SHONTZ	
Incorporating Estimation Error into Optimal Portfolio Allocation	17
D. COTRELL, H. HUANG, N. NIGAM	
Yolk Dynamics in Amphibian Embryos	33
C.S. BOHUN, C. BREWARD	
Global Travel and Severe Acute Respiratory Syndrome (SARS)	51
J. ARINO	
Mathematical Models of Mother/Child Attachment	61
L. BUONO, R. CHAU, G. LEWIS, N. MADRAS, M. PUGH, L. ROSSI, T. WITELSKI	
Normalization and Other Topics in Multi-Objective Optimization	89
O. GRODZEVICH, O. ROMANKO	
List of Participants	103

Preface by the Director of the Fields Institute

During the week of August 14-18, 2006, the Fields Institute experienced a new venture. A casual visitor during that time would have been uncertain whether this was a research institute or a summer camp, as a set of mostly young participants filled the offices, seminar rooms and halls from dawn until well after dark. The occasion was the first Fields-MITACS Industrial Problems Workshop (FMIPW), run on the model of the “Study Groups” pioneered in Europe and the US and introduced to Canada by PIMS and MITACS. FMIPW brought the concept to Eastern Canada, and the success of the first Workshop has ensured that this will become institutionalized here: a CRM-MITACS IPW will take place in Montreal in 2007 and after that the workshops will alternate between Toronto and Montreal (while PIMS continues to conduct an annual IPSW in the West).

This Proceedings volume represents more than a report of the activities that took place during five busy days. The problem-solving groups took the problems home with them and have worked up further results, have added references and details, and have provided further background and conclusions to the brief reports they gave on August 24. Nonetheless, the main part of what you will read here was produced during that one incredible week.

The written words cannot do justice to the atmosphere around the Institute that week. About half of the 65 participants were veterans of the IPSW circuit; they greeted each other as old friends, and welcomed newcomers on the first day. Problems were presented. To my ears, they sounded intriguing, but in many cases hopelessly intractable. The questions came from all over the map (literally: the SARS problem code-named airports all around the world). Some of them (like the mother-child attachment scenario) were presented with no mathematical model whatsoever, and did not offer many handles for “industrial mathematicians” to grasp.

No matter. The eager participants grabbed lunch (the program included a daily buffet set out on trestle tables in the foyer), selected team leaders and started assembling teams. Miraculously, each problem was the first choice of a distinct set of participants. Huaxiong Huang and Nilima Nigam, like experienced camp counselors, combed through the groups each day, adjusting approaches, and occasionally membership. A daily briefing identified any problem where progress was behind schedule, and allowed further changes in team composition. I don’t know if anyone went home on Thursday night before midnight, but on Friday morning they were lined up to present answers to the proposers. An astonishing transformation had occurred. A problem that had been presented on Monday as a jumble of information and questions, with incomplete or censored data, had turned into an elegant model juxtaposed with a tidy solution. One after another, teams walked to the front of the room and announced, “We solved this problem ...”

The youthfulness of the participants surely contributed to the carnival atmosphere (though some of the most enthusiastic team members were senior professors), and the fact that a number of them are mothers or fathers of young children must have contributed to the attraction of the mother-child problem (which had the largest team and produced three distinct solution strategies). But it was equally impressive to observe leaders in each problem emerging from the first-time participants.

The two problems from the financial sector were presented at the start in a mathematical form by mathematically sophisticated presenters, but even here participants got new insights into the kinds of answers needed by the presenters' companies (for example, an algorithm that produced instant results). A third problem, the analysis of micro-array data, also involved analysis of quantitative (numerical) data, though here also the expertise of the participant team, which included statistics but also other disciplines, contributed something new to the solution. The remaining problems broke new ground for most of the participants, and gave a snapshot of the challenges that an initiative like this will encounter as we move away (which we chose to do, deliberately) from a narrow focus on certain kinds of industries to encompass a wider set of practical engineering and societal problems that are faced by government laboratories and medical research establishments. The yolk dynamics problem, the analysis of SARS data and the systematic interpretation of study data in the mother-child problem are remarkable as examples of the variety of problems that are faced by researchers or practitioners, to which mathematical analysis can contribute a piece - perhaps even the key piece - of the solution. The amphibian yolk dynamics problem was almost classical engineering - but only after one had listened to and understood the physiological framework in which it was presented. And it became intensely more interesting when one heard the ecological importance of understanding the solution. The SARS data could not have been analysed without help from the extensive repertory of modelling of infectious disease transmission. To discover that analysis could tease a meaning out of what appeared to be an almost incoherent data set was one of many revelations of the week. And, finally, the richness of modelling that contributed to an understanding of the situation presented in the mother-child problem astonished all the participants. One of the proposers of the problem, Leslie Atkinson (son of the esteemed mathematician F. V. Atkinson) greeted the presentation of the three solutions with the simple words, "I am blown away".

In this volume, you will read the solutions, though nothing can reproduce the confused picture given by the original presentations. So a perusal of these papers, fascinating as they are, can only begin to suggest the genius and innovation that went into the writing of them. For that, you will just have to participate in the next Industrial Problems Workshop. I recommend it highly.

Barbara Lee Keyfitz

Director, The Fields Institute

Message from the Scientific Director of MITACS

As I read about all the wonderful work done at the first Fields-MITACS Industrial Problems Workshop, the enthusiasm and camaraderie of the event is obvious. There's something magical about a team of scientists, many of whom have not previously collaborated, getting together to look at a problem posed by a non-expert. The problem is often not well defined and yet, after careful consideration and discussion with the proposers, a well-formulated problem emerges. And now, with different expertise and working together, a multitude of mathematical techniques are used to attack the problem. And so, after five days, the proposers are amazed at the solutions that come out and the insights gained while the scientists have the satisfaction of having made a real difference to a societal challenge. This is what happened at the Fields on August 20-24, 2006 and these proceedings are a testament to a highly successful workshop run by a dedicated group of scientists, with over 60 participants donating their time all within the confines of a magnificent venue - the Fields Institute.

The MITACS Network of Centres of Excellence is mandated to promote industrial mathematics in Canada. When I think about the beginnings of MITACS, I note that the network, in many ways, arose out of the problem solving workshops that started ten years ago at PIMS. Those workshops gave the Canadian mathematical community the confidence to know that we could make a significant contribution to Canadian industry and society. We saw the need and MITACS allowed us to focus our energy into meeting it. So, in many ways we were overdue to expand these workshops beyond the West. The vibrant industrial community in Central Canada, the excellence of the mathematical community in Ontario and the rest of the country, and the growing numbers of students who are keenly interested in industrial mathematics speaks to the need - this workshop is a realization of that need.

The problems at the workshop were drawn from the biomedical/social sciences and the financial sectors. Both of these are key theme areas of concentration within the MITACS research program. As such, I firmly believe that we will see spin-offs from this workshop with scientists and possibly even the non-academic partners participating in future MITACS scientific programs. I am also pleased to know there will be two workshops in 2007 (one in Montreal at the CRM and one in Edmonton at PIMS) which will give ample opportunity for Canadian scientists to further develop new industrial outreach and to involve still more scientists in this activity.

My sincerest thanks to the organizers, Huaxiong Huang, Barbara Keyfitz, and Nilima Nigam, who put in a tremendous effort in launching this initiative and thought about every aspect to ensure the workshop ran smoothly. They were joined by Sean Bohun, Greg Lewis, and Roderick Melnik to form the scientific committee and the choice of problems is a testament to their efforts. There are many others who deserve to be recognized for their contributions - the editors of these proceedings, Dhavide Aruliah and Greg Lewis, the problem presenters and the scientists who participated and the staff at Fields. To all of them, congratulations on a superb job and I am looking forward to hearing about successes of future workshops.

Arvind Gupta
Scientific Director, MITACS

Acknowledgements

It is due to the hard work of many people that the First Fields-MITACS Industrial Problems Workshop (FMIPW) was a success. An important part of a workshop such as this is the writing of the reports. It is here that the tangible evidence of the productivity of the week can be seen. These reports represent a great effort. Therefore, we would like to thank those individuals who took the responsibility to ensure that the ideas generated at the workshop would be available for all in the form of these Proceedings. These individuals are:

- Suzanne Shontz
- David Cotrell, Huaxiong Huang, Nilima Nigam
- Sean Bohun, Chris Breward
- Julien Arino
- Luciano Buono, Roger Chau, Greg Lewis, Neal Madras, Mary Pugh, Louis Rossi, Thomas Witelski
- Oleg Grodzevich

It is also a tremendous amount of work to collect the problems and organize the workshop itself. We would like to thank the organizers

- Huaxiong Huang (York University)
- Barbara Keyfitz (Fields Institute)
- Nilima Nigam (McGill University)

for putting together this successful event, and the scientific committee for vetting the problems. In addition to the organizers (listed above), the scientific committee consisted of:

- Sean Bohun (University of Ontario Institute of Technology)
- Greg Lewis (University of Ontario Institute of Technology)
- Roderick Melnik (Wilfrid Laurier University)

The organizational details would not have been possible without the help of the Fields Institute staff. In particular, the organizers would like to thank Alison Conway, Judith Munn, Philip Spencer and Luke Chang.

Of course, without the problems the workshop could not have taken place. We would like to thank the participating organizations and the problem presenters for contributing such interesting problems:

- NRC Winnipeg, presented by Chris Bowman
- Manulife (Toronto), presented by Scott Warlow
- Manitoba Institute of Child Health, presented by Richard Gordon
- St. Michael's Hospital (Toronto), presented by Kamran Khan
- Mt. Sinai Hospital (Toronto), presented by Jon Hunter and Bill Lancee with Leslie Atkinson (CAMH)
- Algorithmics (Toronto), presented by Helmut Mausser

Finally, and not least of all, the problems could not have been solved without the tremendous effort put forth by the academic participants. We thank them heartily for the generosity of their time and mental capacity.

Dhavid Aruliah (UOIT)

Greg Lewis (UOIT)

Editors

Nonlinear Dimension Reduction for Microarray Data (Small n and Large p)

Problem Presenter: Christopher Bowman (National Research Council of Canada)

Academic Participants: Dhavide Aruliah (University of Ontario Institute of Technology), Guangzhe Fan (University of Waterloo), Roderick Melnik (Wilfred Laurier University), Suzanne Shontz (Pennsylvania State University), Steven Wang (York University), Jiaping Zhu (University of Waterloo)

Report prepared by: Suzanne Shontz¹

1 Introduction

Over the last decade or so, researchers have developed techniques for measuring the expression level of many genes in an organism simultaneously. One such technique is the cDNA microarray [13, 11]. Such techniques generate a torrent of data that can be used to then learn more about gene functions, response to stimuli, and interactions.

A cDNA microarray is a glass slide on which many (usually thousands) segments of DNA (often genes, but not always) are attached in distinct spots. Messenger RNA is then extracted from two different populations of cells (for example, cancer and normal tissue) and reverse transcribed to complementary DNA (cDNA). Each of the two sets of cDNA is tagged with a molecule of fluorescent dye; usually they are red and green, respectively. The cDNA solutions are then washed over the glass slide and hybridized with the genetic material spotted onto the slide. When a molecule of cDNA matches the DNA spotted onto the slide, it reacts and binds to it, bringing along the fluorescent dye molecule. The greater the number of copies of the appropriate piece of cDNA present in the sample, the greater the number of dye molecules which will bind to that particular spot, creating a stronger signal. If red and green dyes are used, the spots will appear to fluoresce with varying intensities of red, green, and yellow (when cDNA from both samples bind to the spot). These intensities can be measured by a scanner to determine the relative expression level of each gene in each of the two cell populations.

Microarray experiments thus typically have thousands of variables explaining each individual sample in the experiment and typically only a handful (a few hundred at most, often

¹shontz@cse.psu.edu

many fewer) distinct samples. Furthermore, the thousands of genes in an organism are not independent entities, and each reacts to the activation level of other genes in a complicated and not well-understood way. This raises a mathematical challenge. Each experimental sample can be viewed as a point in a space of dimension equal to the number of genes being measured. The question is, can one find a lower-dimensional space in which to work? Or, stated more precisely, given a set of n points in an p -dimensional linear space, drawn from some unknown distribution V , find a d -dimensional (possibly nonlinear, $d \ll p$) manifold that approximates the points well?

There are many measures for determining whether or not a lower-dimensional manifold approximates the points well. The simplest is that the orthogonal distance from each point to the manifold should be minimised, but this is by no means the only choice, and other options will be discussed below. It is important to note, however, that any notion of goodness-of-fit should apply not just to the data that has already been collected, but also to future data points drawn from the distribution V . To ensure this, a cross-validated estimate of error must be used, for example, the leave-one-out error described below.

2 Filtering the data

2.1 Motivation for filtering. Typical microarray data have quite high dimensionality due to the number of genes involved. For example, the simplest biological model, yeast, has more than 6000 genes. In 2003, estimates from gene-prediction programs suggested there might be as many as 24,500 protein-coding genes [12]. The Ensemble genome-annotation system estimates their number at 23,299. Therefore, the dimensionality is very high. On the other hand, the number of observations that is available is usually very low due to fact the microarray experiments are too expensive to produce many replications. This is known as the problem of “*large p and small n* ”.

Although there are many human genes, often medical researchers are only concerned with a dozen or fewer genes if they are interested in one particular disease. Therefore it is not necessary to consider all the genes in the analysis of microarray data. Furthermore, the information or “signal” for the genes of interest could be overwhelmed by the genes that are not relevant to the current analysis. Dimensionality reduction is necessary given the fact that there are not many observations that are scattered in very high-dimensional space.

Furthermore, the filtering is crucial for any data mining technique to work. For example, the clustering procedure is often applied to microarray data to divide the large-dimensional space into subspaces such that the subspaces are much more manageable than the whole space. However, most clustering algorithms would rely on a proper choice of distance function. There are many distance functions proposed in the literature. We will demonstrate our argument by using the most commonly used distance function, *i.e.*, Euclidean distance. To make our argument more transparent, we suppose that there are p random variables that are independent and identically distributed with a standard normal distribution, *i.e.*

$$X_1, X_2, \dots, X_p \sim N(0, 1).$$

Let us further assume that only Y_1 and Y_2 are important or relevant to us. Furthermore, we assume that

$$Y_1 \sim N(10, 1) \quad \text{and} \quad Y_2 \sim N(20, 1)$$

for the observations from the treatment group and $Y_1, Y_2 \sim N(0, 1)$ for the control group.

However, the vector $(Y_1, Y_2, X_1, X_2, \dots, X_p)$ will not be informative if the Euclidean distance is used. Let $O_k = (Y_{k1}, Y_{k2}, X_{k1}, X_{k2}, \dots, X_{kp})$ and $O_j = (Y_{j1}, Y_{j2}, X_{j1}, X_{j2}, \dots, X_{jp})$

represent two observations in a microarray data set. Note that $Y_{k1} \sim N(10, 1)$ and $Y_{k2} \sim N(20, 1)$.

It can be verified that

$$\text{dist}(O_j - O_k)^2 = \sqrt{(Y_{k1} - Y_{j1})^2 + (Y_{k2} - Y_{j2})^2} + \chi^2(p)$$

where $\chi^2(p)$ denotes the central χ^2 distribution with mean p and variance $2p$.

It can be verified that

$$\frac{(Y_{k1} - Y_{j1})^2 + (Y_{k2} - Y_{j2})^2 + \chi^2(p)}{\chi^2(p)} \xrightarrow{P} 1, \quad \text{as } p \rightarrow \infty. \quad (2.1)$$

This implies that the Euclidean distance function will be dominated by those variables that are pure noise in general. Although another distance function might be a better choice, they all suffer from the same problem but to a lesser degree.

Therefore, filtering is very important to quickly reduce the genes of interest and avoid the aforementioned problems introduced by those noisy variables which contain no information at all.

2.2 Example of preprocessing. Various methods of preprocessing have been proposed in the literature. These methods mainly deal with problems having class labels. For example, Golub et al. [3] proposed a univariate ranking criterion for each gene in a two-class situation. The criterion is can be defined as the ratio of the absolute mean difference of gene expression levels of the two classes with respect to the sum of standard deviations of the two classes for each gene considered. Higher ratio indicate higher ranking of the gene. Some other author used the ratio of between-class sum of squares to within-class sum of squares of each gene for multi-class problems. Later, Tibshirani et al. [14] used the shrunken centroids method for gene classification. Shrinkage and gene selection are integrated into a naive Bayes classifier. The univariate gene selection is based on t-statistics for each gene of each class.

Another method is the random forest procedure [1]. Random forest is an ensemble tree approach in data mining. It has been used as a popular approach in gene selection. Basically, random forest build tree classifiers. A tree classifier recursively partition the data to classify. The tree is built by greedily searching locally optimal split rules recursively. Instead of using all variables (genes) to build the trees, random forest uses a random sample of variables (genes) during the tree construction. The randomness causes different trees built even following the same procedure each time. In this sense, we can get many (usually more than 50) different trees using the same data set. These trees are used as an ensemble classifier via voting. Random forest can have high accuracy in classification. It also effectively estimates the performance of these randomly selected variables (genes) and provides an overall measure of variable (gene) importance. Different ways of evaluating the variables (genes) can be found in the random forest manual. These importance measures will consider interactions among the variables (genes) due to the nature of the tree classifiers.

As an example, let us look at the famous Leukemia data. This data set has 38 training samples and 34 test samples of two types of acute leukemias, acute myeloid leukemia (AML) and acute lymphoblastic leukemia (ALL) [3]. Each sample is related to 7129 genes.

Due to the large number of genes, we propose a combination of univariate ranking and random forest. First, univariate ranking is performed to select the best 200 genes. Then the random forest procedure is performed on these 200 genes to obtain their measures of importance. Below is a figure showing the importance measure of the 200 pre-selected genes.

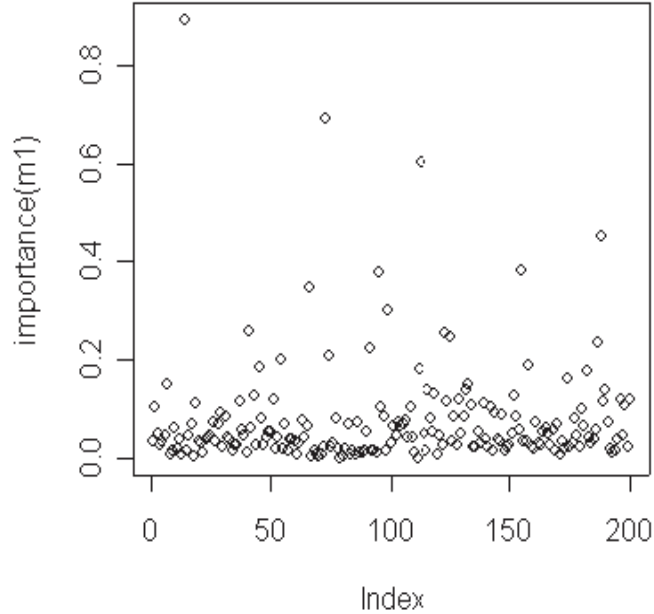


Figure 1 Variable (Gene) Importance using Random Forest for 200 Pre-selected Genes

We see that the variable importance using random forest is not the same as that using univariate ranking when interactions are considered. We can select a number of genes based on the variable importance for our needs.

2.3 Future avenues. As seen in the previous example, univariate ranking methods implicitly assume weak or no interactions or correlations among genes, which may not be true in practice of microarray analysis. The ideal situation would be to have a method which considers all variables together for selection. We now introduce the support vector machine classifier. The support vector machine basically searches for the optimal hyperplane that separates the data. Here an optimal hyperplane is the one that maximizes the geometric margin (the closest distance of the observations to the hyperplane). For a nonlinear pattern, the original space can be mapped to a high-dimensional space using kernel functions and the so-called Reproducing Kernel Hilbert Space (RKHS). So support vector machines can learn very well for a general problem.

In particular, for gene expression data, Guyon et al. [4] proposed a recursive feature eliminating method for gene selection. First, all the variables (genes) are used in model fitting. Then a large number of variables (genes) which are not significant in the model are removed. The model is then rebuilt on the rest of the variables (genes), and we can recursively repeat the procedure until only a small number of genes is left in the model. Zhu and Hastie used penalized logistic regression with similar ideas of gene selection [16].

For example, in the Golub 1999 data set just described in the previous section, Zhu and Hastie report 26 genes selected with two cross-validated errors on the training set and one error on the test set. The support vector machine selects 31 genes with similar performances.

In the future, we could try to combine random forest with support vector machine to perform gene selection.

3 Nonlinear dimension reduction

While filtering the data requires the methodologies to be able to identify in some sense redundant information in the already existing data, the ultimate purpose of dimensionality reduction is to reduce the data to a low-dimensional manifold in such a way that unsupervised learning is possible on new data. In other words, we have to discover the main trend in the existing data in order to be able to deal with newly acquired data in a similar way. Along with the (probabilistic) density estimation techniques, dimensionality reduction is a key methodology in developing algorithms for unsupervised learning [10]. Although these two methodologies can be applied simultaneously, nonlinear reduction can also be developed in a non-probabilistic framework.

Historically, first developed techniques for dimensionality reduction were based on linear versions of principal component analysis (PCA) (described below) and other eigenvalue-based methods such as variants of centre manifold reduction techniques. Due to difficulties with the mapping of the higher-dimensional data (even if represented by clusters) into a single coordinate system of lower dimensionality in applications of such techniques, most recent developments were centered around nonlinear dimensionality reduction methods. These techniques, similarly to traditional linear methods, are essentially based on *spectral embeddings*, but with a key new feature now of being able to generate nonlinear embeddings.

3.1 Spectral embedding methodologies.

3.1.1 *Generic setting for the spectral embedding.* Nonlinear procedures of interest can be cast in the following generic setting:

1. Given the input space, compute neighbourhoods;
2. Construct the cost function to determine the weight matrix as a result of an optimisation procedure (e.g., minimising the generalized error function);
3. Based on the eigenvectors of the above matrix (can be shown with the Rayleigh-Ritz ansatz), calculate the spectral embedding.

3.1.2 *The nearest neighbour parameter as a key to success.* The starting point of spectral embedding methodologies is computing neighbourhoods. In all the algorithms currently available to the National Research Council (NRC) of Canada, our industrial partner, we have one of the two situations:

- either the number of nearest neighbours is predefined by a certain value, denoted further by K (as it is the case, for example, in the Locally Linear Embedding (LLE)),
- or the input information requires the neighbourhood radius, denoted further by ϵ (as is the case, for example, in Isomap).

This may bring difficulties in some of the practical situations where a nonlinear dimensionality reduction algorithm is applied to a set of new data. Indeed, if we choose an estimate for K in the LLE such that K is very small compared to the real situation, a neighbourhood can falsely divide the underlying manifold. On the other hand, if we choose an estimate for K in the LLE such that K is large, the resulting manifold will be excessively smoothed and important small-scale features will be completely missing. Similar difficulties arise in the choice of ϵ .

3.1.3 *Description of some algorithms.* **Locally Linear Embedding (LLE):** The Local Linear Embedding (or LLE) Algorithm is a spectral embedding method for nonlinear dimension reduction developed by Roweis and Saul [8]. This algorithm takes as input X , a $p \times n$ matrix (whose columns contain the n data points in \mathbf{R}^p) and outputs Y , a $d \times n$

matrix, where $d < p$ is the dimensionality of the embedding of the input. The idea behind this algorithm is to characterize the local geometry of patches by linear coefficients that reconstruct each data point from its nearest neighbours when determining the underlying lower-dimensional manifold.

There are three major steps in the LLE algorithm. The first is to determine the neighbours in X -space. The second step is to solve for reconstruction weights W_{ij} which allow each point \mathbf{X}_i to be reconstructed from its neighbours \mathbf{X}_j . The final step is to compute the embedding coordinates Y using the reconstruction weights W . We now describe these three steps in more detail.

The first step is to determine the neighbours for each data point. This can be done in various ways described above. For our purposes, we compute the K -nearest neighbours for each data point.

The second step is to determine the reconstruction weights. To that end, we let W_{ij} denote the contribution of the j^{th} data point to the i^{th} reconstruction. Then, the weights W_{ij} are computed that minimise the following cost function:

$$E(W) = \sum_i \|\mathbf{X}_i - \sum_j W_{ij} \mathbf{X}_j\|^2. \quad (3.1)$$

which is known as the reconstruction error. The minimisation is performed subject to two constraints. The first constraint is that \mathbf{X}_i is reconstructed only from its K nearest neighbours. Thus, we set W_{ij} to 0 if \mathbf{X}_j is not a neighbour of \mathbf{X}_i . The second constraint is that each set of local weights must sum to 1. Determining the optimal weights is a least squares optimisation problem that is described in further detail in Appendix A of [9].

The final step is to compute the embedding coordinates Y using the weights W . This is done by choosing the Y_i that minimise:

$$\Phi(Y) = \sum_i \|\mathbf{Y}_i - \sum_j W_{ij} \mathbf{Y}_j\|^2. \quad (3.2)$$

This specifies a quadratic form in Y which can be minimised by solving a sparse $N \times N$ eigenvector problem. See Appendix B in [9] for more details.

Isomap: The Isomap algorithm consists of three primary steps:

1. Construct the neighbourhood graph G .
As with the LLE method, the first step of the Isomap method is to determine which points are neighbours based on Euclidean distances between points in the input data in \mathbf{R}^p . The neighbours are obtained using one of the two basic approaches for finding nearest neighbours outlined above. The information about the neighbourhoods is collected into a weighted neighbourhood graph G that has a node for each data point in the original input. The nodes of G are connected iff they are neighbours and the weights on the edges connecting nodes are the corresponding Euclidean distances between neighbouring data points in \mathbf{R}^p . The graph G is particularly easy to construct when the number of data points n is smaller than the dimension p of the space in which the data is embedded.
2. Construct the matrix D containing the shortest paths between all pairs of points in the graph G .

Isomap estimates the geodesic distances between all pairs of points on the manifold. This is achieved by computing the shortest path distances between vertices in the

weighted graph G constructed in the first step. Dijkstra's algorithm is known to be a good algorithm to find a shortest path in a weighted graph.

3. Apply Multi-Dimensional Scaling to the matrix D to determine the d -dimensional embedding.

The final step of Isomap applies classical Multi-Dimensional Scaling (MDS) to the matrix of D of graph distances as computed in the second step. The MDS algorithm constructs an embedding of the data in a d -dimensional Euclidean space that best preserves the intrinsic geometry of the manifold as determined by the relative distances of the points. The particular embedding found results from minimising a particular measure of error; the solution of this optimisation problem reduces to an eigenvalue problem.

Some more comments are in order concerning the final step of the Isomap algorithm. Given a set of n input vectors $\{\mathbf{X}_1, \dots, \mathbf{X}_n\} \subset \mathbf{R}^p$, the Isomap algorithm returns a set of n vectors $\{\mathbf{Y}_1, \dots, \mathbf{Y}_n\} \subset \mathbf{R}^d$ where $d < p$ is prescribed. Let

$$X = [\mathbf{X}_1, \dots, \mathbf{X}_n] \in \mathbf{R}^{p \times n} \text{ and } Y = [\mathbf{Y}_1, \dots, \mathbf{Y}_n] \in \mathbf{R}^{d \times n}$$

be rectangular matrices with the input and output column vectors stacked in sequence. The pre-images Y of the input data X are found as the minimisers of a cost function

$$E(Y) = \|\tau(D) - \tau(D_Y)\|_F, \tag{3.3}$$

where $\|A\|_F = \left[\sum_{i,j} |A_{i,j}|^2\right]^{1/2}$ is the usual Frobenius matrix norm. Further, in the definition of the cost function in (3.3), D_Y denotes the matrix of Euclidean distances between all the columns of Y taken pairwise, i.e.,

$$(D_Y)_{i,j} = \|\mathbf{Y}_i - \mathbf{Y}_j\| \quad (i, j = 1, \dots, n).$$

The operator τ in (3.3) is defined as

$$\tau(A) := -\frac{1}{2}H(A \cdot A)H \tag{3.4a}$$

where $A \cdot A$ is the Hadamard (entrywise) product of A with itself and H is a centering matrix; explicitly,

$$(A \cdot A)_{i,j} := A_{i,j}^2, \tag{3.4b}$$

$$H_{i,j} := \delta_{i,j} - \frac{1}{n} \tag{3.4c}$$

where n is the number of data points and $\delta_{i,j}$ is the usual Kronecker delta. The operator τ expresses the (Frobenius) distance between matrices using matrix products and thus makes the minimisation of $E(Y)$ easier.

3.1.4 Optimal number of nearest neighbours. In what follows, we focus on the problem of optimal choice of nearest neighbour numbers.

As proposed by Kouropteva et al. (with modifications recently suggested by Samko et al.) [6], we choose a set of values of K from $[K_{min}, K_{max}]$. The simplest choice of K_{min} in our case is 1.

Next, for each $K \in [K_{min}, K_{max}]$, we calculate the cost function:

$$E = \|\tau(\bar{D}) - \tau(D_Y)\|, \tag{3.5}$$

where

$$D_Y = \{d_{\mathbf{y}}(i, j) = \|\mathbf{Y}_i - \mathbf{Y}_j\| = \sqrt{\sum_{k=1}^d (\mathbf{Y}_i^k - \mathbf{Y}_j^k)^2}\} \quad (3.6)$$

is the matrix of Euclidean distances in the output space, while \bar{D} is different for different spectral embedding algorithms. We focus on a generalization of LLE where we have

$$\bar{D} \equiv D_X = \{d_{\mathbf{x}}(i, j) = \|\mathbf{X}_i - \mathbf{X}_j\| = \sqrt{\sum_{k=1}^p (\mathbf{X}_i^k - \mathbf{X}_j^k)^2}\} \quad (3.7)$$

As usual, the operator τ converts distances to inner products (to simplify the optimisation procedure).

Then all K values where minima of $E(K)$ are achieved will form the set S_K of initial candidates for the optimum value of K .

Finally, the nonlinear reduction algorithm should be run for each $K \in S_K$. And K_{opt} is determined by the following formula based on minimising the residual variance:

$$K_{\text{opt}} = \arg \min_K (1 - \rho_{D_X D_Y}^2), \quad (3.8)$$

where ρ is the linear correlation coefficient taken over all entries of the matrices D_X and D_Y which contain Euclidean distances between pairs of points in the input (dimension p) and output (dimension d) spaces, respectively.

3.1.5 Choice of the cost function and how to avoid ill-posedness. The above choice of the cost function in the form of (3.5) is not the only possible one. In the generalized LLE we worked on, the cost function is taken as a measure of the reconstruction error:

$$E(W) = \sum_i \|\mathbf{X}_i - \sum_j W_{ij} \mathbf{X}_j\|^2. \quad (3.9)$$

To avoid ill-posedness it is essential to add constraints to this optimisation problem. The most natural are related to the weights, and probably the simplest one is

$$\sum_j W_{ij} = 1. \quad (3.10)$$

Further, as we observed in our experiments (described below), it might be essential to precondition the Gram matrix by a regularization procedure.

3.1.6 Further improvements. The search for the neighbours can be improved further if it is carried out with respect to the geodesic distance, rather than the Euclidean distance as it is commonly done. Only a slight modification of the LLE algorithm is required in this case [15]. In order to eliminate the necessity to estimate geodesic distances between faraway inputs on the manifold, and hence to improve the efficiency, we can apply a semidefinite embedding as recently proposed by Weinberger et al.

Finally, further modifications of the spectral embedding algorithms, described here, can be introduced with the stochastic neighbour embedding which could be useful for relatively noisy data.

Potential gaps in existing literature: There is a lot of work and experience to draw upon from the machine learning community to help with the problem of dimensionality reduction for microarray data. However, there are some features of algorithms for nonlinear dimensionality reduction described in the existing literature that complicate the present

study rather than making matters more clear. We describe some of these issues with the hope that they can be resolved in later studies.

A number of nonlinear dimensionality reduction algorithms are based on the assumption that there exists a nonlinear manifold embedded in \mathbf{R}^p that underlies the given set of data. The input of the algorithms usually consists of a set of n data points in \mathbf{R}^p and possibly the dimension d of the manifold sought. The output of the algorithms typically consists of a set of n vectors in \mathbf{R}^d with $d < p$ that would be the pre-images of the input data vectors in a presumably lower-dimensional space. However, manifolds consist of uncountably many coordinate charts (smooth mappings from \mathbf{R}^d into \mathbf{R}^p whose ranges are contained in the points on the manifold) in an atlas that cover the whole manifold. It is not typical for a single coordinate chart to cover the whole manifold. Moreover, when the output from a dimensionality reduction algorithm consists of the pre-images of the data under a particular coordinate chart, it is not obvious which coordinate chart is being used. Some charts have greater utility than others in different regions of the manifold.

To clarify the preceding discussion, assume that the manifold from which the input data is sampled is the unit sphere in \mathbf{R}^3 (i.e., $p = 3$ and $d = 2$). Consider the mappings $\psi_1 : (0, \pi) \times (\pi, \pi) \rightarrow \mathbf{R}^3$ and $\psi_2 : \{(x, y) \in \mathbf{R}^2 : x^2 + y^2 < 1\} \rightarrow \mathbf{R}^3$ that are defined by

$$\begin{aligned} \psi_1(\phi, \theta) &:= (\cos \theta \sin \phi, \sin \theta \sin \phi, \cos \phi) & (\phi, \theta) &\in (0, \pi) \times (\pi, \pi) \\ \psi_2(x, y) &:= (x, y, \sqrt{1 - x^2 - y^2}) & (x, y) &\in \{(x, y) \in \mathbf{R}^2 : x^2 + y^2 < 1\}. \end{aligned}$$

Both of these charts cover portions of the unit sphere in \mathbf{R}^3 . However, while ψ_1 covers the region near the point $(0, 0, 1)$ relatively poorly due to a coordinate singularity in ψ_1 near $\phi = 0$, the chart ψ_2 can be used near that region without difficulty. Similarly, the mapping ψ_2 encounters difficulty near the boundary of the unit disk in \mathbf{R}^2 for exactly the same reason whereas ψ_1 has quite well-behaved derivatives near the region where $\phi = \pi/2$. As such, the output of algorithms such as LLE or Isomap consist of vectors in \mathbf{R}^d , but it is in no way obvious which chart has been selected and whether it is one that is appropriate in the region of the manifold being sampled.

Another problem shared by many algorithms is the number of heuristic parameters inherent even in deterministic algorithms. For instance, in LLE, the dimension d of the lower-dimensional manifold on which the sampled data lies is an input parameter of the algorithm. (Admittedly, the Isomap algorithm does not share this particular shortcoming in that it starts from $d = 1$ and increments d until a suitable value of d is determined.) Other heuristic choices in the development of the algorithms include the number of nearest neighbours to choose, the method by which nearest neighbours are measured, and the choice of metric in the objective function to minimise in finding the reconstruction weights.

The most perplexing difficulty arises when trying to compare the performance of distinct algorithms. If the output of algorithm A is a set of pre-images of the data under one coordinate chart and the output of algorithm B is a similar set of pre-images, does it follow that the outputs can be compared? This is a vexing issue for assessing the numerical accuracy and the asymptotic complexity of dimensionality reduction algorithms. Convergence properties of, say, numerical approximation schemes for partial differential equations, can be estimated by numerical experiments where the exact solution is known even when convergence proofs are unattainable. Such numerical experiments are invaluable when new schemes are suggested for comparison to existing frameworks. It does not seem that the literature on nonlinear dimension reduction algorithms has analogous criteria for comparison of algorithms.

3.2 Kernel Principle Component Analysis (KPCA).

3.2.1 *Description of the PCA method.* Principal component analysis (PCA) is one of the statistical methods to extract the patterns in the data and to represent the original data in another way based on their similarity and dissimilarity. PCA is not only widely-used for pattern extraction but also for dimensionality reduction and data visualization. Once the patterns hidden in the data are identified, we can project the data into lower dimension by selecting several most important patterns and without losing too much information. As one might expect, it is nontrivial to identify these patterns in the high-dimensional data.

PCA is essentially a basis transformation. Suppose the data points are given by $\{\mathbf{X}_1, \mathbf{X}_2, \dots, \mathbf{X}_n\}$, where $\mathbf{X}_i \in R^p$ and are centered, *i.e.*, such that $\sum_{i=1}^n \mathbf{X}_i = \mathbf{0}$. The covariance matrix is then defined by

$$C = \frac{1}{n} \sum_{i=1}^n \mathbf{X}_i \mathbf{X}_i^T.$$

Since the orthonormal eigenvectors of the covariance matrix form a basis in space, we can express the data in terms of the eigenvector basis, instead of Cartesian coordinates. Actually, the eigenvectors show the directions of variance in the data. In addition, the corresponding eigenvalues indicate the proportions of the variances. The eigenvector corresponding to the largest eigenvalue is called the principal component.

It will be easier to analyse the data if their dimension is much smaller. Therefore, we can project the data onto a lower-dimensional space. Then the data are approximated by the linear combination of the selected d eigenvectors ($d < p$) and truncating the tails of the vectors creating vectors of length d . The value of d may be decided by the specific need, such as a value of two or three for visualization, or by minimising the difference between the original data and its approximation.

3.2.2 *Description of the Kernel PCA method.* The principle component analysis has a very long history and is known to be very powerful for the linear case. However, the sample space that many research problems are facing, especially the sample space of microarray data, are considered nonlinear in nature. One reason might be that the interaction of the genes are not completely understood. Many biological pathways are still beyond human comprehension. It is then quite naive to assume that the genes should be connected in a linear fashion.

To handle nonlinear spaces, a natural idea is to make a suitable transformation that tries to make the transformed space linear. Although this idea has been mentioned in the literature many times, the breakthrough did not come until the last 20 years during which time the computational issue has been resolved.

In order to capture nonlinear patterns, it is often useful to consider a nonlinear transformation of the original variables. For example, given two random variables, we might consider only the linear combination, *i.e.*, $a_1x_1 + a_2x_2$. To capture any nonlinear relationship, we might want to consider the ensemble of

$$\mathcal{E} = \{X_1, X_2, X_1^2, X_2^2, X_1X_2, X_1^3, X_2^3, X_1X_2^2, X_1^2X_2, \dots\}.$$

Although this can be done, the computational burden associated with the expansion into a higher-dimensional space is very costly. Given the fact the microarray data already has a very high dimensionality to begin with, this does not appear to be feasible.

To be more specific, we consider a mapping:

$$\mathcal{K} : \mathcal{X} \longrightarrow \mathcal{F} \tag{3.11}$$

where \mathcal{X} and \mathcal{F} are the sample and output spaces, respectively, and K is the kernel function.

However, the Kernel PCA method does exactly this seemingly impossible task. The key element of the Kernel PCA is that the original space is transformed into an output space through kernel functions. Kernel functions are designed to capture the nonlinear nature of the original space by expanding the basis functions into a much higher-dimensional space. However, any computation after the transformation can be done using the kernel function and the inner product of the original space. In other words, no actual transformation is necessary, and the results are obtained without significant computational cost.

Given $f \in \mathcal{F}$ and $g \in \mathcal{F}$, we then have

$$\langle f, g \rangle = \sum_{i=1}^n \sum_{j=1}^n \alpha_i \alpha_j \mathcal{K}(x_i, x_j). \quad (3.12)$$

Detailed discussions of the Kernel PCA can be found in [12].

3.2.3 Choice of kernel functions and future research. There are many kernel functions that have been proposed in the literature. Gaussian functions are commonly used. However, this is no guarantee that a Gaussian function would be applicable all the time. One possible approach is to use the idea of model averaging. To be more specific, one could use an array of kernel functions and evaluate each kernel function for its effectiveness using some loss function, for example, the mean squared error (MSE).

4 Numerical experiments and results

4.1 Available datasets. We now describe the two types of datasets of interest to us: a microarray dataset from the NRC and some synthetic datasets which we have designed.

4.1.1 Microarray dataset. The NRC provided us with an AML microarray dataset of genetic data which sampled 7129 genes in 72 patients; this corresponds to 72 vectors of data in \mathbf{R}^{7129} . The patterns in the microarray data are nonlinear and are thus quite complicated. In addition, the data are noisy due to the nature of the microarray experiment.

4.1.2 Synthetic datasets. The papers of Roweis and Tannenbaum make extensive use of test data sets for their algorithms. These include an S-shaped ribbon (a two-dimensional manifold embedded in \mathbf{R}^3 , the standard unit sphere $S^2 \subset \mathbf{R}^3$, and a number of variants involving translations of a fixed image. These examples support the strength of these algorithms in the event that the number n of samples available is larger than the dimension p of the space from which the data are sampled. Unfortunately, this is not the case with cell microarray data.

We advocate generating synthetic test data known to lie on a manifold with known structure of arbitrary dimensions as a means of testing prospective algorithms. The procedure mentioned here was developed using random sampling on the unit sphere $S^d \subset \mathbf{R}^{d+1}$. This does in fact require some care; randomly sampling points on the unit hypersphere needs to be done in a way to ensure that samples are not clustered near poles. Fortunately, a very simple framework for doing so is provided by Knuth.

1. Generate random vectors $\mathbf{Y}_1, \dots, \mathbf{Y}_n \in \mathbf{R}^{d+1}$, each component being observations of a random variable with Gaussian distribution with mean at 0.
2. $\mathbf{Y}_k \mapsto \mathbf{Y}_k / \|\mathbf{Y}_k\|_2$ ($k = 1, \dots, n$) generates set of n random vectors uniformly-distributed on the unit sphere in \mathbf{R}^{d+1} .
3. Embed vectors \mathbf{Y}_k into column vectors $\mathbf{X}_k \in \mathbf{R}^p$ by padding with zeros.

The vectors generated thusly lie on the unit sphere $S^d \subset \mathbf{R}^p$. This procedure can be adapted to make data points from the manifolds $S^{d_1} \times S^{d_2}$ embedded in \mathbf{R}^p or any similar Cartesian product manifold. To obscure the obvious manifold structure of a set of vectors in \mathbf{R}^p with zeros in most of the components, a number of strategies can be used.

1. Make the substitutions $\mathbf{X}_k \mapsto P\mathbf{X}_k$ where P is a random $p \times p$ permutation matrix.
2. Make the substitutions $\mathbf{X}_k \mapsto Q\mathbf{X}_k$ where $Q = I - 2\mathbf{u}\mathbf{u}^T$ is a random orthogonal Householder reflection ($\|\mathbf{u}\|_2 = 1$).
3. Make the substitutions $\mathbf{X}_k \mapsto \mathbf{X}_k + \mathbf{a}$ where $\mathbf{a} \in \mathbf{R}^p$ is a random translation.
4. Add Gaussian noise to all of the components of each vector.

4.2 Numerical experiments. For our numerical experiments, we tested the LLE algorithm on the NRC microarray dataset described above. In particular, we performed a leave-one-out cross-validation experiment and measured the reconstruction error for several combinations of d and K .

Leave-one-out is a cross-validation technique in which the data is divided into n subsets each corresponding to one data point. Training on the data is performed h times, each time using only the omitted subset to compute the error criterion of interest. The following pseudo-code demonstrates the use of the leave-one-out technique for the LLE algorithm:

```

for i = 1:n
  1. Remove X_i from X, i.e., set Xhat_i = X\{X_i}.
  2. Compute the manifold on Xhat_i.
  3. Project X_i onto Xhat_i.
  4. Compute the reconstruction error for X_i.
end

```

Then, the reconstruction error is the sum of the reconstruction errors for each of the n data points.

We repeated this experiment on the filtered dataset (using the result from the Random Forest algorithm described above). Before discussing our numerical results, we describe three main metrics for analyzing the error in the nonlinear dimension reduction process.

4.3 Measures for error analysis. There are three main measures for the error in the nonlinear dimension reduction algorithms: the distortion of the distances, the residual variance, and the reconstruction error.

To measure the distortion of the distances, we compute $E(W) = \sum_{i < j} W_{ij}(D_{ij} - \Delta_{ij})^2$, where D_{ij} is the distance between the points in \mathbf{R}^p , and Δ_{ij} is the corresponding distance in \mathbf{R}^d . Although an interesting error metric, we have not studied this metric in favor of pursuing others.

The measures for characterizing the quality of the nonlinear dimension reduction procedure described here are based on the following two choices:

- Minimisation of the generalized reconstruction error:

$$E_{\mathbf{y}} = \frac{1}{n} \sum_i \|\mathbf{X}_i - P\mathbf{X}_i\|^2, \quad (4.1)$$

where P is the projection operator, $P^2 = P$ such that $\mathbf{Y}_i = P\mathbf{X}_i$. Note that we go from a space of dimensionality p to a space of dimensionality d where for the linear pieces we have

$$\text{var}(\mathbf{Y}) = \text{Tr}(PCP^T), \quad P = \sum_{\alpha=1}^d \mathbf{e}_\alpha \mathbf{e}_\alpha^T, \quad (4.2)$$

$$C = \frac{1}{n} \sum_i \mathbf{X}_i \mathbf{X}_i^T = \sum_{\alpha=1}^p \lambda_\alpha \mathbf{e}_\alpha \mathbf{e}_\alpha^T, \quad (4.3)$$

$$\lambda_1 \geq \lambda_2 \geq \dots \geq \lambda_p. \quad (4.4)$$

- Minimisation of the residual variance:

$$1 - \rho_{D_X D_Y}^2 \quad (4.5)$$

is as discussed above (see (3.8)).

Determining the error of the reduction with (4.5) was proposed for the original LLE algorithm [8]. Note, however, that since all the available algorithms require computing spectral characteristics of the underlying data in one form or another, the computational dichotomy of spectra may represent a non-trivial problem in practice [7]. Nevertheless, recent applications of spectral embedding non-linear reduction techniques, such as LLE and Isomap, to high-density microarray data sets have demonstrated their robustness [5, 2]. Finally, note that in the linear case, the approach based on (4.5) is the standard maximisation of variance subspace:

$$\text{var}(\mathbf{Y}) = \frac{1}{n} \sum_i \|\mathbf{P}\mathbf{X}_i\|^2, \quad (4.6)$$

and is equivalent to the procedure (4.1) based on the minimum reconstruction error.

4.4 Numerical results. Now that we have described three possible error metrics, we return to a description of the results from obtained from the LLE algorithm by running the leave-one-out cross-validation experiment on the NRC microarray dataset. We will also describe the results from running leave-one-out on the corresponding filtered dataset.

The following two figures show the results from the leave-one-out cross-validation experiment using LLE on the microarray and filtered microarray datasets. We see from both figures that the best results are obtained for roughly $K = 12$ nearest neighbours. This result is independent of the choice of d . When a greater number of nearest neighbours is used, the LLE algorithm is more expensive, and there is little to no additional benefit, *i.e.*, the reconstruction error decreases little. The figures also demonstrate that the reconstruction error is minimised for low-dimensional manifolds of smaller dimension. This result is also independent of whether or not filtering was applied. As was expected, the amount of reconstruction error decreased when filtering was applied to the microarray dataset before the leave-one-out cross validation experiment was performed; this demonstrates the success of the filtering process.

5 Discussion and recommendations

As discussed above, support vector machines may be useful for gene selection when combined with the random forest algorithm. There are other issues to explore within the filtering context such as filtering time trends.

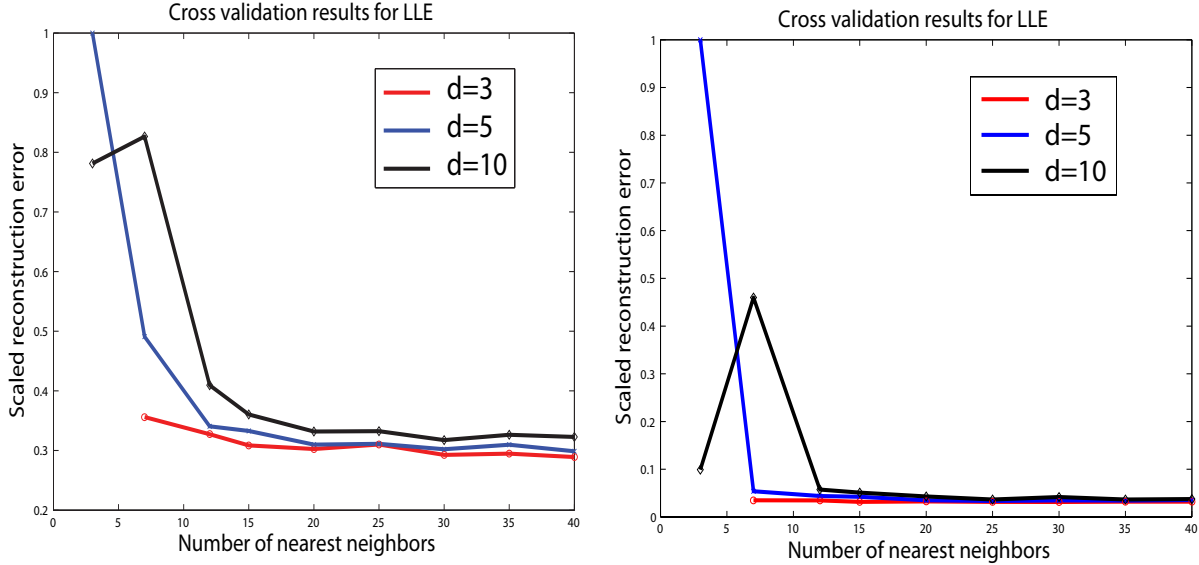


Figure 2 Leave-one-out cross validation results for the LLE algorithm on the NRC microarray (left) and filtered microarray (right) datasets. These figures demonstrate that 12 is a good choice for the number of nearest neighbours in this algorithm. In addition, the reconstruction error is smaller for lower-dimensional manifolds and for the filtered microarray dataset.

Within Kernel PCA, the choice of kernel function should be investigated to find the most useful type of kernel for the microarray and synthetic datasets.

There are several avenues to pursue within the spectral embedding framework for nonlinear dimensionality reduction. First, we would like to experiment with the Isomap algorithm and compare the results of that algorithm with the LLE experiments. Comparisons should also be made with the other spectral embedding algorithms. Thus far, our results indicate that the Random Forest and LLE algorithms were useful for filtering the genes and nonlinear dimensional reduction as tested on the NRC microarray dataset.

A second avenue to explore is the choice of the nearest neighbours in LLE and other spectral-embedding algorithms. There are many options for choosing the neighbours within LLE such as the using the K -nearest neighbours, the points within a ball of a specified radius, or using an adaptive local distance metric to choose the neighbours flexibly within various regions. It is expected that an adaptive choice for the neighbours will produce improved results. Above it was discussed how to pursue an optimal number of neighbours.

A third avenue that needs to be investigated is the choice of cost function. Our experiments measured the reconstruction error because this metric was of interest to the NRC, our industrial partner. It is not clear which error metric would be the most useful for the general case, as we have not run any experiments using the distortion of the distances or the residual variance as our error metric. We have not run any experiments on the synthetic datasets which we have designed; tests will need to be run on this dataset for us to be able to understand how these algorithms perform on additional datasets.

The final issue we have identified for investigation is the choice of cross-validation technique. Our experiments used the leave-one-out cross-validation technique. This can be

generalized to the leave- v -out technique, which is a more complicated version of leave-one-out in which all possible subsets of v data points are left out of the training set. As the choice of cost function changes, the most successful cross-validation technique may change as well.

Numerous experiments need to be performed on the microarray and synthetic datasets in order for us to better understand the performance of the algorithms described in this report on filtering of genes and the nonlinear dimensionality reduction problem.

References

- [1] L. Breiman. (2001), Random forests. *Machine Learning* 45:5–32.
- [2] K. Dawson, R. L. Rodriguez, and W. Malyj (2005), Sample phenotype clusters in high-density oligonucleotide microarray data sets are revealed using Isomap, a nonlinear algorithm. *BMC Bioinformatics* 6(195):1–17.
- [3] T. Golub, D. Slonim, P. Tamayo, C. Huard, M. Gaasenbeek, J. Mesirov, H. Coller, M. Loh, J. Downing, and M. Caligiuri (1999), Molecular classification of cancer: Class discovery and class prediction by gene expression monitoring. *Science* 286:531536–531536.
- [4] I. Guyon, J. Weston, S. Barnhill, and V. Vapnik (2002), Gene selection for cancer classification using support vector machines. *Machine Learning* 46:389–422.
- [5] B. W. Higgs, J. Weller, and J. L. Solka (2006). Spectral embedding finds meaningful (relevant) structure in image and microarray data. *BMC Bioinformatics* 7(74):1–13.
- [6] O. Kouropteva, O. Okun, and M. Pietikainen (2002), Selection of the optimal parameter value for the linear embedding algorithm. In *Proc. of the 1st International Conference on Fuzzy Systems and Knowledge Discovery* pages 359–363.
- [7] R. V. N. Melnik (2000), Topological analysis of eigenvalues in engineering computations. *Engineering Computations* 17(4):386–416.
- [8] S. T. Roweis and L. K. Saul (2000), Nonlinear dimensionality reduction by locally linear embedding. *Science* 290:2323–2326.
- [9] L. Saul and S. Roweis (2001), An introduction to locally linear embedding. Paper located at <http://www.cs.toronto.edu/~roweis/lle/publications.html>
- [10] L. K. Saul and S. T. Roweis (2003), Think globally, fit locally: Unsupervised learning of low dimensional manifolds. *Journal of Machine Learning Research* 4:119–155.
- [11] M. Shena, D. Shalon, R. Heller, A. Chai, P. O. Brown, and R. W. Davis (1996), Parallel human genome analysis: Microarray-based expression monitoring of 1000 genes. In *Proc. Nat. Acad. Sci.* Volume 93, pages 10615–10619. National Academy of Sciences.
- [12] J. Shawe-Taylor and N. Cristianini (2006), *Kernel Methods for Pattern Analysis*. Cambridge University Press.
- [13] M. Shena, D. Shalon, R. W. Davis, and P. O. Brown (1995), Quantitative monitoring of gene expression patterns with complimentary DNA microarray. *Science* 270:467–470.
- [14] R. Tibshirani, T. Hastie, B. Narasimhan, and G. Chu (2002), Diagnosis of multiple cancer types by shrunken centroids of gene expression. In *Proc. Nat. Acad. Sci.* volume 99, pages 6567–6572. National Academy of Sciences.
- [15] C. Varini, A. Degenhard, and T. W. Nattkemper (2006), ISOLLE: LLE with geodesic distance. *Neurocomputing* 69:1768–1771.
- [16] J. Zhu and T. Hastie (2004), Classification of gene microarrays by penalized logistic regression. *Information Processing Systems* 14:427–443.

Incorporating Estimation Error into Optimal Portfolio Allocation

Problem Presenter: Scott Warlow (Manulife)

Academic Participants: David Cottrell (McGill University), Huaxiong Huang (York University), Nilima Nigam (McGill University), Christopher Raymond (New Jersey Institute of Technology), Thomas Salisbury (The Fields Institute and York University), Olga Trichtchenko (McGill University)

Report prepared by: David Cottrell, Huaxiong Huang¹, Nilima Nigam

1 Problem description

In this report, we consider the problem concerned with incorporating estimation error into optimal consumption and portfolio selection in continuous time. The original optimal consumption and asset allocation problem in continuous time was solved by Merton in a series of papers [4, 5] and became widely known as “Merton’s Problem”. Merton made the assumption that the asset price processes $\{S_i\}_{i=1}^N$ are given by Geometric Brownian Motion (GBM), where the parameter values are known. He was able to prove that the investment opportunity set can be generated by two portfolios or mutual funds of assets, which themselves obey Geometric Brownian Motion. This result is sometimes known as a two-fund separation theorem, and does not depend on the market being in equilibrium. Merton utilized the separation theorem in his development of the Inter-temporal Capital Asset Pricing Model in [6], but the mutual fund theorem is only dependent on the assumed properties of the asset price processes.

Subsequent work on this problem has sought to generalize Merton’s work in numerous ways. For instance, some authors have considered more general asset price processes than GBM, e.g. Ito processes with deterministic (and even stochastic) time-dependent drift and diffusion parameters, and other general diffusion and Markov processes, or general semi-martingales. In the latter case, the additional assumption that the market is complete (or more generally, effectively complete) is required, and the method of solution uses the so-called Cox-Huang-Pliska method [9], which involves the use of the Martingale Representation Theorem. Another generalization of the Merton problem involves the inclusion of

¹hhuang@yorku.ca

stochastic income for the investor, with various degrees of generality regarding the structure of the income process and transaction costs, and with investor preferences given by expected utility functions that are non-time-separable (e.g. recursive or stochastic differential utilities), or even non-expected utility preference orderings. However, most of the published work on the consumption/portfolio allocation problem in continuous time has assumed that the parameters of the asset price processes are known with perfect certainty [3, 2, 10, 8]. In reality, these parameters must be estimated, and there will always be some measure of estimation risk [8, 10].

The result of the unavoidable nature of estimation risk is that the optimized consumption/portfolio selection strategy will only truly be optimal in the unlikely event that there is no estimation error; in all other cases, it will be suboptimal. The goal of the workshop is to formulate the optimal consumption and portfolio investment problem such that, given any data sample of the asset price processes, we have a prescription that associates to that sample an optimal strategy; note that this prescription is dynamic, since the sample will enlarge over time, likely resulting in a different optimal strategy from the previous one, going forward. To eliminate unnecessary complications, it would be easiest to work within the original Merton model, except that we wish to consider the case that investors do derive benefit from end-of-period wealth (instead of the overall consumption), and investor wealth is constrained to be nonnegative.

2 Mathematical models

To address the issue related to estimation error and investment strategies, we recall the Merton framework of optimal asset allocation in continuous time. To simplify the discussion, we consider only asset allocation and ignore consumption in this report. Following Merton's approach [4, 5], we assume that

- we have an initial wealth w_0 at time t_0 ;
- we can choose a combination of one risky asset (S_t) and one risk-free asset (R_t), e.g. a bond;
- S_t follows the GBM

$$\frac{S_t}{S_0} = \exp \left[\left(\mu - \frac{\sigma^2}{2} \right) t + \sigma B_t \right] \quad (2.1)$$

with drift μ and volatility σ ;

- the risk-free asset has a rate of return r , and is given by

$$\frac{R_t}{R_0} = \exp(rt). \quad (2.2)$$

Let π_t be a fraction of wealth allocated to S_t such that the utility of wealth is maximized at the end of a fixed period, i.e.,

$$J = \max_{\pi_t} \mathbb{E} [u(W_T) | \mathcal{F}_t], \quad (2.3)$$

where $u(\cdot)$ is a (convex) utility function and the wealth of the portfolio is given by

$$W_t = \pi_t \frac{W_t}{S_t} dS_t + (1 - \pi_t) \frac{W_t}{R_t} dR_t. \quad (2.4)$$

With the assumption that the parameters μ and σ are known with certainty, Merton [4, 5] obtained analytical expressions for the dynamic allocation strategy, π_t when the utility

function takes certain forms. For example, when

$$u(w) = \frac{w^p}{p}, \quad p < 1, \quad (2.5)$$

the optimal allocation is given by

$$\pi_t = \frac{\mu - r}{(1 - p)\sigma^2}, \quad (2.6)$$

and the value function is given as

$$J = \frac{W^p}{p}V, \quad (2.7)$$

where

$$V = \exp \left[\left(pr + \frac{p(\mu - r)^2}{2(1 - p)\sigma^2} \right) (T - t) \right]. \quad (2.8)$$

2.1 Asset allocation under estimation error. During the workshop, we decided to approach the problem as follows. We assume that the risky asset follows the stochastic equation (2.1), where the return of the asset is given by

$$\mu = \mu_0 + \sigma_0 U, \quad (2.9)$$

where $U \sim N(0, 1)$. Solving the asset equation (2.1) yields

$$\frac{S_t}{S_0} = \exp \left[\left(\mu_0 - \frac{\sigma^2}{2} \right) t + \sigma X_t \right], \quad (2.10a)$$

where

$$X_t = aUt + B_t, \quad a = \frac{\sigma_0}{\sigma}. \quad (2.10b)$$

We now write

$$dX_t = H_t dt + K_t dZ_t, \quad (2.11a)$$

where Z_t is a Brownian motion with respect to the same filtration as the asset S_t . It can be shown that

$$H_t = ag_t X_t, \quad K_t = 1, \quad (2.11b)$$

where

$$g_t = \frac{a}{1 + a^2 t}. \quad (2.11c)$$

Thus,

$$dX_t = ag_t X_t dt + dZ_t.$$

Applying Ito's lemma, we can rewrite the process for the risky asset in terms of the observable parameters:

$$\frac{dS_t}{S_t} = (\mu_0 + \sigma ag_t X_t) dt + \sigma dZ_t. \quad (2.12)$$

Therefore, the wealth process can now be written as

$$\frac{dW_t}{W_t} = [r + \pi_t(\mu_0 + \sigma ag_t X_t - r)] dt + \pi_t \sigma dZ_t. \quad (2.13)$$

We now write the value function defined in (2.3) as $J = J(W_t, X_t, t)$, and apply Ito's lemma (note J is a martingale when we use the optimal allocation strategy) to obtain

$$dJ = (J_t + \mathcal{A}_t J) dt + J_w dW_t + J_x dX_t, \quad (2.14a)$$

with

$$\mathcal{A}_t J = \frac{1}{2} J_{xx} + \frac{\pi_t^2}{2} \sigma^2 w^2 J_{ww} + \pi_t \sigma w J_{wx}. \quad (2.14b)$$

Because J is a martingale, we have $J_t + \mathcal{A}_t J = 0$ when π_t is optimal; or

$$J_t + \frac{1}{2} J_{xx} + r w J_w + a g_t x J_x + \frac{1}{2} \pi_t^2 \sigma^2 w^2 J_{ww} + \pi_t [(\mu_0 + a \sigma g_t x - r) w J_w + \sigma w J_{wx}] = 0, \quad (2.15)$$

with $J(w, x, T) = u(w)$. Using the constant relative risk aversion (CRRA) utility $u(w) = w^p/p$, and assuming $J = V(x, t)u(w)$, we obtain the following Hamilton-Jacobi-Bellman (HJB) equation for V :

$$\begin{aligned} V_t + \frac{1}{2} V_{xx} + a g_t x V_x + p r V \\ + \max_{\pi_t} \left\{ \frac{p(p-1)}{2} \pi_t^2 \sigma^2 V + p \pi_t [(\mu_0 + \sigma a g_t x - r) V + \sigma V_x] \right\} = 0 \end{aligned} \quad (2.16)$$

for $p > 0$, and

$$\begin{aligned} V_t + \frac{1}{2} V_{xx} + a g_t x V_x + p r V \\ + \min_{\pi_t} \left\{ \frac{p(p-1)}{2} \pi_t^2 \sigma^2 V + p \pi_t [(\mu_0 + \sigma a g_t x - r) V + \sigma V_x] \right\} = 0 \end{aligned} \quad (2.17)$$

for $p < 0$. The terminal condition is $V(x, T) = 1$. The allocation strategy is given by the first order condition

$$\pi_t^* = \frac{\mu_0 + a \sigma g_t x - r}{(1-p)\sigma^2} + \frac{V_x}{(1-p)\sigma V}. \quad (2.18)$$

The first order condition is only the necessary condition for optimality. Applying the second order condition yields

$$p(1-p)\sigma^2 V < 0, \quad \text{for } p > 0; \quad \text{and} \quad p(1-p)\sigma^2 V > 0, \quad \text{for } p < 0. \quad (2.19)$$

Because $V > 0$ and $p < 1$, this condition is satisfied for both positive and negative values of p .

2.2 An alternative formulation. One approach to incorporate estimation error is to treat the problem as an optimal asset allocation problem with learning. In [1], Brennan analyzes the effect of uncertainty about the mean return on the risky asset on the portfolio decision, while assuming the volatility is a known constant. To be more specific, he assumes that the change in the conditional expectation of the stock return is given by

$$dm = \frac{v_t}{\sigma^2} \left(\frac{dS}{S} - m dt \right), \quad (2.20)$$

where the conditional variance, v_t , is determined by its initial value v_0 and the differential equation

$$dv_t = -\frac{v_t^2}{\sigma^2} dt. \quad (2.21)$$

We can solve for the conditional variance to get

$$v_t = \frac{v_0 \sigma^2}{v_0(t - t_0) + \sigma^2}. \quad (2.22)$$

Using Bellman's principle, under the optimal allocation policy, we have $\mathbb{E}[dJ] = 0$, which leads to the following Hamilton-Jacobi-Bellman (HJB) equation (after applying Ito's lemma):

$$J_t + rwJ_w + \frac{v^2}{2\sigma^2}J_{mm} + \max_{\pi_t} \left[\pi_t(m-r)wJ_w + \pi_tvJ_{wm} + \frac{1}{2}(\pi_t\sigma w)^2J_{ww} \right] = 0, \quad (2.23)$$

with terminal condition $J(w, m, T) = w^p/p$. If we assume $J = Vw^p/p$, (2.23) can be further simplified as

$$V_t + rpV + \frac{v^2}{2\sigma^2}V_{mm} + \max_{\pi_t} p \left[\pi_t(m-r)V + \pi_tvV_m + \frac{p-1}{2}(\pi_t\sigma)^2V \right] = 0 \quad (2.24)$$

for $p > 0$ and

$$V_t + rpV + \frac{v^2}{2\sigma^2}V_{mm} + \min_{\pi_t} p \left[\pi_t(m-r)V + \pi_tvV_m + \frac{p-1}{2}(\pi_t\sigma)^2V \right] = 0 \quad (2.25)$$

for $p < 0$. The terminal condition now becomes $V(m, T) = 1$.

Once again, the optimal allocation strategy is given by the first order condition

$$\pi_t^* = \frac{m-r}{(1-p)\sigma^2} + \frac{vV_m}{(1-p)\sigma^2V}. \quad (2.26)$$

Note that π_t^* consists of two terms where the first term, denoted by π_t^m , corresponds to the ad hoc strategy in which Merton's formula is used by replacing μ with m . Note that the Merton's formula should only be applicable when there is no uncertainty, in which case the initially estimated return m_0 is used. The second term in (2.26) is the "correction" due to learning. This correction reflects how well the ad hoc strategy approximates the true strategy.

2.3 Relationship between the two formulations. We now show that the two approaches described above are equivalent. Note that the two variables m of (2.23) and x of (2.16) are related by the following equation

$$m = \mu_0 + \sigma ag_t x = m_0 + \sigma_0 g_t x. \quad (2.27)$$

Treating (2.27) as a coordinate transformation, and using simple straightforward calculations, we have the following:

$$V_t|_x = V_t|_m + V_m \frac{\partial m}{\partial t} = V_t + \sigma ag'_t x V_m, \quad (2.28a)$$

$$V_x = V_m \frac{\partial m}{\partial x} = \sigma ag_t V_m, \quad (2.28b)$$

$$V_{xx} = (\sigma ag_t)^2 V_{mm}. \quad (2.28c)$$

Substituting these equations into the HJB equation (2.16) (with π_t the optimal strategy), we obtain

$$\begin{aligned} V_t + \frac{1}{2}(\sigma ag_t)^2 V_{mm} + [\sigma a^2 g_t^2 x + p\sigma^2 ag_t \pi_t + \sigma ag'_t x] V_m \\ + p \left[r + \pi_t(\mu_0 + \sigma ag_t x - r) + \frac{p-1}{2}\sigma^2 \pi_t^2 \right] V = 0. \end{aligned} \quad (2.29)$$

Using (2.11c), we have $g' = -ag_t^2$. Noting that $v_0 = \sigma_0^2$, we obtain

$$\sigma ag_t = \frac{\sigma a^2}{a^2 t + 1} = \frac{\sigma \sigma_0^2}{\sigma_0^2 t + \sigma^2} = \frac{\sigma v_0}{v_0 t + \sigma^2} = \frac{v}{\sigma},$$

and (2.29) becomes

$$V_t + \frac{v^2}{2\sigma^2} V_{mm} + pv\pi_t V_m + p \left[r + \pi_t(m - r) + \frac{p-1}{2} \sigma^2 \pi_t^2 \right] V = 0, \quad (2.30)$$

which is the same as (2.31) derived by Brennan [1] when π_t is optimal.

Remark 2.1 In [1], the HJB equation is solved directly using a finite difference method. In this report, we will present a more efficient method, which reduces the problem to solving a system of ordinary differential equations instead of the highly nonlinear partial differential HJB equation. We will also extend the model by including constraints on the allocation strategy. In practise, there are often restrictions on short selling of the risky asset as well as on the amount one can borrow. Therefore, we will impose a constraint on borrowing as well as on short-selling by considering portfolio strategies in a bounded region, i.e., $0 \leq \pi_t \leq 1$. Finally, learning, as well as portfolio selection, are carried out in discrete time. Therefore, it is of practical interest to study the problem under discrete time settings. We will present the continuous time approach first, and defer discussion of the discrete time approach to later in the report.

2.4 Asset allocation under estimation error and borrowing constraints. It is straightforward to implement the constraint $0 \leq \pi_t \leq 1$. Bellman's principle applies in a similar fashion and the simplified HJB equation can be written as

$$V_t + rpV + \frac{v^2}{2\sigma^2} V_{mm} + \max_{0 \leq \pi_t \leq 1} p \left[\pi_t(m - r)V + \pi_t v V_m + \frac{p-1}{2} (\pi_t \sigma)^2 V \right] = 0, \quad (2.31)$$

where the value function is $J = Vw^p/p$, and the terminal condition is also the same $V(m, T) = 1$. We have implicitly assumed that $p > 0$. Otherwise, we take the minimum instead of the maximum.

The asset allocation strategy can be obtained by applying the first order condition to (2.31), which is

$$\pi_t = \max\{0, \min\{1, \pi_t^*\}\}, \quad \pi_t^* = \frac{m - r}{(1 - p)\sigma^2} + \frac{vV_m}{(1 - p)\sigma^2 V}. \quad (2.32)$$

3 Solution methodologies

In this report we discuss two methods for solving the HJB equation: direct numerical method and a dimension reduction technique.

3.1 Numerical method for solving the Hamilton-Jacobi-Bellman (HJB) equation. For simplicity, instead of solving (2.16) or (2.17) backwards in time from terminal time T , we introduce the following change of variable:

$$s = T - t, V(x, t) \longrightarrow V(x, s), g_t \longrightarrow g_s = \frac{a}{1 + a^2(T - s)}.$$

We thus get an initial value problem for V :

$$V_s = \frac{1}{2} V_{xx} + [p\pi_s \sigma + ag_s x] V_x + p \max_{\pi_s} \left[r + \pi_s (\mu_0 + \sigma ag_s x - r) + \frac{(p-1)\pi_s^2 \sigma^2}{2} \right], \quad (3.1)$$

with initial condition $V(x, 0) = 1$. In this case, using the first order condition, the optimal allocation strategy (unconstrained) is

$$\pi_s = \frac{\mu_0 + \sigma a g_s x - r}{(1-p)\sigma^2} + \frac{V_x}{(1-p)\sigma V}, \quad (3.2)$$

with constraints $0 \leq \pi_s \leq 1$.

At this juncture, we must fully specify the conditions on V for large x . Because the partial differential equation (PDE) is defined for $x \in \mathbb{R}$, we need to truncate the computational region to $x \in [-X_{max}, X_{max}]$. This requires us to impose boundary conditions at the endpoint $\pm X_{max}$. Assuming that for large x , the solution V behaves like the Merton solution $V \sim \exp(sp[r + (\mu_0 - r)^2 / (2(1-p)\sigma^2)])$, we shall impose the time-varying Robin conditions

$$V_x = \frac{p(x-r)s}{(1-p)\sigma^2} V, \quad x = \pm X_{max}. \quad (3.3)$$

Even though other choices of numerical boundary conditions are possible, we will provide more insights in Section 3.2 to show that (3.3) is probably the best choice.

A few qualitative comments are in order. First, the same method can be applied to (2.24) or (2.25). Second, the constrained problem can be solved similarly. In all the cases, the PDE is highly nonlinear. However, one may naively expect that the linear diffusive term will ameliorate numerical difficulties, as long as p is much smaller than 0. This observation motivates the choice of the method of lines for discretizing the PDE.

In the x direction, we pick a mesh size $h \ll 1$, and define a uniform grid $\{x_i\}_{i=1}^N$ on $[-X_{max}, X_{max}]$. We use a centred difference scheme to evaluate both the first and second ‘‘spatial’’ derivatives, taking care to incorporate the Robin condition specified above. The resulting nonlinear system of ordinary differential equations (ODEs) is solved using a built-in Matlab routine.

3.2 A dimension reduction solution method. Even though we could apply the numerical method directly to the HJB equations, as in [1] for the unconstrained case, we are able to find a semi-analytic method that gives more insight into the solution behaviour. In addition it is much more efficient and avoids the problem of seeking artificial boundary conditions. Motivated by the Merton solution (2.8), we seek the solution in the following form

$$V = \exp[\alpha(t)(m-r)^2 + \beta(t)(m-r) + \gamma(t)], \quad (3.4a)$$

where α , β and γ are functions of t . It is a simply calculation to verify from (3.4a) that

$$V_t = \left[\dot{\alpha}(m-r)^2 + \dot{\beta}(m-r) + \dot{\gamma} \right] V, \quad (3.4b)$$

$$V_m = [2\alpha(m-r) + \beta] V, \quad (3.4c)$$

$$V_{mm} = \left[2\alpha + (2\alpha(m-r) + \beta)^2 \right] V, \quad (3.4d)$$

where the dots denote the derivative with respect to time.

3.2.1 Optimal allocation strategy. Using (3.4a)–(3.4d), the optimal allocation becomes

$$\pi_t^* = \frac{2\alpha v + 1}{(1-p)\sigma^2} (m-r) + \frac{\beta v}{(1-p)\sigma^2}. \quad (3.5)$$

Substituting (3.4b)-(3.5) into (2.24) and rearranging the terms, we obtain

$$\dot{\alpha} + \frac{2v^2}{\sigma^2}\alpha^2 + \frac{p}{2(1-p)\sigma^2}(1+2\alpha v)^2 = 0, \quad (3.6a)$$

$$\dot{\beta} = 0, \quad (3.6b)$$

$$\dot{\gamma} + rp + \left(\frac{v}{\sigma}\right)^2 \alpha = 0, \quad (3.6c)$$

subject to

$$\alpha(T) = \beta(T) = \gamma(T) = 0. \quad (3.6d)$$

We note immediately in this case that $\beta \equiv 0$. Thus the optimal allocation strategy becomes

$$\pi_t^* = \frac{2\alpha v + 1}{(1-p)\sigma^2}(m-r), \quad (3.7)$$

and the problem at hand becomes extremely simple: in order to find the optimal allocation strategy, we only need to solve (3.6a), an *ordinary differential equation* (ODE) instead of the full HJB equation. Furthermore, the optimal asset allocation strategy is a *linear* function of m . Because the Merton solution is

$$\pi_t^m = \frac{m-r}{(1-p)\sigma^2}, \quad (3.8)$$

the difference between the current strategy and the Merton solution is also a linear function of m , i.e.,

$$\Delta\pi_t = \frac{2\alpha v}{(1-p)\sigma^2}(m-r). \quad (3.9)$$

We note that the value of γ has no effect on the allocation strategy, and its value is only needed if we want to compute the value function V (or J). The value function defined in (3.4a) becomes

$$V = \exp[\alpha(t)(m-r)^2 + \gamma(t)], \quad (3.10)$$

which takes a similar form as the original Merton solution (2.8). Furthermore, when $v \ll \sigma$ and $v \ll 1$, (3.6a) and (3.6c) can be approximated by

$$\dot{\alpha} + \frac{p}{2(1-p)\sigma^2} = 0, \quad (3.11a)$$

$$\dot{\gamma} + rp = 0. \quad (3.11b)$$

In this case we recover the Merton solution. This explains that the numerical boundary condition (3.3) is indeed a very good choice.

Finally, we note that there is a difference between the Merton strategy (where m is a constant) and the Merton's solution. If we use Merton's solution as an allocation strategy for stochastic return, we would be using the *ad hoc* strategy, and the solution of the value function could also be obtained using a similar approach, which is shown below.

3.2.2 Solution using the ad hoc strategy. When the ad hoc strategy

$$\pi_t^m = \frac{m-r}{(1-p)\sigma^2} \quad (3.12)$$

is used, the HJB equation (2.31) can also be simplified by substituting (3.4b)-(3.4d) and (3.12) into (2.31). In this case, we need to solve the following system of three ODEs

$$\dot{\alpha} + \frac{2v^2}{\sigma^2}\alpha^2 + \frac{1 + 4v\alpha}{2(1-p)\sigma^2} = 0, \quad (3.13a)$$

$$\dot{\beta} + 2\left(\frac{v}{\sigma}\right)^2\alpha\beta + \frac{pv\beta}{(1-p)\sigma^2} = 0, \quad (3.13b)$$

$$\dot{\gamma} + rp + \left(\frac{v}{\sigma}\right)^2\left(\alpha + \frac{\beta}{2}\right) = 0, \quad (3.13c)$$

subject to

$$\alpha(T) = \beta(T) = \gamma(T) = 0. \quad (3.13d)$$

Note that from (3.13b) and $\beta(T) = 0$, we have $\beta \equiv 0$. As a consequence, the equation for γ is the same as (3.6c). Compared with the solution using optimal allocation, the solution using the ad hoc strategy takes a similar form with minor differences, reflected in the equations for α . The difference in the equations for α in the two equations (3.6a) and (3.13a) is $2v^2\alpha^2/(1-p)\sigma^2$. Since $(v/\sigma)^2$ is normally small, the difference in the solution is also small except when α is large.

Remark 3.1 For the unconstrained case, the solution methodology used here is very effective and provides insights into the behaviour of the solution. It also gives justification for the boundary conditions when numerical methods are applied directly to the HJB equation. However, for the optimal allocation with constraints, the methodology is not applicable in general, despite the fact that similar procedure can be applied to $\pi_t = 0$ or 1 separately. It is possible that approximate solutions can be found under special circumstances, such as when $v/\sigma \ll 1$ and $v \ll 1$. Since we can solve the HJB with constraints using the finite difference method, we will not discuss it any further in this report.

4 Numerical experiments

4.1 Outline. We now describe some numerical experiments and our investigations include:

- The allocation strategy in the presence of uncertainty in the parameters, but without constraints on the allocation (Brennan's approach);
- The allocation strategy with constraints;
- A comparison of the actual allocation strategy to the "ad hoc" strategy obtained by simply replacing $\mu = m = \mu_0 + \sigma a g_t x$ in the Merton solution, i.e. using

$$\pi_t^m = \frac{m - r}{(1-p)\sigma^2} = \frac{\mu_0 + a\sigma g_t x - r}{(1-p)\sigma^2};$$

- Computations using the simpler dimension reduction formulation when applicable.

4.2 Results. In order to compare with the results presented by Brennan [1], in this section we make the following choices for parameters:

- Rate of return on risk-free asset $r = 5\%$;
- Volatility of the market $\sigma = 20.2\%$;
- Initial mean return of the risky asset $\mu_0 = 13\%$;
- Variance around the mean return $v_0 = 0.0243^2$;
- Risk aversion parameter $p = -2$ and $p = 0.2$;
- Time horizon $T = 5$ and $T = 20$;

- Size of the computational domain for HJB is set to be $X_{max} = 0.5$ (or $m_{max} = 0.5$ when Brennan's formulation is used).

Table 1 Comparisons of the optimal allocations obtained by solving the HJB, using the dimension reduction technique as well from the case with constraint. The results from Brennan [1] are also presented.

	p	T	σ	π_t^*	π_t^m	$\pi_t^m - \pi_t^*$
HJB (2.24)	-2	5	0.202	0.6236	0.6535	0.02995
Brennan [1]				0.624	0.654	0.030
Dimension reduction (3.5)-(3.6c)				0.6235	0.6535	0.03007
HJB (2.31)				0.6236	0.6535	0.02995
HJB (2.24)	-2	20	0.202	0.5497	0.6535	0.1039
Brennan [1]				0.551	0.654	0.103
Dimension reduction (3.5)-(3.6c)				0.5478	0.6535	0.1039
HJB (2.31)				0.5497	0.6535	0.1039
HJB (2.25)	0.2	5	0.202	2.4960	2.4507	-0.0453
Brennan [1]				2.495	2.451	-0.044
Dimension reduction (3.5)-(3.6c)				2.4959	2.4507	-0.0451
HJB (2.31)				1	2.4517	1.4507
HJB (2.25)	0.2	20	0.202	2.6449	2.4507	-0.1941
Brennan [1]				2.643	2.451	-0.192
Dimension reduction (3.5)-(3.6c)				2.6419	2.4507	-0.1997
HJB (2.31)				1	2.4507	1.4507

In Table 1, we have presented the results obtained using the finite difference method for HJB equations (2.24) and (2.25), the dimension reduction method, and those from Brennan [1]. We have also presented the results for the constrained allocation case, obtained by solving the HJB equation (2.31) by finite difference method. It can be seen that all the results for the unconstrained case agree with each other. It is interesting to note that when the constraint is not active, the values of the optimal allocation stay unchanged. As pointed by in [1], the correction to the ad hoc strategy is positive for $p > 0$ and negative for $p < 0$, under economic viable conditions. This can also be explained by the sign of α in the dimension reduction solution. Because the correction is given by

$$\frac{2\alpha v}{(1-p)\sigma^2}(m-r),$$

and $v > 0$ and $p < 1$, the sign of the correction is determined by the sign of α for $m > r$ ("economically viable"). The sign of α , on the other hand, is the same as p , which can be seen clearly from (3.6a), when $v/\sigma \ll 1$, as is the case here. In Figure 1, the numerically computed values of α and γ are given for the optimal allocation (both exact and approximated) and the ad hoc allocation strategies. We can see from the graphs that the difference between the optimal and ad hoc strategies is small. The approximation (Merton's solution) is reasonably close to the exact value of α . We also present the numerically computed value functions in Figure 2. Finally, the optimal allocation π_t^* at $t = 0$ is given in Figure 3. Linear variation with m is apparent in all cases, even for the constrained problem when the constraints are not active.

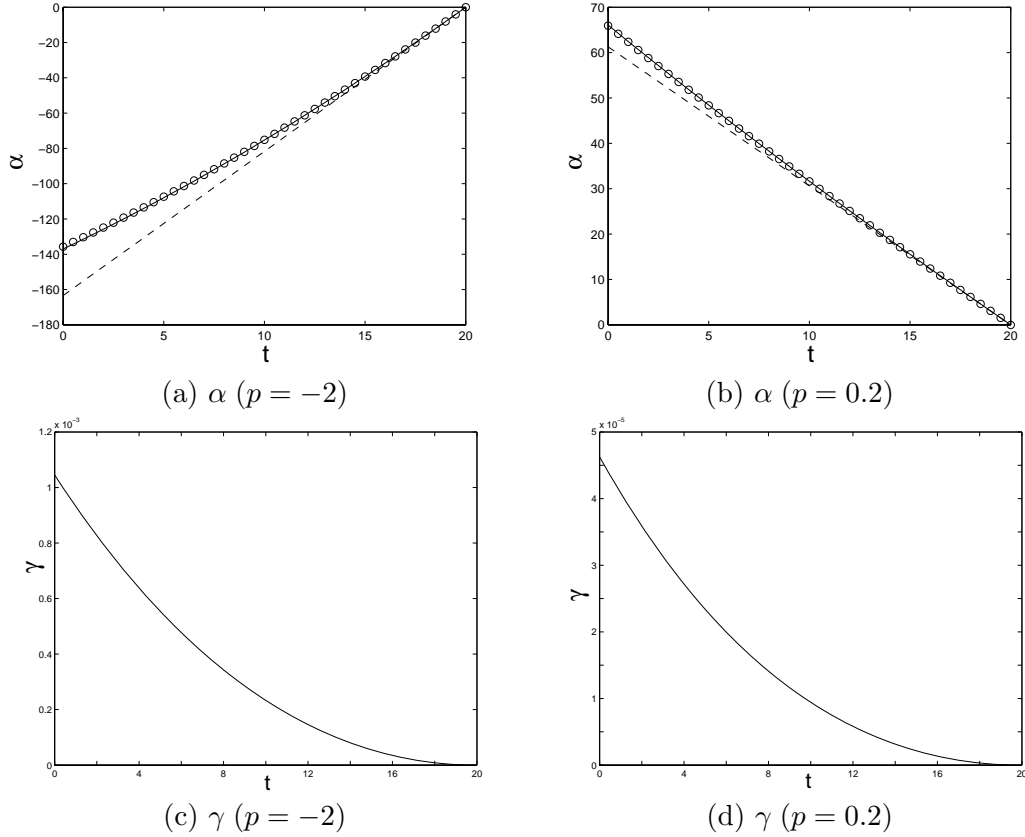


Figure 1 Numerically computed values of α and γ , using (3.6a) and (3.6c). The solid line corresponds to the optimal allocation and the circles are for the ad hoc allocation. The dashed line is from the approximation of the optimal allocation (Merton’s solution).

5 Discrete time model

In this section we describe a time-discrete formulation of the asset allocation problem with learning. This is a more realistic approach in the sense that both market transactions and learning occur in discrete time intervals (rather than continuously).

5.1 Illustration A: one period. Consider a market consisting of one risky asset S_t and a bond R_t . The prices can be written as (with respect to the ‘full’ sigma field \mathcal{G}_t)

$$\begin{cases} dS_t = \mu S_t dt + \sigma S_t dZ_t \\ dR_t = r R_t dt \end{cases} \Rightarrow \begin{cases} S_t = S_0 e^{(\mu - \frac{1}{2}\sigma^2)t + \sigma Z_t} \\ R_t = R_0 e^{rt} \end{cases}$$

where we take μ to be Gaussian with mean μ_0 and standard deviation σ_0 . With respect to the sigma field generated by the market up to time t_0 , $\mathcal{F}_{t_0} = \sigma\{S_k, k < t_0\}$, the price of the stock can then be written

$$S_t = S_{t_0} e^{(\mu_0 - \frac{1}{2}\sigma^2)(t-t_0) + \sigma(X_t - X_{t_0})},$$

where

$$X_t = X_0 + \frac{\sigma_0}{\sigma} tU + Z_t, \quad U \sim \mathcal{U}(0, 1).$$

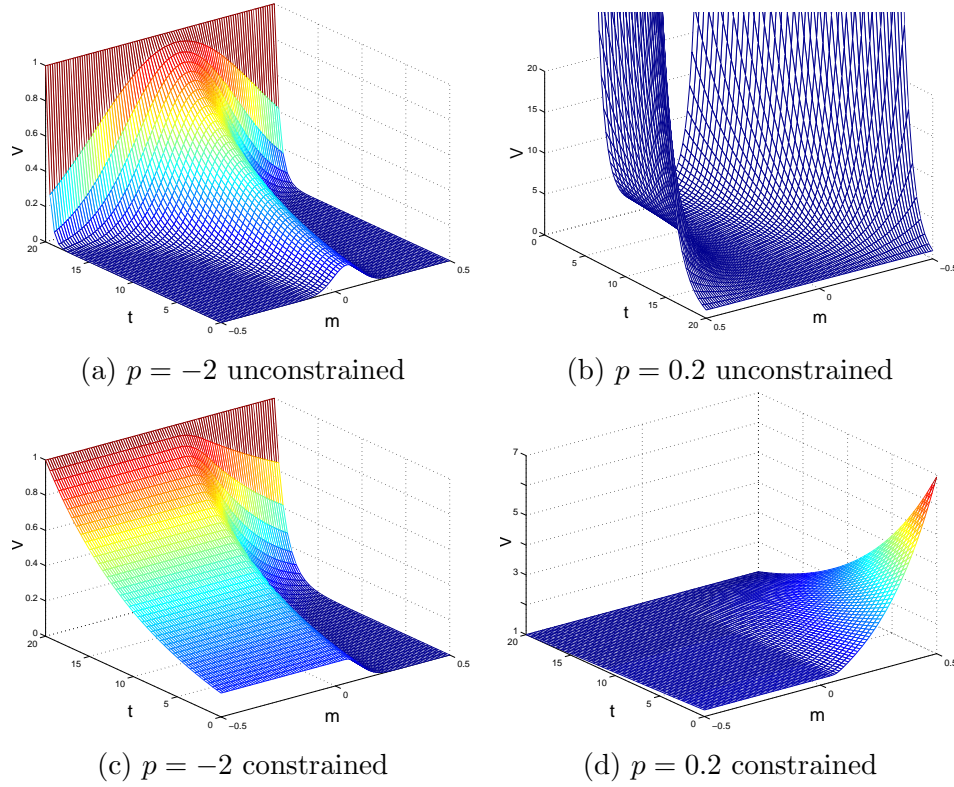


Figure 2 Numerically computed value function V , using (2.24) and (2.25).

We now consider the discrete time one period portfolio allocation problem. Let us assume $t_0 = 0$ and $(t - t_0) = 1$. The total wealth after investing in the market for one period with a strategy given by the *starting* strategy π_0 will be

$$W_1 = W_0 \left(\pi_0 \frac{S_1}{S_0} + (1 - \pi_0) \frac{R_1}{R_0} \right).$$

The goal of the investor is to maximize the expectation of the utility of wealth

$$V(\pi_0, W_0, t_0) = \mathbb{E}(U(W_1)|\mathcal{F}_0).$$

If we take a linear utility function, $U(x) = x$, we can easily calculate the expectation and solve the maximizing problem explicitly:

$$\begin{aligned} V(\pi_0, W_0, t_0) &= \mathbb{E}(W_1|\mathcal{F}_0) \\ &= W_0 \mathbb{E} \left(\pi_0 e^{\mu_0 - \frac{1}{2}\sigma^2 + \sigma(X_1 - X_0)} + (1 - \pi_0)e^r \right) \\ &= W_0 \left(\pi_0 \left(e^{\mu_0 + \frac{1}{2}\sigma_0^2} - e^r \right) + e^r \right) \\ &= W_0 \frac{1}{2\pi} \int \left[\pi \exp \left(\mu_0 - \frac{1}{2}\sigma^2 - \frac{-X^2 - 2\hat{\sigma}^2 X + \hat{\sigma}^4}{2\hat{\sigma}^2} + \frac{\hat{\sigma}^2}{2} \right) \right. \\ &\quad \left. + (1 - \pi) \exp \left(r - \frac{X^2}{2\hat{\sigma}^2} \right) \right] dX. \end{aligned}$$

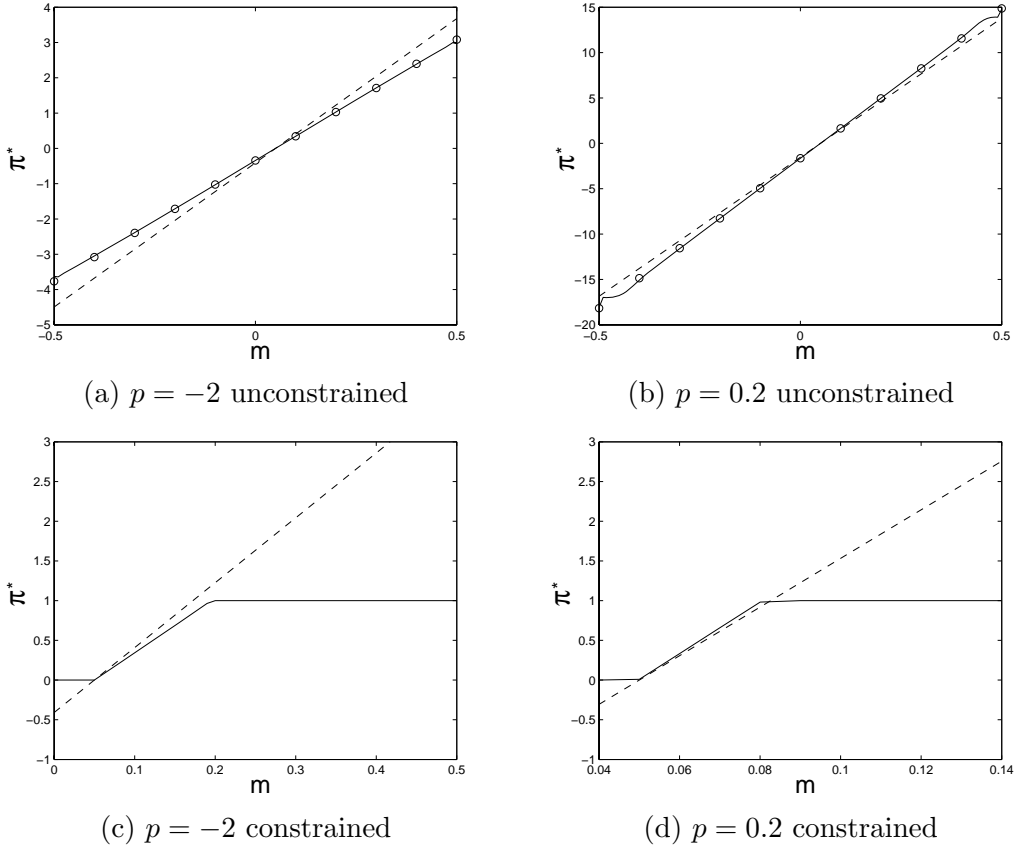


Figure 3 Numerically computed values of optimal allocation π_t^* at $t = 0$. The solid line is the solution by solving the HJB equation using finite difference method, the dashed line is the ad hoc strategy, and the circles are the solution using the dimension reduction method.

Here X is a normally distributed random variable with mean zero and standard deviation $\hat{\sigma} = \sqrt{\sigma^2 + \sigma_0^2}$. V is maximized with the allocation strategy

$$\pi_0 = \begin{cases} 0 & \text{if } \mu_0 + \frac{1}{2}\sigma_0^2 < r, \\ 1 & \text{if } \mu_0 + \frac{1}{2}\sigma_0^2 > r, \end{cases}$$

and the investor is indifferent if $\mu_0 + \sigma_0^2/2 = r$. In other words, the allocation strategy is determined by the relation of the uncertainty in the market parameter μ , and *not* on the standard deviation σ of the stock. This is to be contrasted to the result for the optimal allocation problem with deterministic μ , where the optimal strategy π_0 is

$$\pi_0 = \begin{cases} 0 & \text{if } \mu + \frac{1}{2}\sigma^2 < r, \\ 1 & \text{if } \mu + \frac{1}{2}\sigma^2 > r. \end{cases}$$

5.2 Illustration B: two periods. Now consider investing in the same market for two investment periods. The investor must make two allocation decisions represented by π_0 and

π_1 (at time 0 and 1 respectively). The problem facing the investor can be phrased

$$\max_{(\pi_0, \pi_1)} \mathbb{E}(U(W_2)|\mathcal{F}_0), \quad W_2 = W_1 \left(\pi_1 \frac{S_2}{S_1} + (1 - \pi_1) \frac{R_2}{R_1} \right).$$

The expectation can be rewritten

$$\begin{aligned} & \mathbb{E}(\mathbb{E}(W_2|\mathcal{F}_1)|\mathcal{F}_0) \\ &= \mathbb{E} \left[\mathbb{E} \left[W_0 \left(\pi_0 \frac{S_1}{S_0} + (1 - \pi_0) \frac{R_1}{R_0} \right) \left(\pi_1 \frac{S_2}{S_1} + (1 - \pi_1) \frac{R_2}{R_1} \right) \middle| \mathcal{F}_1 \right] \middle| \mathcal{F}_0 \right] \\ &= \mathbb{E} \left[W_0 \left(\pi_0 \frac{S_1}{S_0} + (1 - \pi_0) \frac{R_1}{R_0} \right) \left(\pi_1 \mathbb{E} \left(\frac{S_2}{S_1} \middle| \mathcal{F}_1 \right) + (1 - \pi_1) \frac{R_2}{R_1} \right) \middle| \mathcal{F}_0 \right] \\ &= W_0 \pi_0 \mathbb{E} \left(\pi_1 \frac{S_1}{S_0} \mathbb{E} \left(\frac{S_2}{S_1} \middle| \mathcal{F}_1 \right) \middle| \mathcal{F}_0 \right) + W_0 \pi_0 \frac{R_2}{R_1} \mathbb{E} \left((1 - \pi_1) \frac{S_1}{S_0} \middle| \mathcal{F}_0 \right) \\ &\quad + W_0 (1 - \pi_0) \frac{R_1}{R_0} \mathbb{E} \left(\pi_1 \mathbb{E} \left(\frac{S_2}{S_1} \middle| \mathcal{F}_1 \right) \middle| \mathcal{F}_0 \right) + W_0 (1 - \pi_0) \frac{R_2}{R_0} \mathbb{E} \left((1 - \pi_1) \middle| \mathcal{F}_0 \right). \end{aligned}$$

Writing out S_1 and S_2 explicitly in the above expression, we see that we only need to calculate

$$\mathbb{E} \left(\pi_1 \frac{S_1}{S_0} \mathbb{E} \left(\frac{S_2}{S_1} \middle| \mathcal{F}_1 \right) \middle| \mathcal{F}_0 \right), \quad (5.1)$$

$$\mathbb{E} \left((1 - \pi_1) \frac{S_1}{S_0} \middle| \mathcal{F}_0 \right), \quad (5.2)$$

$$\mathbb{E} \left(\pi_1 \mathbb{E} \left(\frac{S_2}{S_1} \middle| \mathcal{F}_1 \right) \middle| \mathcal{F}_0 \right), \quad (5.3)$$

$$\mathbb{E} [1 - \pi_1 | \mathcal{F}_0]. \quad (5.4)$$

Note that π_1 depends on the market σ field \mathcal{F}_1 (i.e. $\pi_1 = \pi_1(S_1)$) in an, as yet, undetermined way. To simplify these expectations as much as possible we note that with respect to \mathcal{F}_{t_0} , we have

$$dX_t = ag_t X_t dt + dZ_t, \quad a = \frac{\sigma_0}{\sigma}, \quad g_t = \frac{a}{a^2 t + 1}.$$

Thus, X_t with respect to \mathcal{F}_{t_0} is an Ornstein-Uhlenbeck process, and

$$X_t \sim \mathcal{N}(\mu_x(t_0, t), \sigma_x(t_0, t)^2) = \mathcal{N} \left(e^{\int_{t_0}^t ag_s ds} X_{t_0}, \int_{t_0}^t e^{2 \int_{t_0}^t ag_s ds} dt' \right). \quad (5.5)$$

We then have

$$\begin{aligned} \mathbb{E} \left[\frac{S_2}{S_1} \middle| \mathcal{F}_1 \right] &= e^{\mu_0 - \frac{1}{2} \sigma^2 - \sigma X_1} \mathbb{E} [e^{\sigma X_2} | \mathcal{F}_1] \\ &= e^{\mu_0 - \frac{1}{2} \sigma^2 + \sigma \mu_x(1,2) + \frac{1}{2} \sigma^2 \sigma_x(1,2)^2 - \sigma X_1}. \end{aligned}$$

The expectations (5.1), (5.2), (5.3), (5.4) then simplify to

$$\begin{aligned}\mathbb{E}(\pi_1 \frac{S_1}{S_0} \mathbb{E}(\frac{S_2}{S_1} | \mathcal{F}_1) | \mathcal{F}_0) &= \mathbb{E}(\pi_1 | \mathcal{F}_0) e^{2(\mu_0 - \frac{1}{2}\sigma^2) + \sigma\mu_x(1,2) + \frac{1}{2}\sigma^2\sigma_x(1,2)^2 - \sigma X_0}, \\ \mathbb{E}((1 - \pi_1) \frac{S_1}{S_0} | \mathcal{F}_0) &= \mathbb{E}((1 - \pi_1) e^{\sigma X_1} | \mathcal{F}_0) e^{\mu_0 - \frac{1}{2}\sigma^2 - \sigma X_0}, \\ \mathbb{E}(\pi_1 \mathbb{E}(\frac{S_2}{S_1} | \mathcal{F}_1) | \mathcal{F}_0) &= \mathbb{E}(\pi_1 e^{-\sigma X_1} | \mathcal{F}_0) e^{\mu_0 - \frac{1}{2}\sigma^2 + \sigma\mu_x(1,2) + \frac{1}{2}\sigma^2\sigma_x(1,2)^2}, \\ \mathbb{E}[1 - \pi_1 | \mathcal{F}_0] &= 1 - \mathbb{E}[\pi_1 | \mathcal{F}_0].\end{aligned}$$

In principle one could now attempt to solve the constrained optimization problem by setting up the Lagrangian and differentiating with respect to $\{\pi_1\}$, being careful about switching the order of expectation and differentiation. That is for each s we would need to set the derivative of the expected utility of wealth (E.U.W.) to zero. However, we can save a lot of effort by noting that the E.U.W. depends only linearly on $\{\pi_1\}$. This means that, once again, the optimal solution for each path $s = \{S_t, 0 \leq t \leq 1\}$ is either zero or one. Writing the E.U.W. as

$$\text{E.U.W.} = \mathbb{E}(A(X_1) + B(X_1)\pi_1(s) | \mathcal{F}_0),$$

we see that the optimal π_1 only depends on X_1 . Since π_1 can only depend on information derived from observables (S_t), we must build a ‘best inference’ of X_1 , say $\hat{X}_1(s)$, in order to estimate the sign of $B(X_1)$. Then the optimal investment decision for the second period would be

$$\pi_1^* = \begin{cases} 0 & \text{if } B(\hat{X}_1(s)) > 0, \\ 1 & \text{if } B(\hat{X}_1(s)) \leq 0. \end{cases}$$

5.3 A non-linear utility function. In researching the best possible utility function that describes investment portfolio strategies, a concave function of the form $u(W) = -e^{\frac{1}{\gamma}W_0}$, $\gamma > 0$, was found to capture the required behaviour [8] (p.419).

The solution to the one-step discrete model is already analytically not possible without making some approximations. The solution process is the following:

$$\begin{aligned}\max_{\{\pi\}} E[u(W_0) | \pi] &= \text{const} \int e^{-W_0 \frac{1}{\gamma} \pi e^{\mu - \frac{\sigma^2}{2} + \sigma z}} e^{-W_0 \frac{1}{\gamma} (1-\pi) e^r} e^{-\frac{z^2}{2}} dz \\ &\approx -\frac{1}{\gamma} e^{-\frac{1}{\gamma}(1-\pi)e^r} \pi e^{m\mu - \frac{1}{2}\sigma^2 + \frac{\sigma^2}{2}} + \frac{1}{\gamma^2} e^{-\frac{1}{\gamma}(1-\pi)e^r} \pi^2 e^{2\mu - \frac{\sigma^4}{4} + \sigma^2}.\end{aligned}$$

When the above is provided as input in Maple, the solution obtained is of the form

$$-\frac{1}{2}\gamma \left(-e^r + 2e^{\mu - \sigma^4/4 + \sigma^2} - \sqrt{e^{2r} + 4e^{2\mu - \sigma^4/2 + 2\sigma^2}} \right) e^{-\mu - r + \sigma^4/4 - \sigma^2}.$$

6 Conclusion

In this report, we investigate the impact of uncertainty in the market parameters to the optimal allocation problem. An alternative derivation to the one proposed by Brennan is presented. A dimension reduction solution is obtained by reducing the HJB equation into a system of simpler ODEs. Numerical results demonstrate the validity of these approaches, and the impact of the constraints on the allocation strategy is discussed. Discrete-time allocation models are also presented. To simplify the discussion, we focus on asset allocation

and do not consider consumption. The methodology that we present in this report can be extended to include consumption, which will be pursued in a future study.

Acknowledgements

We would like to thank Moshe Milevsky for helpful comments during the workshop.

References

- [1] Brennan, M. (1998), The Role of Learning in Dynamic Portfolio Decisions. *European Finance Review* 1: 295-306.
- [2] Karatzas, I. and S.E. Shreve (1998), *Methods of Mathematical Finance*, Springer, New York, NY.
- [3] Korn, R. (1997), *Optimal Portfolios: Stochastic Models for Optimal Investment and Risk Management in Continuous Time*, World Scientific, River Edge, NJ.
- [4] Merton, R.C. (1969), Lifetime Portfolio Selection Under Uncertainty: The Continuous- Time Case. *Review of Economics and Statistics* 51 (August): 247-257.
- [5] Merton, R.C. (1971), Optimum Consumption and Portfolio Rules in a Continuous-Time Model. *Journal of Economic Theory* 3 (December): 373-413.
- [6] Merton, R.C. (1973), An Intertemporal Capital Asset Pricing Model. *Econometrica* 41 (September): 867-887.
- [7] Merton, R.C. (1992), *Continuous-Time Finance*, revised edition, Blackwell Publishers, Cambridge, MA.
- [8] Meucci, A. (2005), *Risk and Asset Allocation*, Springer, New York, NY.
- [9] Pliska, S.R. (1997), *Introduction to Mathematical Finance: Discrete Time Models*, Blackwell Publishers, Oxford, UK.
- [10] Scherer, B. (2004), *Portfolio Construction and Risk Budgeting*, 2nd edition, Risk Books, London, UK.

Yolk Dynamics in Amphibian Embryos

Problem Presenter: Richard Gordon (University of Manitoba)

Academic Participants: C. Sean Bohun (University of Ontario Institute of Technology), Chris Breward (University of Oxford), Ellis Cumberbatch (Claremont Graduate University), George Djounna (Université Laval), Ahmed ElSheikh (McMaster University), J.F. Williams (Simon Fraser University), Jonathan Wylie (City University of Hong Kong)

Report prepared by: C. Sean Bohun¹ and Chris Breward².

1 Introduction

This problem was proposed by the Manitoba Institute of Child Health and investigated at the First Fields-MITACS Industrial Problem-Solving Workshop. The impetus for this work is to attempt to understand the role that gravity plays in the development of embryos. One of the most serious obstacles that the group found in this field is the lack of a complete set of physical parameters for any given embryo. Consequently, it was decided early on that no time would be spent modelling behaviour for which there was no experimental evidence.

Three processes observed in development of the egg prior to the first cell division were investigated. These include:

- the up-righting phase (first minute),
- the delay until cortical rotation initiates (up to one hour),
- the cortical rotation (~ 30 minutes).

The hope was that in understanding these simple processes, one would be able to understand some of the interesting behaviour of the egg described in Section 1.3 when it is rotated manually.

1.1 Structure of the egg. Figure 1 illustrates a mature amphibian oocyte (unfertilized egg) and its internal structure. Contained within the oocyte is a nucleus containing nucleoplasm, and suspended in viscous cytoplasm are yolk platelets, ribosomes, and mitochondria. The yolk platelets store lipoproteins that are packed into a regular array and provide energy for the developing cell. They vary in size and density with an average diameter of $12\ \mu\text{m}$ [23] for those platelets located in the vegetal hemisphere.

¹sean.bohun@uoit.ca

²breward@maths.ox.ac.uk

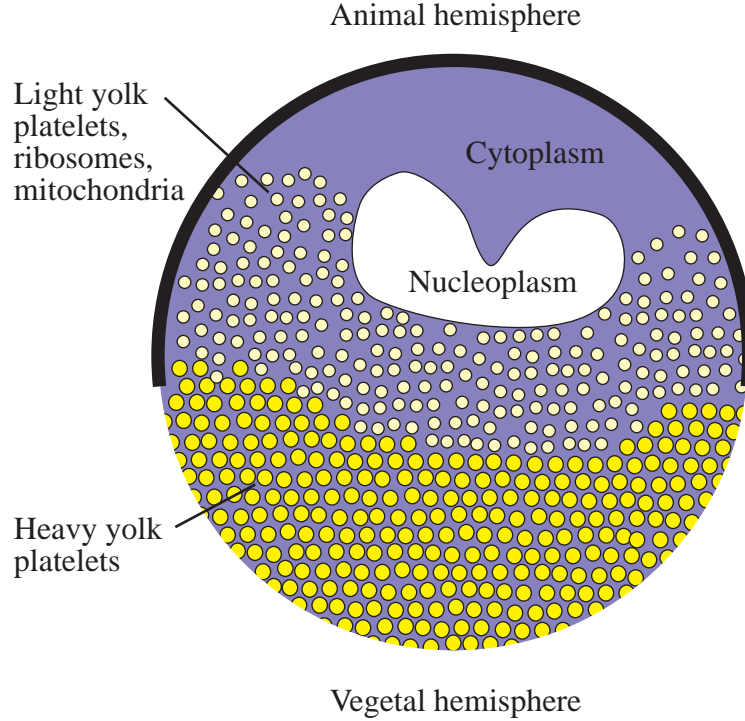


Figure 1 Structure of a mature oocyte.

The periphery of the cell is quite complicated consisting of a series of interconnected layers. Outermost is a monolayer of follicle cells which are bound to the follicular epithelium that encases the oocyte. Beneath the follicular epithelium is the vitelline envelope which is roughly $1 - 2 \mu\text{m}$ in thickness and consists of a network of fibres that range in diameter from $40 - 70 \text{ nm}$. Within 200 nm of the surface of the plasma membrane are the cortical and pigment granules. Stereo micrographs of these structures can be found in [8]. The animal hemisphere is characterized by many pigment granules and cortical granules of $1.5 \mu\text{m}$ in diameter whereas the vegetal hemisphere has significantly less pigment granules and cortical granules of $2.5 \mu\text{m}$ in diameter [5]. A detailed view of the cell periphery can be found in [16] or in [5] and the references cited therein.

1.2 Egg activation. Fertilized eggs are released from the female in random orientations which persist even though they were activated through fertilization before release. In urodele amphibians such as the axolotl, many sperm enter the egg, but only one sperm nucleus fuses with the egg nucleus. When a fertilizing sperm penetrates the plasma membrane, the cortical granules break down and release their contents to the surface of the egg. Swelling on contact with water, the contents of the granules expand the space that lies between the plasma membrane and the vitelline envelope forming the perivitelline space [9]. At the same time the vitelline envelope hardens and prevents any further penetration by sperm. Once the perivitelline space has formed and the animal hemisphere contracts, the egg is freed of its connections to its surrounding membranes permitting the reorientation of the eggs via gravity. Average rates of rotation are typically 0.26 rpm [9] and the up-righting itself is hypothesized to be a result of the different yolk densities. Figure 2 shows



Figure 2 Typical axolotl eggs and their encapsulating gel after the up-righting phase (Courtesy of Susan Crawford-Young).

axolotl eggs after up-righting. They appear to be axially symmetric, though inversion experiments [13, 21, 22] suggest that this may only apply to the cortex (cell membrane and underlying attached cytoplasm), i.e., developmentally the embryo may be spherically symmetric at this stage.

Further asymmetry within the egg is introduced by a reorganization of the cytoplasm at about the halfway point between the moment of fertilization and time of first cell division. The reorganization occurs with a 30° rotation³ of the cortex relative to the rest of the cell body [9] and is depicted in Figure 3. The portion of the egg exposed by moving the animal hemisphere becomes covered with the clear vegetal hemisphere and as a result forms a grey crescent. This region of the egg becomes the dorsal (back) side of the embryo and the opposite side of the egg forms the ventral (belly) side of the embryo. The grey crescent is only visible in certain amphibian eggs but many different techniques have been developed to visualize the subcortical rotation in many species.

1.3 The role of gravity. Gravity does seem to play a role in the development of the embryo but its effect is paradoxical. This was demonstrated in a sequence of experiments where the egg was immobilized and rotated manually. Four situations were examined with an initially inverted egg.

1. An initial rotation of $15^\circ - 90^\circ$ for 30 minutes and then manually up-righting the egg causes the dorsal lip of the embryo to reposition to the side of the egg opposing gravity but otherwise produces normal offspring [3].

³Vincent [20] indicates rotations of $20^\circ - 38^\circ$ with an average of 28° . Maximum linear displacement is $300\ \mu\text{m}$ at rates up to $10\ \mu\text{m}/\text{minute}$.

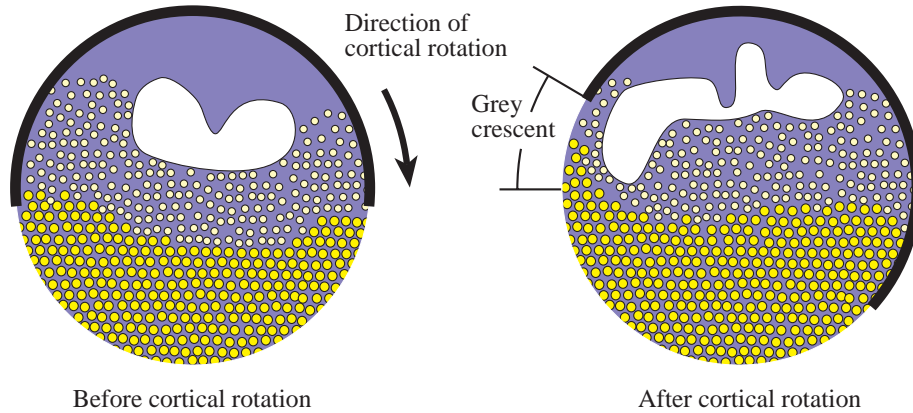


Figure 3 Eggs before and after cortical rotation.

2. Eggs irradiated with ultraviolet light typically create offspring with morphological defects. These defects can be corrected with a manual rotation of the egg for 30 minutes [3].
3. A sustained rotation of 165° (nearly inverted) produces offspring that have an altered pigmentation. Sterility is enhanced for those eggs with a lower viscosity [21].
4. A sustained inversion at 180° creates eggs that divide normally but fail to produce offspring [22].

A centrifuge has also been shown to be effective at orientating the cytoplasm, provided the procedure starts before the initiation of cortical rotation. Conjoined twin tadpoles were formed by first irradiating the egg with ultraviolet light, centrifuging at $30g$ for 4 minutes at a 90° inclination and then centrifuged at $10g$ for 4 minutes at a 0° inclination. These offspring were characterized as doubly rescued from the irradiation [1]. Despite the strength of the acceleration in this latter case the eggs produce viable offspring.

1.4 Overall timeline. Each of the processes discussed above occurs at a specific time within the first cell cycle. Figure 4 depicts the various events and is an accumulation of data from several sources [1, 9, 10, 11, 20, 24]. The time units are labelled in both normalized time (NT) and in minutes. A time of 0 NT corresponds to the moment of fertilization and 1 NT is the time when the egg divides for the first time. There is some ambiguity in the literature with respect to the absolute time scale since 1 NT can take anywhere from 85 – 120 minutes depending on the temperature [1]. For the remainder of this report we have assumed the upper bound of $1 \text{ NT} = 120$ minutes.

1.5 Physical data. We end this section with a summary of the geometry and physical constants that were inferred from the embryological literature. Reported sizes of yolk platelets range from $2 - 14 \mu\text{m}$ in diameter, Neff et al. [14] identified three categories (small, medium and large) with densities of 1208 , 1240 , and 1290 kg/m^3 respectively. Wall et al. [23] specifies two sizes at different concentrations with a preponderance of the platelets about $12 \mu\text{m}$ in diameter. Light yolk platelets were found to have a density of 1210 kg/m^3 in concentrations of 7 g/ml whereas heavy platelets are more dense and occur in higher concentrations: 1230 kg/m^3 at 40 g/ml . Values used in the remainder of this report as well

as a characteristic viscosity for the various regions of the egg are listed in Table 1. Most of the data is taken from the African clawed frog (*Xenopus laevis*) species.

Figure 5 illustrates the overall geometry of an amphibian egg showing the various regions of interest. The pigmentation variation seen in the previous images is represented by the dark and light grey shaded regions.

2 Up-righting phase

As previously described, once the eggs are released from the female and fertilized (or reverse, for urodele amphibians), the contents of the cortical granules are released into the gap between the plasma membrane and the vitelline membrane. Upon hydration this gap expands to form the perivitelline space, freeing the egg and causing it to rotate with the

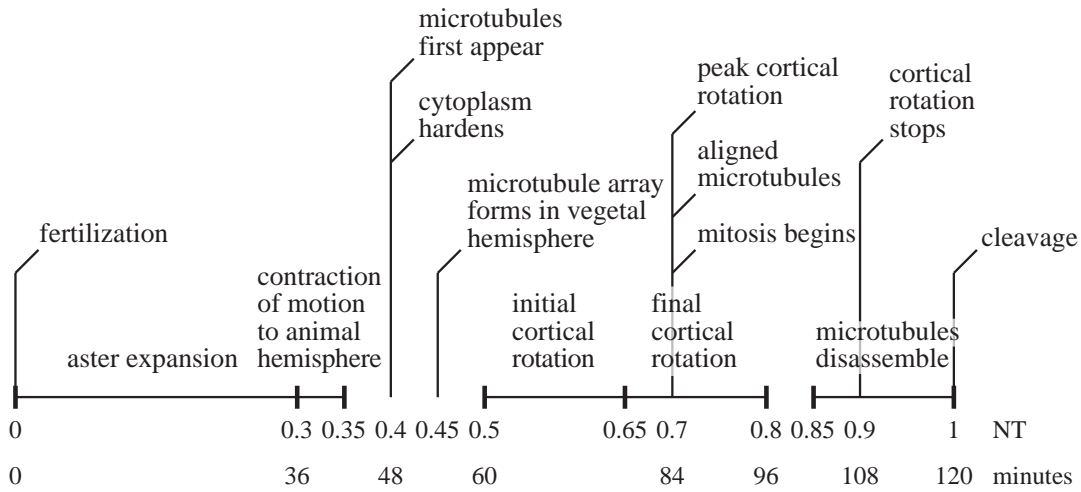


Figure 4 A timeline of significant events in the oocyte from fertilization to first cleavage.

Table 1 Physical properties of a typical amphibian egg.

Density (kg/m^3)	
Nucleoplasm	$\rho_0 = 1000$
Cytoplasm	$\rho_1 = 1100$
Yolk platelets	$\rho_2 = 1200$ [14]
Dynamic Viscosity ($\text{kg}/\text{m}/\text{s}$)	
Nucleoplasm	$\mu_0 = 5 \times 10^{-3}$ [12]
Cytoplasm	$\mu_1 = 20 \times 10^{-3}$ [18]
Water	$\mu_2 = 1 \times 10^{-3}$
Lengths (m)	
Nucleus diameter	$2r_0 = 7 \times 10^{-4}$
Egg diameter	$2r_1 = 2 \times 10^{-3}$ [14]
Yolk platelet diameter	$a = 12 \times 10^{-6}$ [14]
Nucleus displacement	$s = 7 \times 10^{-4}$
Cortex width	$h_1 = 20 \times 10^{-6}$ [16]
Perivitelline space	$h_2 = 3 \times 10^{-6}$ [25]

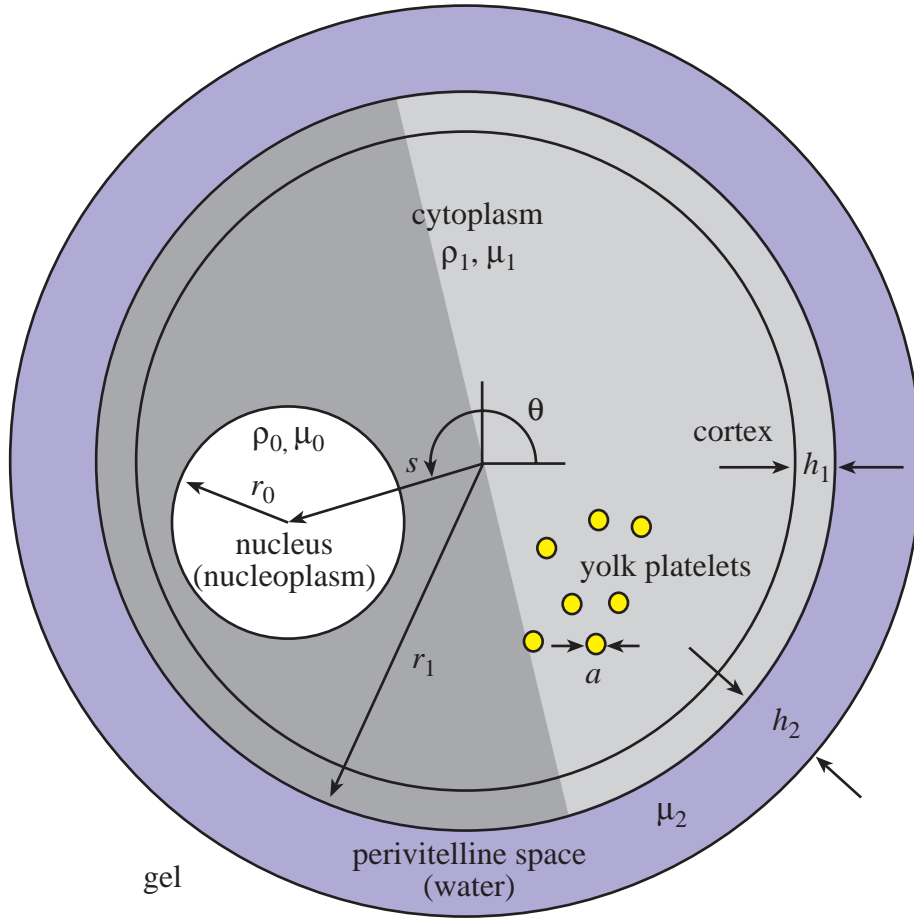


Figure 5 An idealized amphibian egg and its physical parameters.

dark pigmentation area towards the top. Some of the characteristics of this up-righting motion are that it takes about a minute to complete [9] and appears to be overdamped [6].

If the interior of the cell is sufficiently viscous then the up-righting can be approximated with a rigid body rotation. As discussed earlier, two of the main components of the interior of the egg are yolk platelets and cytoplasm. The platelets are membrane-bound spheres containing high concentrations of yolk protein so that interior can be thought of as a colloidal suspension. To determine how long it would take a yolk platelet of diameter a to traverse the length of the egg we apply Stokes' law to find the terminal velocity

$$v_{\infty} = \frac{1}{18} \frac{(\rho_2 - \rho_1)ga^2}{\mu_1} = 3.92 \times 10^{-7} \text{ m/s}$$

using the data in Table 1. This implies that it would take 5.1×10^3 seconds for the platelet to fall the 2 mm length of the egg. Since the up-righting occurs on the time scale of a minute, during this phase the interior of the egg can be approximated as solid.

Referring back to Figure 5, the nucleus is set inside a cell body and has three forces acting on it. The gravitational force acts through its centre of mass. Buoyancy acts through the centre of buoyancy which is simply the centre of mass of the displaced fluid. Finally, the

viscous drag force opposes the motion in the fluid bearing region of the perivitelline space. Denoting θ as the angular displacement of the nucleus and I_0 as the moment of inertia of the cell,

$$I_0\ddot{\theta} = \tau_{\text{buoy}} + \tau_{\text{gravity}} + \tau_{\text{drag}}, \quad \theta(0) = \theta_0, \quad \dot{\theta}(0) = 0. \quad (2.1)$$

Using the values in Table 1 we find that

$$I_0 \lesssim \frac{2}{5}m_1r_1^2 = \frac{8}{15}\pi\rho_1r_1^5 \simeq 2.8 \times 10^{-11}, \quad (2.2)$$

and

$$\tau_{\text{buoy}} + \tau_{\text{gravity}} = \frac{4}{3}\pi r_0^3(\rho_1 - \rho_0)gs \cos \theta \simeq 3.7 \times 10^{-10} \cos \theta, \quad (2.3)$$

where I_0 neglects the effect of the lower density region occupied by the nucleus. For the drag we need to take into account the variation in speed over the surface of the sphere. At an azimuthal angle of φ , the infinitesimal torque is

$$d\tau_{\text{drag}} = -\mu_2(r_1 \sin \varphi)\dot{\theta} \left(\frac{r_1 \sin \varphi}{h_2} \right) dA = -2\pi r_1^4 \frac{\mu_2 \dot{\theta}}{h_2} \sin^3 \varphi d\varphi.$$

Integration over $0 \leq \varphi \leq \pi$ gives the expression

$$\tau_{\text{drag}} = -\frac{4}{3}\pi r_1^4 \frac{\mu_2 \dot{\theta}}{h_2} \sim -1.4 \times 10^{-9} \dot{\theta}. \quad (2.4)$$

Due to their relative smallness, the inertial terms do not contribute significantly to the motion. Neglecting them reduces (2.1)-(2.4) to the simplified expression

$$\dot{\theta} \simeq \frac{sr_0^3 h_2 g (\rho_1 - \rho_0)}{r_1^4 \mu_2} \cos \theta, \quad \theta(0) = \theta_0, \quad \dot{\theta}(0) = 0 \quad (2.5)$$

with solution curves illustrated in Figure 6. Notice that the time to up-right is typically less than a minute and the behaviour is essentially exponential. Using reported rotational speeds of anywhere from 0.026 to 0.54 rpm [9] and the fact that the maximal rate of rotation occurs when $\theta = 0$ we can determine the size of the perivitelline space as

$$\frac{0.026(2\pi)}{60} \frac{r_1^4 \mu_2}{sr_0^3 g (\rho_1 - \rho_0)} \leq h_2 \leq \frac{0.54(2\pi)}{60} \frac{r_1^4 \mu_2}{sr_0^3 g (\rho_1 - \rho_0)}$$

or $0.092 \mu\text{m} \leq h_2 \leq 1.9 \mu\text{m}$. These values are quite possible since this space is created by the swelling contents of corticle granules that are themselves typically only $1.5 \mu\text{m}$ in diameter.

3 Delay until cortical rotation

Once the egg has up-righted, the yolk platelets in the cytoplasm will settle out until they reach an equilibrium distribution. To study this behaviour, we approximate the interior of the egg with a one-dimensional two phase flow model⁴ (see [7]) for the yolk/cytoplasm colloid as illustrated in Figure 7. In what follows, α and β are the volume fractions of the yolk and cytoplasm which move with speeds u_α and u_β respectively. Conservation of mass for each phase can then be written as

$$\alpha_t + (\alpha u_\alpha)_y = 0, \quad \beta_t + (\beta u_\beta)_y = 0. \quad (3.1)$$

⁴We neglect the presence of the nucleus in this section.

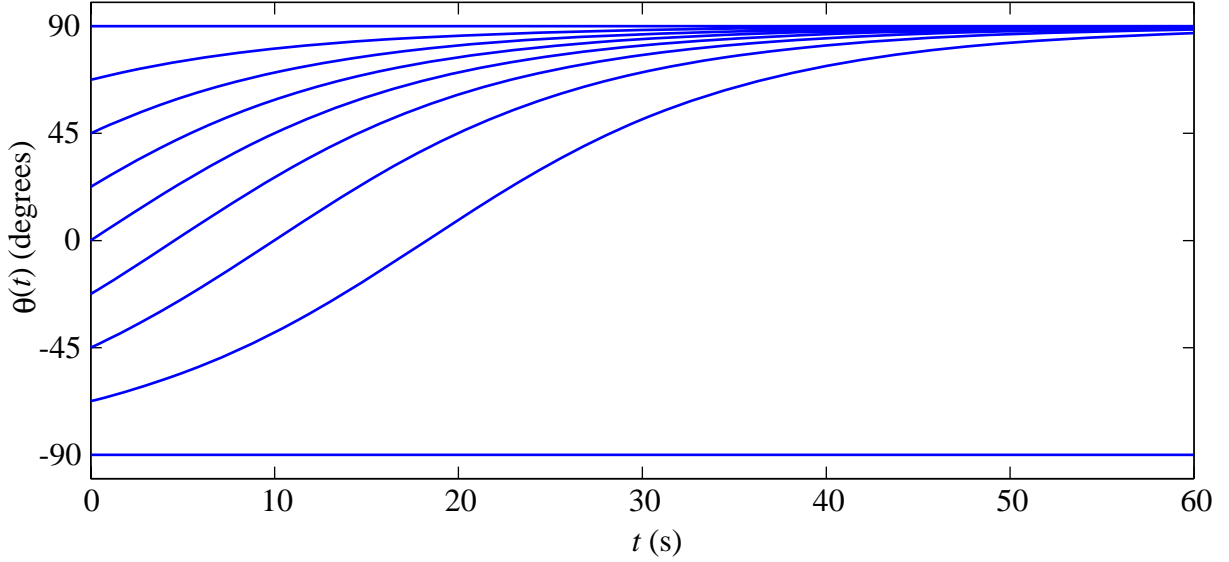


Figure 6 Solution curves to (2.5) with various initial values $-\pi/2 \leq \theta_0 \leq \pi/2$.

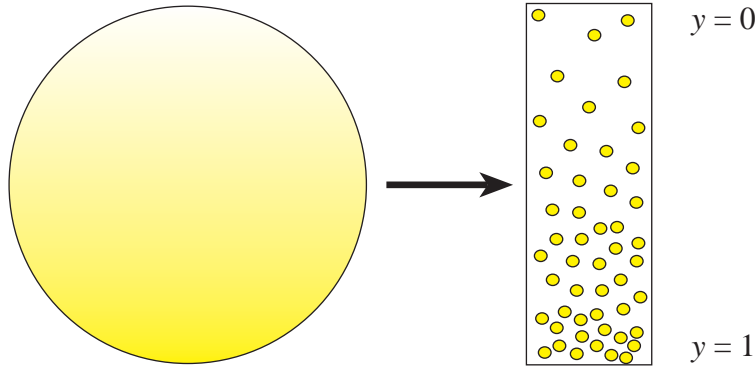


Figure 7 One-dimensional approximation of the interior of the egg.

Assuming that space is completely filled by yolk and cytoplasm, we write

$$\alpha + \beta = 1, \quad (3.2)$$

which is known as the no-voids condition. Neglecting inertia and introducing p_α and p_β for the averaged isotropic pressure in each phase, μ_α and μ_β for the viscosity of each phase, g as the acceleration due to gravity, and τ_α and τ_β for the deviatoric stresses, conservation of momentum for each phase leads us to

$$(-\alpha p_\alpha + \alpha \tau_\alpha)_y + (p_\alpha - \tau_{\alpha i})\alpha_y - \frac{\mu_\alpha}{a^2} \alpha f(\alpha)(u_\alpha - u_\beta) + \rho_\alpha g \alpha = 0, \quad (3.3)$$

$$(-\beta p_\beta + \beta \tau_\beta)_y + (p_\beta - \tau_{\beta i})\beta_y + \frac{\mu_\alpha}{a^2} \alpha f(\alpha)(u_\alpha - u_\beta) + \rho_\beta g \beta = 0, \quad (3.4)$$

where $\tau_{\alpha i}$ and $\tau_{\beta i}$ are the stresses at the interfaces. The first two terms are the bulk-averaged and surface-averaged contributions to the stress from the phases themselves, the third term in these equations represents drag one phase on the other (modelled by f), and the final

term represents the gravitational force. Continuity of stress at the interface between yolk and cytoplasm gives

$$-p_\alpha + \tau_{\alpha i} - (-p_\beta + \tau_{\beta i}) = -\gamma\kappa, \quad (3.5)$$

where γ is the average interfacial tension and κ is the average interfacial curvature.

In order to close the model we have to pose four constitutive laws, describing the behaviour of the two fluids and what happens with the stress at the interface. Assuming both phases behave as viscous liquids, we write

$$\tau_\alpha = \mu_\alpha u_{\alpha y}, \quad \tau_\beta = \mu_\beta u_{\beta y}, \quad \tau_{\alpha i} = -\mu_\alpha f_1(\alpha) u_{\alpha y}, \quad \tau_{\beta i} = -\mu_\beta f_2(\beta) u_{\beta y},$$

where f_1 and f_2 are functions associated with the geometry of the system and the ease of motion of the liquids.

It is straightforward to reduce these ten expressions to three. We nondimensionalise the resulting equations using

$$y = L\hat{y}, \quad u = U\hat{u} = \frac{\rho_\alpha g a^2}{\mu_\alpha} \hat{u}, \quad t = \frac{L\mu_\alpha}{\rho_\alpha g a^2} \hat{t}, \quad p = \frac{\mu_\alpha U L}{a^2} \hat{p}, \quad \epsilon = \frac{a}{L},$$

to yield, dropping hats,

$$\alpha_t + (\alpha u)_y = 0, \quad (3.6)$$

$$\alpha p_y = \alpha \left(1 - \frac{f u}{1 - \alpha} \right) + \epsilon^2 \left((\alpha u_y)_y + f_1 \alpha_y u_y \right), \quad (3.7)$$

$$p_y = \bar{\rho} + (1 - \bar{\rho})\alpha + \epsilon^2 \left((\alpha u_y)_y + f_1 \alpha_y u_y - (1 - \alpha)(f_1 u_y)_y + \Gamma \right) \quad (3.8)$$

where $\bar{\rho} = \rho_\beta/\rho_\alpha$, and

$$\Gamma = -\frac{\mu_\beta}{\mu_\alpha} \left[\left((1 - \alpha) \left(\frac{\alpha u}{1 - \alpha} \right)_y \right)_y - f_2 \alpha_y \left(\frac{\alpha u}{1 - \alpha} \right)_y + (1 - \alpha) \left(f_2 \left(\frac{\alpha u}{1 - \alpha} \right)_y \right)_y \right]. \quad (3.9)$$

To leading order in ϵ , we find that

$$\alpha_t + (\alpha u)_y = 0, \quad u = (1 - p_y) \frac{1 - \alpha}{f}, \quad p_y = \bar{\rho} + (1 - \bar{\rho})\alpha,$$

in other words,

$$\alpha_t + \left(\frac{(1 - \bar{\rho})\alpha(1 - \alpha)^2}{f} \right)_y = 0. \quad (3.10)$$

We suppose that we know the initial distribution of the yolk platelets, so that we write

$$\alpha(y, 0) = \alpha_0(y). \quad (3.11)$$

At the top and bottom of the egg, we suppose that there is no motion of either phase (that is, since the fluids are viscous we impose the no slip condition) and so we set $u = 0$. This is not possible at both the top and bottom surfaces as seen by the leading-order outer solution, so the viscous stresses that we have neglected to leading order become important. Scaling into the boundary layers at the top and bottom of the egg, we find that conservation of mass leads to the condition

$$u\alpha = 0$$

at $y = 0$ and $y = 1$. We pick $u = 0$ throughout the bottom boundary layer (with consequence that $\alpha = 1$ at $y = 1$). In the top boundary layer, we choose $\alpha = 0$. We now consider the evolution of three relevant initial conditions (a) a linear yolk gradient, (b) an inverted egg

(with a linear gradient) and (c) a well-mixed egg. We set $f = 1$ for simplicity, since we are unsure of the actual functional form, and we scale $t = \tau/(1 - \rho)$ to remove the explicit dependence on ρ . The timescale, T , for the drainage problem is therefore given by

$$T = \frac{L\mu_\alpha}{(\rho_\alpha - \rho_\beta)ga^2} \sim 700 \text{ s}, \quad (3.12)$$

using the values given in Table 1.

Our problem is then to solve

$$\alpha_\tau + (\alpha(1 - \alpha)^2)_y = 0, \quad y \in (0, 1), \quad \tau > 0, \quad (3.13)$$

with an initial condition appropriate to each case and keeping in mind the boundary conditions discussed in the previous paragraph.

3.1 Settling of yolk from a linear gradient. We suppose that

$$\alpha(y, 0) = y, \quad (3.14)$$

and we note that the initial linear gradient satisfies the boundary conditions discussed in the previous section. We solve (3.13) and (3.14) using the method of characteristics, which, for $\tau < 1/4$, yields

$$\alpha(y, t) = \begin{cases} 0 & 0 \leq y < \tau \\ \frac{1}{6} \left[4 - \frac{1}{\tau} + \sqrt{\left(4 - \frac{1}{\tau}\right)^2 - 12 \left(1 - \frac{y}{\tau}\right)} \right] & \tau < y \leq 1. \end{cases} \quad (3.15)$$

At $\tau = 1/4$ a shock forms and we use the Rankine-Hugoniot condition (see [15]) to find the position of the shock. Denoting the shock position by $y = s(\tau)$, we have

$$\frac{ds}{d\tau} = \frac{[\alpha(1 - \alpha)^2]}{[\alpha]}, \quad (3.16)$$

where the square brackets denote the jump in the quantity inside the brackets as the shock is traversed. In this case, since the volume fraction of yolk platelets is zero above the shock, (3.16) becomes

$$\frac{ds}{d\tau} = (1 - \alpha_+)^2, \quad (3.17)$$

where α_+ is the solution given in (3.15) and evaluated at $y = s$, i.e.

$$\alpha_+ = \frac{1}{6} \left[4 - \frac{1}{\tau} + \sqrt{\left(4 - \frac{1}{\tau}\right)^2 - 12 \left(1 - \frac{s}{\tau}\right)} \right]. \quad (3.18)$$

The initial condition for the shock position is $s = 1/4$ at $\tau = 1/4$. We solve (3.17) numerically and show the position of the shock in (y, τ) space in the upper figure of Figure 8. As $\tau \rightarrow \infty$, $s \rightarrow 1/2$, and the liquid separates into cytoplasm at the top of the egg, and yolk at the bottom. We show the volume fraction of the yolk platelets as it evolves in the lower figure of Figure 8. We note that the yolk takes an infinite amount of time to reach its steady state and that the drainage is fastest at the start. Indeed after 15 minutes, the yolk platelets reside below $y = 0.45$ (i.e. within 10% of their final position).

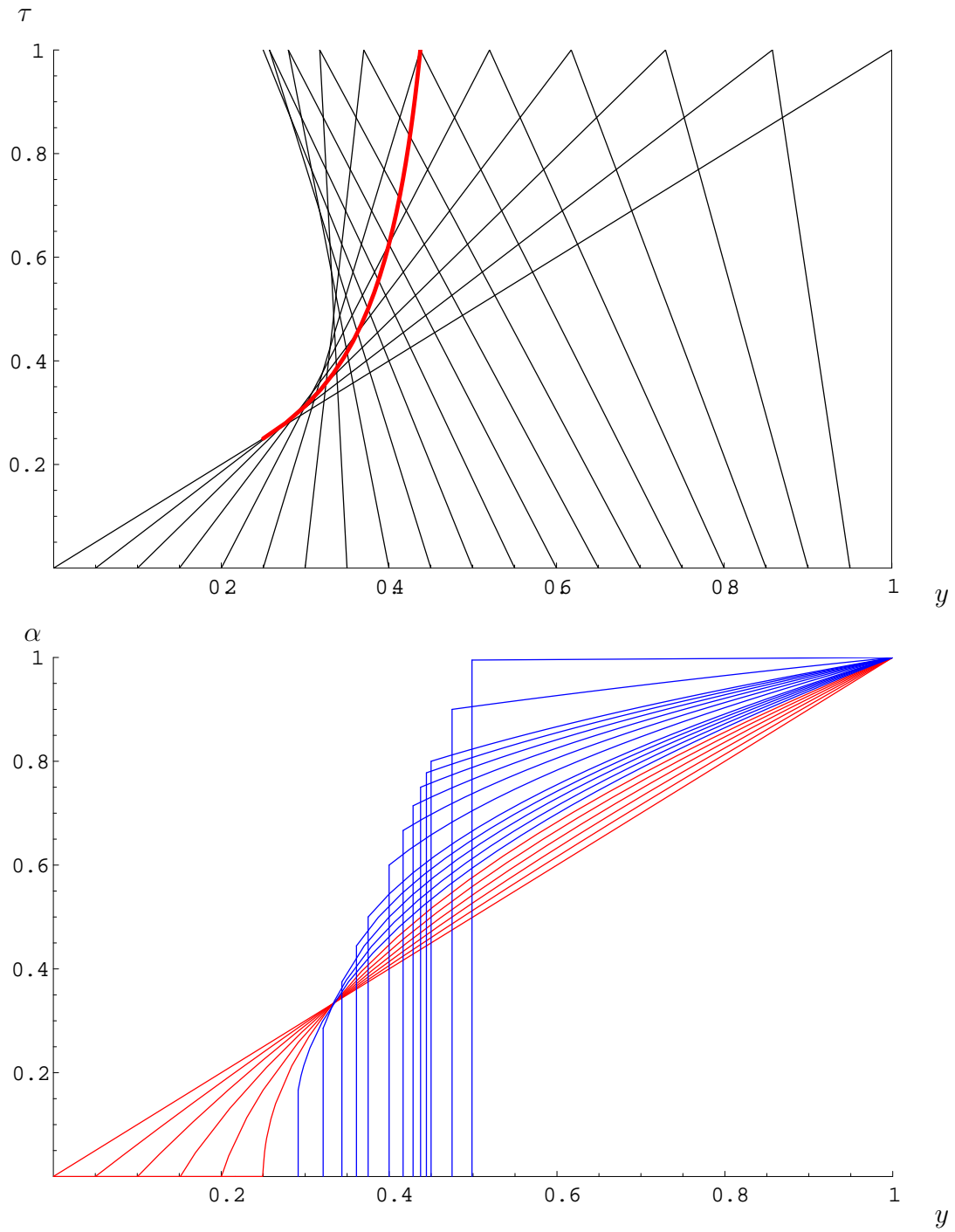


Figure 8 (upper) Characteristic projection in (y, τ) space. The red line shows the position of the shock. (lower) Graph showing the evolution of the yolk volume fraction. The red profiles are before the shock develops, the blue ones, afterwards.

3.2 Settling of an inverted egg. In this case, we set

$$\alpha(y, 0) = 1 - y. \quad (3.19)$$

We find that a shock immediately develops at the bottom of the egg, across which the yolk volume fraction jumps to unity. A second shock propagates in from the top of the egg, initiating at $\tau = 1/2$, across which the volume fraction jumps from zero. Denoting these two shocks as $s_{\text{top}}(\tau)$ and $s_{\text{bot}}(\tau)$ respectively, we find that the solution is

$$\alpha(y, t) = \begin{cases} 0 & 0 \leq y \leq s_{\text{top}}(\tau) \\ \frac{1}{6} \left[4 - \frac{1}{\tau} + \sqrt{\left(4 - \frac{1}{\tau}\right)^2 - 12 \left(1 + \frac{1}{\tau} - \frac{y}{\tau}\right)} \right] & s_{\text{top}}(\tau) \leq y \leq s_{\text{bot}}(\tau), \\ 1 & s_{\text{bot}}(\tau) \leq y \leq 1. \end{cases} \quad (3.20)$$

where the position of the shocks can be found by solving

$$\frac{ds_{\text{top}}}{d\tau} = (1 - \alpha(s_{\text{top}}, \tau))^2, \quad s_{\text{top}}(1/4) = 0, \quad (3.21)$$

and

$$\frac{ds_{\text{bot}}}{d\tau} = -\frac{\alpha(s_{\text{bot}}, \tau) (1 - \alpha(s_{\text{bot}}, \tau))^2}{1 - \alpha(s_{\text{bot}}, \tau)} \quad s_{\text{bot}}(0) = 0. \quad (3.22)$$

These two shocks collide at $y = 1/2$, $\tau = 2.6$ and the solution becomes

$$\alpha(y, t) = \begin{cases} 0, & 0 \leq y < 1/2 \\ 1, & 1/2 \leq y \leq 1, \end{cases} \quad (3.23)$$

for subsequent times, since the new shock created when these two collide satisfies $ds_{\text{end}}/d\tau = 0$. We show the characteristic projections and the evolution of the yolk volume fraction in Figure 9. We note that, in this case, the yolk reaches its steady state after a finite time, which is equivalent to 30 minutes.

3.3 Settling of a well-mixed egg. The final case we consider is the settling of an egg where the yolk is well mixed, so that the initial condition is

$$\alpha(y, 0) = 1/2. \quad (3.24)$$

In this case, the solution is $\alpha = 1/2$ along parallel lines $\tau = 4(y_0 - y)$. However, the initial data cannot propagate into the triangle $1 - \tau/4 \leq y \leq 1$, and we introduce an expansion fan there (with α ranging from $1/2$ to 1). Some of the characteristics in the fan intersect with those generated from the initial data so, as in the previous case, we have a shock propagating in from the base of the egg. The solution reads

$$\alpha(y, t) = \begin{cases} 0 & 0 \leq y \leq s_{\text{top}}(\tau) \\ 1/2 & s_{\text{top}}(\tau) \leq y \leq s_{\text{bot}}(\tau) \\ \frac{2 + \sqrt{1 - \frac{1-y}{\tau}}}{3}, & s_{\text{bot}}(\tau) \leq y \leq 1. \end{cases} \quad (3.25)$$

In this situation, it's easy to find $s_{\text{top}} = \tau/4$, and that s_{bot} satisfies

$$\frac{ds_{\text{bot}}}{dt} = \frac{\alpha^*(1 - \alpha^*)^2 - \frac{1}{8}}{\alpha^* - \frac{1}{2}}, \quad s_{\text{bot}}(0) = 1, \quad (3.26)$$

where

$$\alpha^* = \frac{2 + \sqrt{1 - \frac{1-s(\tau)}{\tau}}}{3}. \quad (3.27)$$

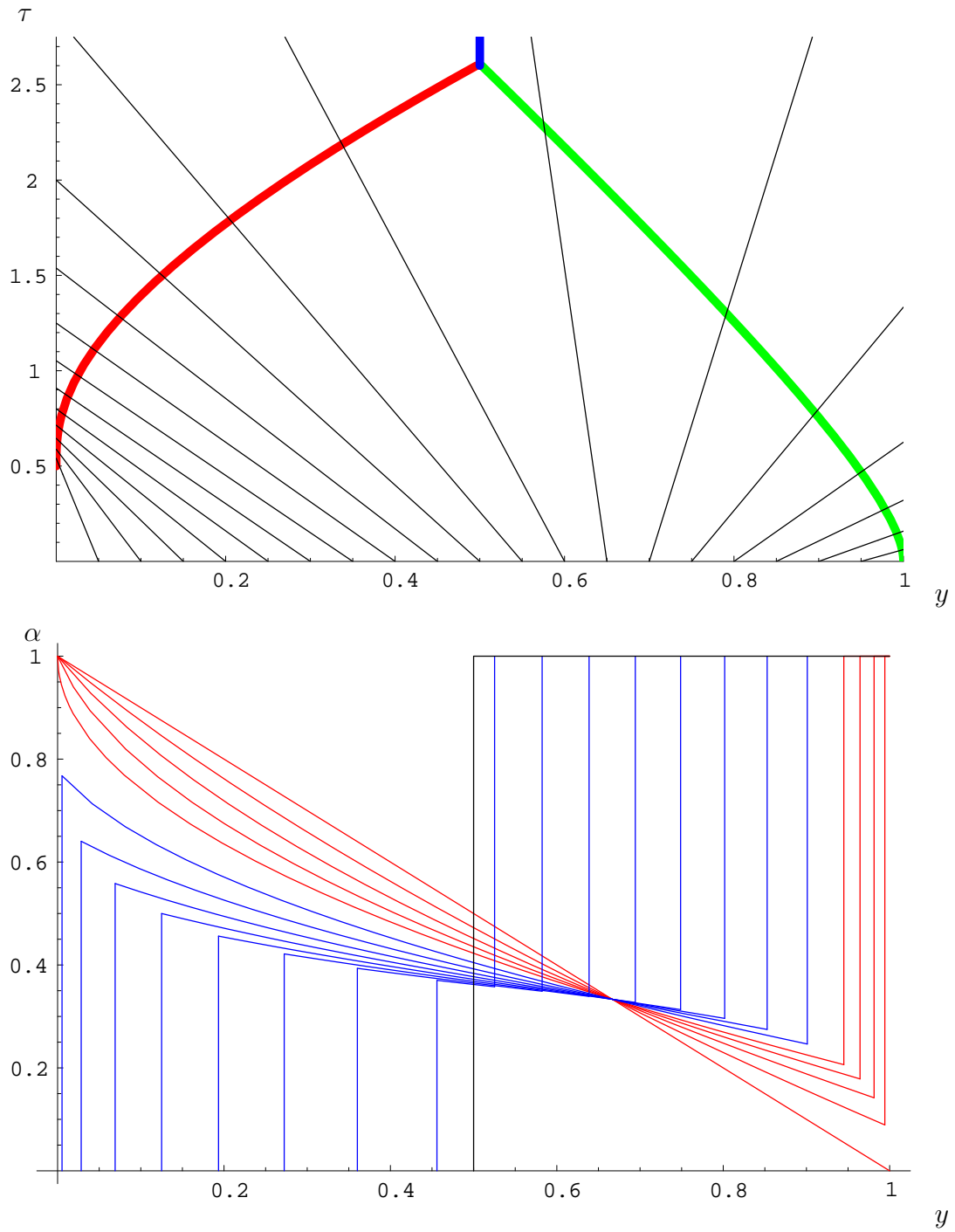


Figure 9 (upper) Characteristic projection in (y, τ) space. The red line shows the position of s_{top} , the green line shows the position of s_{bot} and the blue line shows the position of s_{end} . (lower) Graph showing the evolution of the yolk volume fraction. The red profiles are before the shock s_{top} develops, the blue ones, afterwards. The final state is shown in black.

This solution holds until the two shocks collide, which occurs at τ^* , found by solving $s_{\text{top}}(\tau^*) = s_{\text{bot}}(\tau^*)$, and yielding $\tau = 1.788$, $y = 0.444$ and subsequently a final (slowly moving) shock propagates back down the egg allowing a relaxation to the steady state. The final shock initiates from $s_{\text{bot}}(\tau^*)$, and moves according to

$$\frac{ds_{\text{end}}}{dt} = (1 - \alpha^*)^2, \quad s_{\text{end}}(\tau^*) = s_{\text{bot}}(\tau^*). \quad (3.28)$$

We show the characteristic projection and the evolution of the yolk volume fraction in Figure 10, in which we can see that the yolk takes an infinite time to settle to the steady state. However, after 22 minutes, the yolk platelets are all below $y = 0.45$.

4 Cortical rotation

We now turn our attention to the rotation of the cortex that takes place typically around $t = 0.5$ in normalized time units or at about 60 minutes. Some recent developments [2, 10, 11, 24] have begun to identify components involved in the cortical rotation but there is still a poor understanding of the details of the actual mechanism. What is known with some certainty is that the motor molecules dynein and kinesin both play a role in the process. In addition, recent measurements [4] have determined that one motor molecule is capable of producing about 6.2×10^{-12} N of force.

Even though the electrokinetics of microtubules is still in its infancy [19], it is possible to determine the number of motor molecules that would be required to perform the cortical rotation. We know that the rotation rate is typically $\dot{\theta} = 30^\circ$ in 30 minutes $= \pi/180/60$ rad/s. As a result the linear speed at the surface of the egg ($r_1 = 1 \times 10^{-3}$ m) is $v_1 = r_1 \dot{\theta}$ or $v_1 = 2.9 \times 10^{-7}$ m/s.

The drag force on the cortex is to a first approximation simply the surface area of the cortex multiplied by the viscous drag per unit area. Using the data in Table 1,

$$F_{\text{drag}} = 4\pi r_1^2 \mu_1 \left. \frac{\partial v}{\partial r} \right|_{r=r_1} = 4\pi r_1^2 \mu_1 \frac{v_1}{h_1} = 3.6 \times 10^{-9} \text{ N}$$

indicating that about 590 of the roughly 10^4 available motor molecules would be required to achieve the observed rotation rate. Irrespective of the actual mechanism chosen there seems to be enough energy available to allow the rotation to occur.

There are two main difficulties that need to be overcome before any further modelling can commence. First, the generation of microtubules inside the egg and the motion of motor molecules along these microtubules could be modelled but as mentioned earlier, it is not clear in the literature as to the actual mechanism. The second problem to overcome is an understanding of the switching on and off for the cortical rotation. It seems that this is biological in nature and there does not seem to be an appropriate model for this process. It is possible that cortical rotation is merely stopped by cell division. Artificially induced rotation in sea urchin eggs continues indefinitely [17].

5 Conclusions and future work

In our analysis of the yolk dynamics of the egg prior to the first cell division, three sub-problems were investigated. The up-righting phase was modelled with a simple buoyancy argument for a low density nucleus trapped inside a viscous cytoplasm and predicts an up-righting behaviour consistent with observations.

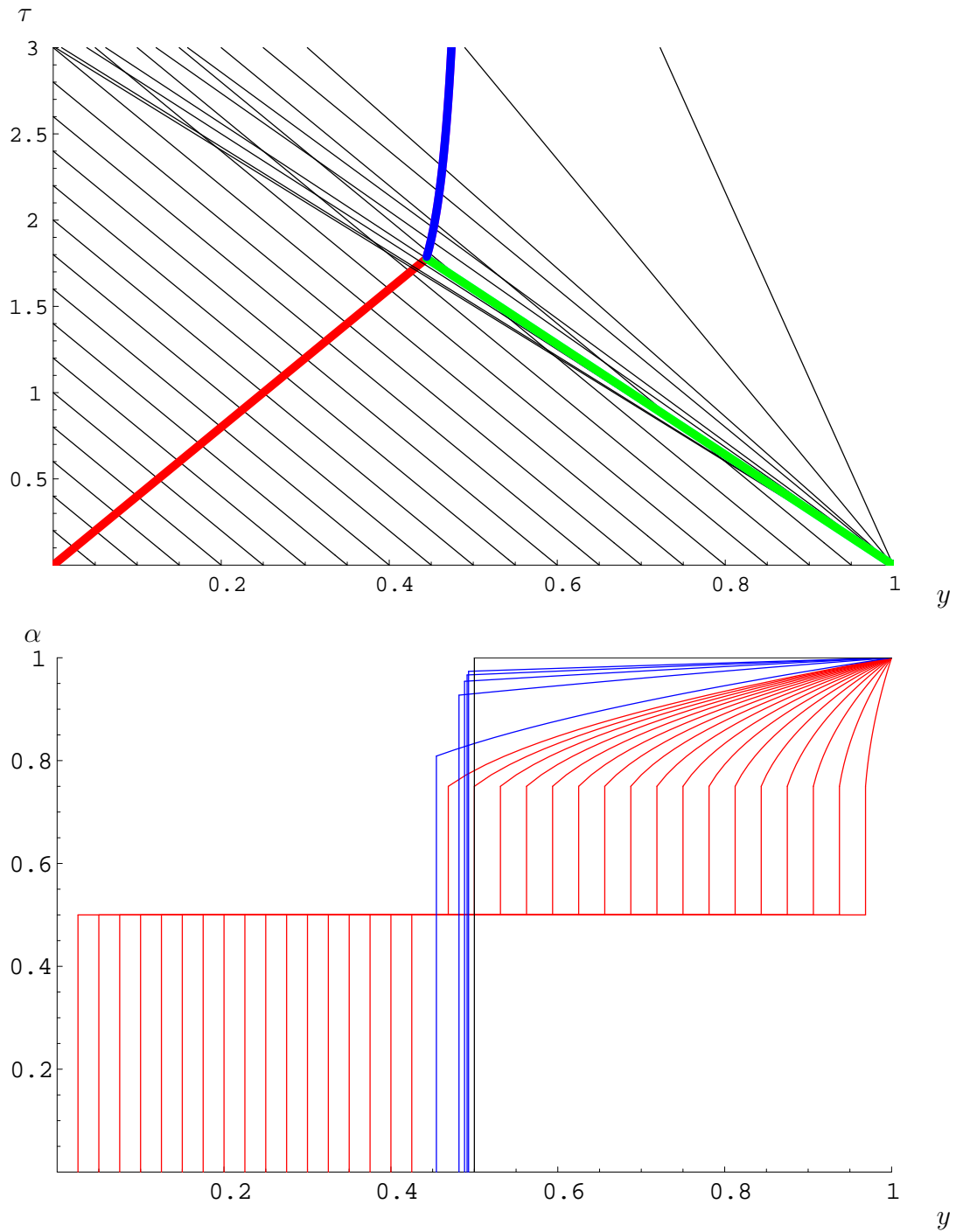


Figure 10 (upper) Characteristic projection in (y, τ) space. The red line shows the position of s_{top} , the green line shows the position of s_{bot} and the blue line shows the position of s_{end} . (lower) Graph showing the evolution of the yolk volume fraction. The red profiles are before the shock s_{end} develops, the blue ones, afterwards. The final state is shown in black.

Once the egg has up-righted, the yolk platelets in the cytoplasm will settle out until they reach an equilibrium distribution. We described the settling of yolk platelets through the cytoplasm using a two phase model. We reduced the model to the simplest form possible and solved the resulting model analytically in three cases: a linear initial gradient of yolk platelets, an inverted egg, and a well mixed egg. We found that the inverted egg settled in finite time, while the other cases settled in infinite time (with the evolution being 90% complete within 15 minutes and 22 minutes respectively). In all three cases, a region devoid of yolk platelets formed near the top of the egg, and we were able to track the point at which the volume fraction became non-zero.

In the case where one inverts the egg, the yolk platelets are stationary after 30 minutes, in contrast with the upright egg case, where there is *always* motion of the fluid in the egg, albeit slow. This might suggest that yolk *motion* is needed for correct development of embryos. However, further speculation about links between the yolk platelet evolution and the development of the embryo will require further experimentation.

With respect to cortical rotation, we verified that motor molecules with the egg will have sufficient energy to cause the cortical rotation. However, a clear mechanism for how the rotation takes place has not been identified.

Future work along these lines could involve further development of the two-phase model to allow the inclusion of the nucleus and/or utilization of the correct egg geometry. An important step in the verification and refinement of the models used in this preliminary work is the direct observation of yolk platelets during the critical moments between fertilization and the first cell division.

6 Acknowledgements

The authors would like to acknowledge the Fields Institute and MITACS for their sponsorship of the FMIPW event. We would also like to take this opportunity to thank Huaxiong Huang, Barbara Keyfitz and Nilima Nigam for organizing the event. Their hard work and dedication ensured the success of the workshop.

References

- [1] Black, S.D. & Gerhart, J.C. (1986), High-Frequency Twinning of *Xenopus laevis* Embryos from Eggs Centrifuged before First Cleavage. *Developmental Biology*, 116, 1, pp. 228-240.
- [2] Brito, D.A. et al. (2005), Pushing Forces Drive the Comet-like Motility of Microtubule Arrays in Dictyostelium. *Molecular Biology of the Cell*, 16, 7, 3334-3340.
- [3] Chung, H. & Malacinski, G.M. (1980), Establishment of the Dorsal/Ventral Polarity of the Amphibian Embryo: Use of Ultraviolet Irradiation and Egg Rotation as Probes. *Developmental Biology*, 80, 1, pp. 120-133.
- [4] Fisher, M.E. & Kolomeisky, A.B. (1999), The force exerted by a molecular motor. *Proceedings of the National Academy of Sciences of the United States of America*, 96, 12, pp. 6597-6602.
- [5] Gentry, M. (2006), Ultrastructure of the coelomic oocyte of *Xenopus laevis*. <http://131.229.114.77/microscopy/student%20projects/MilliecentGentry.html>
- [6] Personal communication with Richard Gordon.
- [7] Howell, P.D. & Muldoon, M. (2003), Two-phase modelling of air bubbles in ice cream. *Proceedings of the 46th ESGI* <http://www.maths-in-industry.org/24/>
- [8] Larabell, C.A. (1993), A New Technique for Isolation and Visualization of the *Xenopus* Egg Cortex Reveals a Complex Cytoskeleton. *Journal of Structural Biology*, 110, 2, pp. 154-159.
- [9] Malacinski, G.M. & Neff, A.W. (1989), The Amphibian Egg as a Model System for Analyzing Gravity Effects. *Advances in Space Research*, 9, 11, pp. 169-176.

- [10] Marrari, Y. et al. (2003), Analysis of microtubule movement on isolated *Xenopus* egg cortices provides evidence that the cortical rotation involves dynein as well as Kinesin Related Proteins and is regulated by local microtubule polymerisation. *Developmental Biology*, 257, 1, pp. 55-70.
- [11] Marrari, Y., Rouvière, C. & Houliston, E. (2004), Complementary roles for dynein and kinesins in the *Xenopus* egg cortical rotation. *Developmental Biology*, 271, 1, pp. 38-48.
- [12] Marshall, W.F. et al. (1997), Interphase chromosomes undergo constrained diffusional motion in living cells. *Current Biology*, 7, 12, pp. 930-939.
- [13] Neff, A.W., Wakahara, M., Jurand, A. & Malacinski, G.M. (1984), Experimental analyses of cytoplasmic rearrangements which follow fertilization and accompany symmetrization of inverted *Xenopus* eggs. *Journal of Embryology and Experimental Morphology*, 80, pp. 197-224.
- [14] Neff, A.W., Smith, R.C. & Malacinski, G.M. (1986), Amphibian Egg Cytoplasm Response to Altered g-Forces and Gravity Orientation. *Advances in Space Research*, 6, 12, pp. 21-28.
- [15] Ockenden J.R., Howison, S.D., Lacey, A.A. & Movchan, A. (1999), Applied Partial Differential Equations. Oxford University Press.
- [16] Sardet, C. et al. (2002), Structure and Function of the Cell Cortex from Oogenesis through Fertilization. *Developmental Biology*, 241, 1, pp. 1-23.
- [17] Schroeder, T.E. & D.E. Battaglia (1985), "Spiral asters" and Cytoplasmic Rotation in Sea Urchin Eggs: Induction in *Strongylocentrotus purpuratus* Eggs by Elevated Temperature. *Journal of Cell Biology*, 100, 4, pp. 1056-1062.
- [18] Valentine, M.T. et al. (2005), Mechanical Properties of *Xenopus* Egg Cytoplasmic Extracts. *Biophysical Journal*, 88, 1, pp. 680-689.
- [19] van den Heuvel, M.G.L., de Graaff, M.P. & Dekker, C. (2006), Molecular Sorting by Electrical Steering of Microtubules in Kinesin-Coated Channels. *Science*, 312, 5775, 910-914.
- [20] Vincent, J., Oster, G.F. & Gerhart, J.C. (1986), Kinematics of Gray Crescent Formation in *Xenopus* Eggs: The Displacement of Subcortical Cytoplasm Relative to the Egg Surface. *Developmental Biology*, 113, 1, pp. 484-500.
- [21] Wakahara, M., Neff, A.W. & Malacinski, G.M. (1984), Topology of the germ plasm and development of primordial germ cells in inverted amphibian eggs. *Differentiation*, 26, 3, pp. 203-210.
- [22] Wakahara, M., Neff, A.W. & Malacinski, G.M. (1985), Development of delayed gastrulae and permanent blastulae from inverted *Xenopus laevis* eggs. *Acta embryologiae et morphologiae experimentalis*, 6, pp. 193-209.
- [23] Wall, D.A. & Meleka, I. (1985), An Unusual Lysosome Compartment Involved in Vitellogenin Endocytosis by *Xenopus* Oocytes. *The Journal of Cell Biology*, 101, 5, part 1, pp. 1651-1664.
- [24] Weaver, C. & Kimelman, D. (2004), Move it or lose it: axis specification in *Xenopus*. *Development*, 131, 15, pp. 3491-3499.
- [25] Inferred from the data in [8] and [9].

Global Travel and Severe Acute Respiratory Syndrome (SARS)

Problem Presenter: Kamran Khan (St. Michael’s Hospital)

Academic Participants: Julien Arino (University of Manitoba), Natalie Baddour (University of Ottawa), Chris Breward (University of Oxford), Abba Gumel (University of Manitoba), Xiamei Jiang (University of Toronto), Chandra Podder (University of Manitoba), Bobby Pourziaei (York University), Oluwaseun Sharomi (University of Manitoba), Naveen Vaidya (York University), J.F. Williams (Simon Fraser University), Jianhong Wu (York University)

Report prepared by: Julien Arino¹

1 Introduction

Severe Acute Respiratory Syndrome (SARS) first appeared in November 2002 in the Guangdong province of China. First reported in Asia in February 2003, the illness spread to more than two dozen countries in Asia, North America, South America and Europe within months. By the time the disease had been declared ‘eradicated’ in May 2005 by the World Health Organization (WHO), a total of 8098 people in 28 countries world wide had been infected, and of those, 774 had died.

The advance of commercial air traffic plays an ever increasing role in the spread of infectious diseases and in the potential for these diseases to reach pandemic proportions. Despite the significance of commercial air traffic and its role in the worldwide dissemination of infectious diseases, our understanding of global air traffic dynamics remains limited. It is the goal of this paper to give insight into the nature of air traffic as it pertains to the spread of diseases.

The models developed are specifically related to the SARS disease. They can be further generalized to fit other similar (in terms of transmission) diseases, but modifications are necessary in order to take into account diseases with latency periods that are short relative to the flight time.

¹arinoj@cc.umanitoba.ca

Questions. The problem presenter posed the following questions:

- Q1.** Is it possible to develop a mathematical model to forecast the movement of disease from a given point source location?
- Q2.** Can these models be developed such that their predictions agree with the SARS data provided?
- Q3.** Was the movement of SARS random in nature or did the cases travel in a systematic fashion?
- Q4.** Were these movements predictable?

2 The data

The data that was provided by Khan was abundant. It allowed us to get a good idea of three important aspects:

1. infrastructure,
2. connections,
3. disease.

Infrastructure. The data details the busiest 802 airports worldwide. Due to a data sharing agreement, each airport had been assigned a random number, while their names had been deleted from the database. Below, we refer to these airports as A_i , $i = 1, \dots, 802$. Only Hong Kong International airport was identified, which was the point of origin of SARS once it left mainland China. In the random ordering chosen for the airports, Hong Kong International has number 7. The total number per year of inbound and outbound passengers for each airport is included in the database. Also, information is provided that localizes these airports within 12 major geographical zones.

Connections. We are given a 802×802 table, detailing, for any pair $i, j = 1, \dots, 802$, the number of seats on flights between airports A_i and A_j . This is different from the actual number of passengers between A_i and A_j , but the latter information is sensitive commercial data and is not available. Also provided in the table is the distance between A_i and A_j , computed by taking the distance between them on a sphere.

Disease importation. For each of the airports, the number of imported cases into that airport is provided. A case is defined as imported in the airport if, following a careful epidemiological enquiry, it is identified as having arrived into the airport while either in the latent or the active stage of the disease. A case identified in the city that the airport serves, and for which the transmission was clearly local, is not counted. Not available is the time course of the cases: we are given the total number of imported cases over the course of the SARS epidemic, with no finer temporal detail.

3 Dynamics in the airports

3.1 Choice of modelling paradigm. We elaborate two different models. One uses ordinary differential equations both for the population and the movement. The other uses ordinary differential equations at the population level, and a stochastic process for movement of individuals between locations.

Because of the nature of the data, and in particular, the absence of geographical information about the airports (and in particular, about the urban centers they are close to), we choose to consider airports as the units of analysis. Two airports are then considered as directly connected one to another if the number of seats between them is nonzero in the database.

3.2 The model within each airport. From now on, we denote by n the total number of airports. (Here, $n = 802$). The model in each airport $i = 1, \dots, n$ is based on the classical SEIR model, which has individuals in one of the epidemiological states: susceptible, exposed, infectious and recovered, with numbers at time t denoted $S_i(t)$, $E_i(t)$, $I_i(t)$ and $R_i(t)$, respectively.

The following are remarks concerning these epidemiological states, in the present context. This discussion will allow us to greatly simplify the model.

Susceptibles represent almost all the population. They are potentially affected by the disease, if subject to an infecting contact.

Exposed (or latent) individuals are susceptibles who have become carriers of the disease. In the case of SARS, estimates of the incubation period (the length of time between infection and the onset of symptoms) vary between 2-10 and 7-10 days, meaning that in any case, the inclusion of a class of exposed individuals is necessary in our model. It is generally assumed that patients in this stage of infection do not transmit the disease.

Infectious individuals actively spread the infection, through contacts with susceptible individuals. Several functions are used to model this transmission, but in the case of large populations such as those traveling through airports, it is generally assumed that *incidence*, the rate of apparition of new cases, takes the form

$$\beta_i \frac{S_i I_i}{N_i}$$

in airport A_i , where $N_i = S_i + E_i + I_i + R_i$ is the population in the airport and β_i is the disease transmission coefficient in airport i . This type of incidence is called *mass action* incidence. The disease transmission coefficient β_i represents the probability that infection occurs, given contact. We allow it to vary from location to location, because factors such as hygiene or social distance play a role in the transmission of the disease.

Recovered individuals are individuals who, having recovered from infection, are immune to reinfection (permanently in the case of an SEIR model, temporarily in the case of an SEIRS model).

Simplifications. Because we are interested in the course of the epidemic over a short time interval of about one year, and that our focus is on the appearance of new cases in new airports rather than the global course of the epidemic, we make a certain number of simplifying assumptions.

First, we suppose that the total population in each airport is large and roughly constant, and that $N_i \approx S_i$, that is, the total number $E_i + I_i + R_i$ is negligible compared to N_i (or S_i). This implies that proportional incidence takes the form

$$\beta_i I_i.$$

Note that this implies that the incidence function, which is typically the only nonlinearity in basic epidemiological models, is linear here; this may not be true for other diseases. It is also not true if the disease is considered on a longer time period, because in this case, $E_i + I_i + R_i$ might increase to such a point that S_i is no longer approximately equal to N_i . Finally, we interpret the class of recovered individuals as in the first meaning it was given [4], in terms of *removed* individuals. Individuals are removed from the I class either by recovery or by death. Individuals in the R class play no role in the short term transmission of the disease, and thus we neglect this class from now on.

These assumptions imply that the only epidemiological states of interest in our model are the E and I classes. Independent of transport between locations, the equations in a

given airport i are

$$\begin{aligned}\frac{d}{dt}E_i(t) &= \beta_i I_i(t) - \alpha E_i(t), \\ \frac{d}{dt}I_i(t) &= \alpha E_i(t) - \gamma_i I_i(t),\end{aligned}$$

where $1/\alpha$ is the mean duration of the latent period, and $1/\gamma_i$ is the mean duration of infection before removal by either death or recovery. (Implicit in this formulation is the assumption that the duration of the latent stage and the infectious stage are both exponentially distributed random variables.) The parameter α is the same in all airports, as it represents a pre-diagnosis disease-specific aspect, and is thus independent of location. On the other hand, the parameter γ_i is influenced by treatment, and thus depends on the location.

Accounting for travel. The model we have described thus far accounts for disease transmission in each location, but does not implement movement between locations. To do this, we consider each airport as a vertex in an undirected graph, and set an edge in the graph between airports A_i and A_j if the database shows a nonzero number of seats between airports A_i and A_j . In airport i and for individuals in epidemiological state X (where X is E or I), we then use an operator

$$\mathbf{T}_i^X(t, \mathbf{X}(t))$$

to describe the travel of individuals, where $\mathbf{X} = (X_1, \dots, X_n)^T$ is the vector of individuals in state X . These operators depend on the type of modelling paradigm used, and are detailed later.

Model equations. In each of the $i = 1, \dots, n$ airports, we use the following equations:

$$\frac{d}{dt}E_i(t) = \beta_i I_i(t) - \alpha_i E_i(t) + \mathbf{T}_i^E(t, \mathbf{E}(t)) \quad (3.1a)$$

$$\frac{d}{dt}I_i(t) = \alpha_i E_i(t) - \gamma_i I_i(t) + \mathbf{T}_i^I(t, \mathbf{I}(t)). \quad (3.1b)$$

4 Deterministic modelling of transport

4.1 The transport operator. In the deterministic model, it is assumed that movement between airports occurs continuously, with the rate of transport of individuals for airport i to airport j equal to $p_{ji}^X X_i$, for individuals in epidemiological state $X = \{E, I\}$. Individuals inbound to airport i arrive at the rate

$$\sum_{j=1}^n p_{ij}^X X_j,$$

where it is assumed for simplicity of notations that $p_{ii} = 0$ for all i . Thus,

$$\mathbf{T}_i^X(t, \mathbf{X}(t)) = \sum_{j=1}^n p_{ij}^X X_j - p_{ji}^X X_i. \quad (4.1)$$

Note that in this case, the transport operator is autonomous. Also, we assume (and this is satisfied by the data provided) that the transport graph is strongly connected, i.e., that any airport can be reached from any other airport in a finite number of steps (flights).

4.2 Model equations. The model equations are thus given, for $i = 1, \dots, n$, by

$$\frac{d}{dt}E_i(t) = \beta_i I_i(t) - \alpha_i E_i(t) + \sum_{j=1}^n p_{ij}^E E_j - p_{ji}^E E_i, \quad (4.2a)$$

$$\frac{d}{dt}I_i(t) = \alpha_i E_i(t) - \gamma_i I_i(t) + \sum_{j=1}^n p_{ij}^I I_j - p_{ji}^I I_i. \quad (4.2b)$$

Non-dimensionalizing time so that $t = \tilde{t}/\alpha$ leads to

$$\frac{d}{dt}E_i(t) = \frac{\beta}{\alpha} I_i(t) - \left[1 + \sum_{j=1}^n \frac{p_{ji}^E}{\alpha} \right] E_i(t) + \sum_{j=1}^n \frac{p_{ij}^E}{\alpha} E_j(t), \quad (4.3a)$$

$$\frac{d}{dt}I_i(t) = E_i(t) - \left[\frac{\gamma}{\alpha} + \sum_{j=1}^n \frac{p_{ji}^I}{\alpha} \right] I_i(t) + \sum_{j=1}^n \frac{p_{ij}^I}{\alpha} I_j(t). \quad (4.3b)$$

Depending on the purpose, we use one of these systems: (4.2) is easier to interpret, making the mathematical analysis easier, while (4.3) is more robust numerically.

4.3 Mathematical analysis. The model (4.2) is a particular case of the models of [1, 2, 3]. Therefore, we do not go into details of the analysis, referring to these papers for precisions.

Grouping disease dependent terms and transportation-dependent terms and writing $\tilde{I} = [I_1 \ I_2 \ \dots \ I_n \ E_1 \ E_2 \ \dots \ E_n]^T$, we can write the above system of $2n$ equations in matrix notation as

$$\frac{d}{dt}\tilde{I} = (D + C)\tilde{I}, \quad (4.4)$$

where the disease dependent matrix D is given by

$$D = \begin{bmatrix} -\frac{\gamma}{\alpha}\mathbb{I}_n & \mathbb{I}_n \\ \frac{\beta}{\alpha}\mathbb{I}_n & -\mathbb{I}_n \end{bmatrix}, \quad (4.5)$$

and the connectivity matrix C is given by

$$C = \begin{bmatrix} P_n^I & \mathbb{O}_n \\ \mathbb{O}_n & P_n^E \end{bmatrix}, \quad (4.6)$$

where \mathbb{I}_n denotes the $n \times n$ identity matrix, and \mathbb{O}_n denotes the $n \times n$ zero matrix. The matrix P_n^I is the $n \times n$ matrix given by

$$P_n^I = \frac{1}{\alpha} \begin{bmatrix} -\sum_j p_{j1}^I & p_{12}^I & \cdots & p_{1n}^I \\ p_{21}^I & -\sum_j p_{j2}^I & \cdots & \vdots \\ \vdots & \vdots & \ddots & \vdots \\ p_{n1}^I & \cdots & \cdots & -\sum_j p_{jn}^I \end{bmatrix}. \quad (4.7)$$

The matrix P_n^E is similar to P_n^I with the superscript I replaced with E .

The first result concerns the asymptotic behavior of the movement problem. A matrix such as (4.7) is singular. However, the analysis can be conducted as explained in [3], by considering the augmented matrix incorporating the total population. This allows us to state the following:

Theorem 4.1 *Assume that there are initially individuals in the system, and that each of the travel matrices is irreducible. Then*

$$\lim_{t \rightarrow \infty} N(t) = N^* \gg 0.$$

Note that it was assumed earlier that the connection graph is strongly connected. The assumption of irreducibility of P_n^E and P_n^I simply translates this fact in matrix terms.

The next step in the analysis is to establish the existence of disease free equilibria (DFE), that is, of equilibria for which $E_i = I_i = 0$ for all $i = 1, \dots, n$. Clearly, setting $E_i = I_i = 0$ for $i = 1, \dots, n$ in (4.2) implies that $E_i = I_i = 0$ remain zero. Thus the DFE of (4.2) is unique and equal to N^* .

Finally, we conclude this brief analysis with considerations on the *basic reproduction number*, \mathcal{R}_0 . The basic reproduction number represents the average number of secondary cases generated in a wholly susceptible population by the introduction of one infective individual. This is a measure of the ability of the disease to spread.

To compute \mathcal{R}_0 , we proceed as in [3], using the method of [5]. We consider only the infected classes E and I , and form the matrices F and V representing new infections and other movements within the infected classes, respectively. Then F takes the form

$$F = \begin{pmatrix} 0 & F_{12} \\ 0 & 0 \end{pmatrix},$$

with

$$F_{12} = \text{diag} (\beta_1, \dots, \beta_n).$$

The matrix V is the block matrix

$$V = \begin{pmatrix} V_{11} & 0 \\ -V_{21} & V_{22} \end{pmatrix},$$

with

$$V_{11} = -P_n^E + \text{diag} \left(\alpha_i + \sum_{j=1}^n p_{ji}^E \right), \quad V_{21} = \text{diag} (\alpha_i),$$

and

$$V_{22} = -P_n^I + \text{diag} \left(\gamma_i + \sum_{j=1}^n p_{ji}^I \right).$$

It can be established as in [3] that V_{11} and V_{22} are $n \times n$ irreducible M-matrices, giving the *next generation matrix*

$$FV^{-1} = \begin{pmatrix} F_{12}V_{22}^{-1}V_{21}V_{11}^{-1} & F_{12}V_{22}^{-1} \\ 0 & 0 \end{pmatrix},$$

and the following result holds.

Theorem 4.2 ([3]) *Let $\mathcal{R}_0 = \rho(FV^{-1}) = \rho(F_{12}V_{22}^{-1}V_{21}V_{11}^{-1})$, with $\rho(\cdot)$ the spectral radius. If $\mathcal{R}_0 < 1$, then the DFE is globally asymptotically stable, whereas if $\mathcal{R}_0 > 1$, the DFE is globally asymptotically unstable.*

4.4 Numerical simulations. For the disease related parameters, we use the following values:

- transmission coefficient $\beta = 0.5$,
- mean incubation period $1/\alpha = 7$ days,
- mean sojourn time in the infectious stage $1/\gamma = 21$ days.

The latter two values are obtained from the literature on SARS. Estimating β is probably one of the hardest tasks in epidemiological modeling, and the value we use is deduced from running the simulation several times and observing realistic spread times. In the case of system (4.2), the p_{ij} represent the strength of the connection between airports i and j . To estimate values, we use the following formula:

$$p_{ij} = \frac{\text{Number of seats between } i \text{ and } j}{\text{Total number of seats (between all airports)}} \tag{4.8}$$

$$= \frac{N_{ij}}{\sum_{i,j} N_{ij}}. \tag{4.9}$$

For example, consider the link from airport 7 to airport 9. The number of available seats is 4,364,182. The total number of seats between all airports is 920,641,841. Therefore, $p_{7,9} = 0.0047404$.

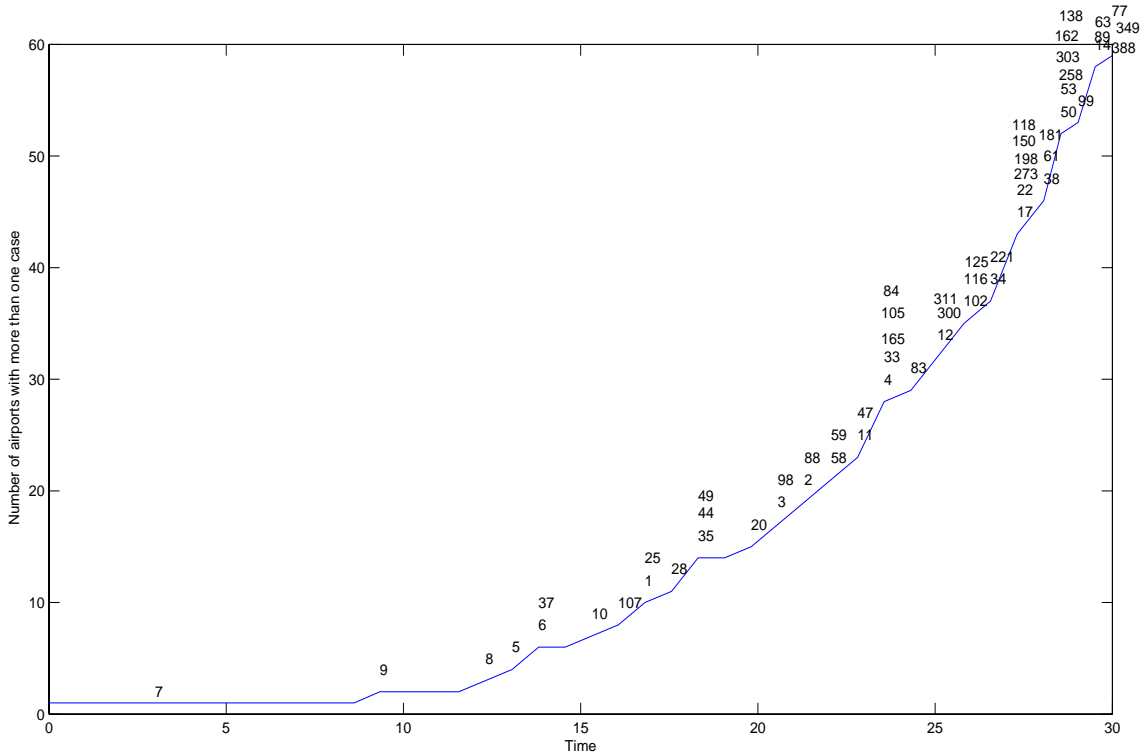


Figure 1 Time of onset of cases in airports for an epidemic initiated in airport 7 (Hong Kong), where the numbers above the curve represent the airports that report their first case at the corresponding time.

Here, we assume that travelers restrain from going to airports where there are known cases. Inbound flows, in airport i , takes the form

$$\sum_{k=1}^{802} p_{ik}^E e^{-cI_i} E_k$$

for exposed, and

$$\sum_{k=1}^{802} p_{ik}^I e^{-cI_i} I_k$$

for infectious. Figure 1 then shows the time of activation of some airports, following an epidemic initiated in airport 7 (Hong Kong). In this figure, we assume that an airport becomes active once the number of cases in that airport becomes larger than 1. For example, we see that after about 10 days, airport 9 becomes active, followed by airports 8, 5, 6 and 37 (the latter two becoming active at the same time).

Comparing the results shown on Figure 1 with the data, we see that over 70% of the airports that become active within the first 30 days of simulation had SARS cases in the data. We also observe that the agreement between simulations and data is better during the initial phase of the simulation (the first 20 days) than later. Indeed, most of the airports becoming active in the simulation, during the first phase, had SARS cases. This proportion then decreases, and most of the airports becoming active in the simulations during the second phase did not have SARS cases in the data. This is easy to understand: the model assumes instantaneous travel between sites. Therefore, a very small time after the simulation is initiated, there are infectives in all patches (since the connection graph is strongly connected), albeit in very small numbers. The initial spread is then governed by the strength of the connections, while the process homogenizes for larger times, with the number of infectives becoming larger (and larger than 1) in most patches.

5 Stochastic modelling of transport

Consider that the travel of individuals is described by the operator

$$\mathbf{T}_i^X(t, \mathbf{X}(t)) = \Delta_T(t) \times \text{a dispersion kernel,}$$

where $\Delta_T(t) = \sum_{k=0}^{\infty} \delta(t - kT)$ is a Dirac comb for the Dirac delta function δ , and T is the period of the movements, e.g., $T = 1$ day if the movement phase is assumed to take place every day. The dispersion kernel then takes the exposed and infective individuals to other patches. An example is the kernel resulting from drawing, at random, a destination among the airports to which an airport has access, with uniform probability density weighted by the volume of the route relative to all routes out of that airport, i.e., with probabilities p_{ij} given as in (4.8).

Preliminary results (not presented here) that were obtained with this model are also quite promising, although they are of course more prone to variability, and thus a larger number of simulations is required in order to deduce some general trends. This will be an area of future study.

6 Conclusions

Due to the limited time imparted to this exercise, it is of course difficult to produce detailed results. However, we are able to draw some positive conclusions. The models developed give remarkably good indications on the future spread of the disease, when it is initiated in the same point of origin as SARS. Thus, even though our approach was extremely simplified, it seems that we can answer questions **Q1** and **Q2** of the introduction by the affirmative. To answer **Q3** is harder: even the deterministic model uses an average approach, because the rates of movement from one airport to another describe the movement of “average individuals”. Further investigations of the stochastic model would probably allow for a more definitive answer to this question. Finally, to answer **Q4** is also difficult; to do so would require the ability to more precisely compare the predictions of our models with the time course of the epidemic, which was not available in our data.

References

- [1] J. Arino, J.R. Davis, D. Hartley, R. Jordan, J.M. Miller, and P. van den Driessche. A multi-species epidemic model with spatial dynamics. *Mathematical Medicine and Biology*, 22(2):129–142, 2005.
- [2] J. Arino, R. Jordan, and P. van den Driessche. Quarantine in a multi-species epidemic model with spatial dynamics. *Mathematical Biosciences*, 2006.
- [3] J. Arino and P. van den Driessche. Metapopulation epidemic models. A survey. *Fields Institute Communications*, 2006.
- [4] W.O. Kermack and A.G. McKendrick. A contribution to the mathematical theory of epidemics. *Proc. Roy. Soc. London, Ser. A*, 115:700–721, 1927.
- [5] P. van den Driessche and J. Watmough. Reproduction numbers and sub-threshold endemic equilibria for compartmental models of disease transmission. *Math. Biosci.*, 180:29–48, 2002.

Mathematical Models of Mother/Child Attachment

Problem Presenters: Leslie Atkinson (Centre for Addiction and Mental Health), Jon Hunter (Mt. Sinai Hospital), Bill Lancee (Mt. Sinai Hospital)

Academic Participants: Lionel Alberti (Université de Nice), Luciano Buono (UOIT), Roger Chau (University of Waterloo), Redhouane Henda (Laurentian University), Andrew King (McGill University), Greg Lewis (UOIT), Neal Madras (York University), Mary Pugh (University of Toronto), Louis Rossi (University of Delaware), Thomas Witelski (Duke University)

Report prepared by: Luciano Buono, Roger Chau, Greg Lewis¹, Neal Madras, Mary Pugh, Louis Rossi, Thomas Witelski

1 Introduction

Attachment theory is a branch of psychology in which the bond between one person with another is studied. Of particular importance is the attachment of a child with her mother.² The form of this attachment will not only affect the ability of the mother to regulate the anxiety of the child, but, also, it has been postulated that the child uses her mother as a secure base from which she can explore her world [1, 2, 9]. Furthermore, the attachment that a child forms with her mother during the first year of her life will not only affect a child’s relationship with her mother, but will affect the attachments she forms with others for the rest of her life.

As part of a larger observational study, Ainsworth developed the “strange situation” laboratory experiment to probe the attachment of a child with her mother [1]. In the experiment, a toddler’s response to her mother and the environment is observed during a series of high and low anxiety situations. Of particular interest, is how the child interacts with her mother to help regulate her anxiety, and the quality of the child’s play and exploration of her new environment.

The strange situation takes place over a period of twenty minutes, and consists of a series of eight episodes: (1) the mother and child enter a laboratory playroom that contains

¹greg.lewis@uoit.ca

²Although, for consistency, we will refer to the child as a female, the theory does not distinguish the sex of the child, and the experiments described in this report involved children of both sexes. Thus, the discussion throughout this report is meant to hold equally regardless of the sex of the child.

toys, (2) a stranger enters the room, and attempts to engage the child, (3) the mother leaves the room for approximately 3 minutes, during which time the stranger attempts to comfort/engage the child if the child appears distressed, (4) the mother re-enters and attempts to comfort the child, (5) the child and mother stay for a time in the room, while the child is once again free to play, (6) after a time, the mother and the stranger leave the room, (7) while the mother is still not present the stranger re-enters the room and attempts to comfort the child, (8) the mother re-enters the room and attempts to comfort the child.

Based on the observations of the experiment, the children are placed into three categories of attachment, (1) secure, (2) avoidant, or (3) ambivalent. The avoidant and ambivalent categories correspond to insecure attachment. Upon first entering the laboratory playroom, a child exhibiting secure attachment will be willing to explore the room, coming back to her mother or glancing at her mother periodically. When the mother returns after her short absence, such a child will seek out her mother, and will subsequently calm down rapidly. Once calm, the child will quickly return to play and exploration of the room. A child exhibiting avoidant attachment will tend not to seek contact with her mother during the first phase when she first enters the room with her mother. However, the quality of play and exploration is not as high as that of the secure child. During her mother's absence, the avoidant child may not show any outward signs of distress, and when the mother re-enters the room, she may not show signs that she has noticed her return. Indeed she may avoid eye contact with her mother. However, the avoidant child will still seek out her mother if she feels a heightened sense of anxiety for a prolonged period of time. Upon initially entering the room, an ambivalent child will tend to hover close to her mother, and will only be willing to explore the new environment very tentatively. Although such a child will seek out the mother upon her return after the short absence, she will not immediately derive comfort from her mother, and may even show outward signs of hostility, such as hitting her mother, or pushing her mother away.

The heart of attachment theory is that the category of attachment in which a child falls is correlated with the history of the mother's response to the child's requests for comfort during times of increased anxiety. As the main part of her study, Ainsworth made home-based observations, noting the quality of a mother's interaction with her child. She found that if a mother consistently responded to her child's call for attention with sensitivity, the child tended to develop a secure attachment. If a mother consistently tended to ignore the child's calls for comfort, the child tended to develop an avoidant attachment. If a mother sometimes responded to her child with sensitivity, and sometimes did not, the child tended to develop an ambivalent attachment.

The presenters of this problem requested the academic participants to develop mathematical models of the decision-making and behaviour that occur when a child is subjected to a stressful episode, e.g. as in the strange situation. The overall goal was to determine the factors that are most relevant in determining the type of attachment the child exhibits toward her mother, and to determine whether these factors are associated with the sensitivity and consistency with which the mother generally responds to the child's requests for comfort and attention. Such a model would shed light on the mechanism by which the mother's behaviour influences the character of her child's attachment to her, and it would provide evidence in support of attachment theory itself.

This report is structured as follows. In Section 2, we use game theory to probe the mother and child's decision making process in the hopes that we can classify the three distinct mother-child behaviours. In Section 3, we develop a dynamical system that models

the relevant features that determine the child’s response to situations of varying levels of stress, e.g. as experienced in the “strange situation.” The goal is to reproduce the distinct dynamics associated with the three different attachment categories as parameters related to the mother’s sensitivity and consistency are varied. Finally, in Section 4, we give a brief introduction to the application of control theory to this problem.

2 Game theory

In this section, we apply game theory to the decision making process of the child and mother. The analysis of payoffs and strategies associated with game theory and the later theory of moves has been used for decades in many fields such as economics, diplomacy, religion, politics and biology (see [3, 6, 15, 16, 18] for overviews and discussion). There are two key ideas that arise from such analyses. The first is that of an equilibrium strategy where both players (in this case for a two-player game) have no incentive to change their strategy and receive a different payoff. The second idea is that of moving or changing strategies. Of the two, the second requires additional assumptions about the rationality, motivations and desires within each player, and some of these can be contested. Needless to say, we will focus on the former and dodge the latter. We will use game theoretic approaches to try and understand how behaviours like “secure”, “ambivalent”, and “avoidant” emerge as equilibrium choices for the child, given her upbringing. We focus on the situation immediately after the mother has returned to the room. At this moment, the child must decide whether or not to approach her mother to seek comfort. At the same time, the mother must decide whether or not to attend to the child.

2.1 A one-person game. First, we describe the simplest possible game. Here, the child has to choose what to do (what “strategy” to use) given the situation she’s been presented with. This corresponds to the clinical observation that the mother’s behaviour is independent of the child’s. To start, we define the game. This requires modelling the situation, modelling the child’s strategies, and constructing a payoff matrix for the child. Strictly speaking, this scenario is an optimization problem for the child rather than a game theoretic problem because only the child is playing; however, we shall use the game-theoretic language throughout this section.

When her mother re-enters the room, the child is anxious because she’d been left alone with a stranger for two minutes. The mother has two possible strategies: to attend to her child or to ignore her. The mother executes these strategies with probability $\vec{q} = (q, 1 - q)$ where $0 \leq q \leq 1$. If $\vec{q} = (1, 0)$ then the mother is the Perfect Mother: unfailingly attentive. If $\vec{q} = (0, 1)$ then the mother is made of stone. Real mothers would have $0 < q < 1$. Whether or not the mother attends in a particular instantiation of the game would be determined by the flip of a q -weighted coin.

In a one-person game, the player (the child) knows what her opponent (the mother) will do and needs to choose a response. Given this information, the child has to choose a strategy (choose an action). For each possible strategy the payoff is the amount of comfort she would receive — the amount that her anxiety would be reduced — should she choose that strategy. In using a one-person game as a model, we are bearing in mind that the mother and child come to the experiment with a long history of prior stressful situations. The child already has a measure of her mother — she knows her mother’s \vec{q} .

2.1.1 A child with two choices. We first consider a model in which the child has only two choices: to go to her mother seeking comfort or to not to go. The child’s payoff matrix

		Mother's action	
		Attend	Ignore
Child's action	Go	1	$-s$
	Don't Go	0	0

Table 1 The child's payoff matrix for the one-person game in which she has two choices.

is given in Table 1. We have normalized the payoffs by the amount of comfort or stress reduction the child receives when she seeks comfort and her mother attends to her. Thus, it is possible for the value in the upper left to be -1 in the pathological case where the mother comforting the child *raises* the child's stress level. When the child seeks comfort but her mother ignores her, the payoff is $-s$. If the child is stressed by such rejection, then $s > 0$. If she would be comforted by being close to her mother, even if she is being ignored, then $s < 0$. We do assume that $s > -1$: being ignored by her mother provides less comfort than if her mother attends to her. Finally, if the child does not go to her mother for comfort then she receives no comfort, whether or not her mother attends to her.

The model has two parameters: q and s . These reflect the parenting strategy and the quality of the mother-child interaction, respectively.

Since the model is a one-person game, the optimal strategy will be a pure strategy: the child will always go to her mother or will never go to her mother. This is to be contrasted with a "mixed" strategy in which the child would go to her mother with probability p where $0 < p < 1$.

If $s \leq 0$ then "Go" is a dominant strategy: no matter what the mother does, the child is better off seeking comfort than not. If $s > 0$ then there is no dominant strategy. What the child chooses to do will depend on the values of q and s .

Assume $s > 0$. The child's expected payoffs are

$$\begin{aligned} P_{\text{Go}} &= q - (1 - q)s, \\ P_{\text{Don't Go}} &= 0. \end{aligned}$$

This means that if the child always plays "Go" then after many plays of the game, the average payoff per game will be approximately P_{Go} and the more times the game has been played, the closer the average payoff will be to P_{Go} . We see $P_{\text{Go}} > P_{\text{Don't Go}}$ if and only if $s < q/(1 - q) =: s_{\text{crit}}$.

At first sight, it seems odd to imagine that the child plays this game many times (which is required in order to use P_{Go} and $P_{\text{Don't Go}}$ to analyze the child's options.) Indeed, if one only counts the number of times that the child goes through the "Strange Situation" protocol then it would be unusual. We suggest, however, that the mother and child played this game many times before they reached the laboratory situation — every time the child cried out for food, a fresh diaper, reassurance, or entertainment. The "Strange Situation" protocol is designed to try and extract the essence of these interactions, rather than being a completely novel situation. And so we view it as yet another play of a game played many times before. Secondly, it may seem odd to imagine that a child is capable of statistical thinking. It is our understanding that children as young as six months old have demonstrated statistical inference in early language acquisition.

If the child seeks comfort but is ignored this causes her stress s . If this stress is less than s_{crit} then she is better off seeking comfort and risking stress than not — her strategy

is always “Go”. If $s > s_{\text{crit}}$ then her optimal strategy is always “Don’t Go”. If $s = s_{\text{crit}}$ then it doesn’t matter what she does; on average she will have zero stress reduction whether she chooses “Go” or “Don’t Go”.

It remains to understand how the parenting strategy, q , determines s_{crit} . If the mother is unfailingly attentive ($q = 1$) then the child should always seek comfort because $P_{\text{Go}} > P_{\text{Don't Go}}$ no matter what the value of s . If the mother is never attentive ($q = 0$) then the child should never seek comfort because $P_{\text{Go}} < P_{\text{Don't Go}}$ (recall that we’ve assumed $s > 0$). If the mother is generally quite attentive then q is close to 1 and s_{crit} is large. This means that the child can have a relatively large stress response to rejection (s) but still be better off always seeking comfort because the chances of rejection are relatively low. Similarly, if the mother is generally inattentive then q is close to 0 and s_{crit} is small. This means that only the thick-skinned child would be better off choosing “Go” — only a child with a low stress response to rejection can afford the risk.

If q and s are such that $s > s_{\text{crit}}$ then we would say the child is “avoidant” and observe that there is no stress mediation because the child’s expected payoff is 0. If $s < s_{\text{crit}}$ then the child is either “secure” or “ambivalent”. In both of these behaviours, the child goes to her mother for stress reduction.

We finish our discussion by noting that in practise one would not expect the child’s stress response, s , to be independent of the mother’s parenting strategy q . This, in turn, makes it hard to predict what the child’s behaviour will be. If the mother is reliably attentive then s_{crit} would be large and one might expect the child to be secure. But one might also expect the child of such a reliably attentive mother to be truly stressed out should her mother not attend to her: her s could be quite large and might exceed s_{crit} . Similarly, if the mother is not at all reliable in her attentiveness then s_{crit} would be close to zero. But one might also expect the child of such a mother to have become quite thick-skinned: her s could be quite small. We also note that the child’s stress response will also have a biological component, one that is not caused by her upbringing. Different people have different pain thresholds and sensitivities; this would certainly enter into the child’s value of s . This biological component would provide a lower bound on the child’s s value. As a result, it provides a threshold for how unreliable the child’s mother could be: if q becomes too close to zero then s_{crit} will be less than the biological component of the child’s stress response and the child will be avoidant no matter what.

2.1.2 A child with three choices. We now consider what might happen if the child had a third strategy, one of guarded behaviour.

From the video footage, the ambivalent child is observed to approach her mother for comfort, and yet is not entirely willing or able to accept full comfort. For example, we see the child asking to be picked up, but holding a hand between herself and her mother, as if making sure that her mother does not get too close. At mildly stressful times, the child stays close to the mother but does not interact with her. We call this the “Half-Go” action: the child is making a guarded request for comfort. If the child chooses the “Half-Go” action and her mother attends to her then she gets some reduction of stress, but not as large a reduction had she approached in an unguarded manner. On the other hand, if her mother ignores her, then she is not as upset as she would have been had she approached in an unguarded manner. And so, the payoffs for the “Half-Go” strategy would be somewhere between the payoffs for the “Go” and “Don’t Go” strategies.

The child’s payoff matrix is shown in Table 2. The payoffs for the “Go” and “Don’t Go” strategies are as before (Section 2.1.1). If the child half-goes to the mother for comfort

		Mother's action	
		Attend	Ignore
Child's action	Go	q	$1 - q$
	Don't Go	1	$-s$
	Half-Go	0	0
		h	$-t$

Table 2 The child's payoff matrix for the one-person game in which she has three choices.

and her mother attends to her, then her payoff is h where $0 < h < 1$. If she half-goes to her mother and is ignored, then her payoff is $-t$. As before, there are two cases for the sign of t . If $t < 0$ then she receives comfort from being around her mother even if her mother ignores her; in this case, we assume $-1 < s < t < 0$. If $t > 0$ then she is stressed by her mother's ignoring her; in this case, we assume $0 < t < s$.

Is it ever rational for the child to choose this new strategy? As before, if $t \leq 0$ then "Go" is a dominant strategy. No matter what the mother does, the child should never choose "Half-Go" or "Don't Go".

We now consider the $0 < t < s$ case, for which there is no dominant strategy. If the child plays the game many times, always choosing the same option, then her expected payoff will be one of

$$\begin{aligned} P_{\text{Go}} &= q - (1 - q)s, \\ P_{\text{Don't Go}} &= 0, \\ P_{\text{Half-Go}} &= hq - (1 - q)t. \end{aligned}$$

Figure 1 gives the graphs of these expected payoffs as a function of q . In both plots, the

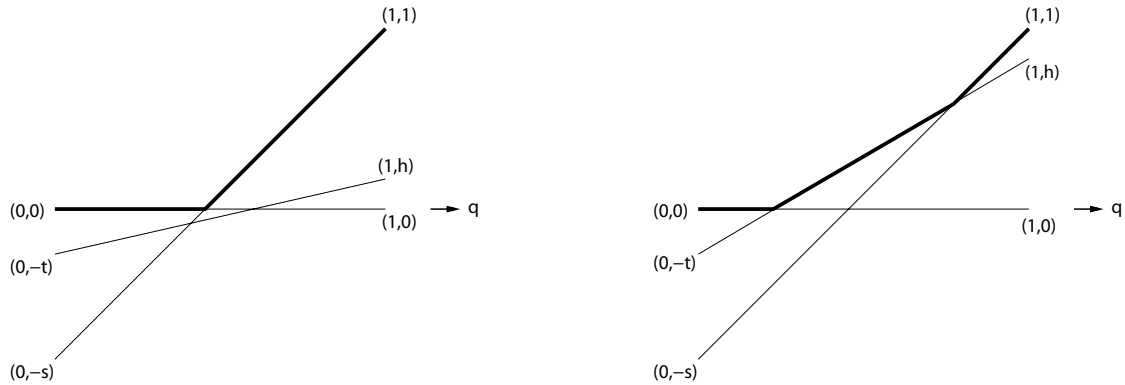


Figure 1 The lighter lines are the graphs of the expected payoffs P_{Go} , $P_{\text{Half-Go}}$, and $P_{\text{Don't Go}}$ for the one-person game with the payoff matrix given in Table 2. The heavy curve is the maximum expected payoff. Left: $h < t/s$, Right: $h > t/s$.

line connecting $(0, -s)$ to $(1, 1)$ is the graph of P_{Go} , the line connecting $(0, -t)$ to $(1, h)$ is $P_{\text{Half-Go}}$, and the line connecting $(0, 0)$ to $(1, 0)$ is $P_{\text{Don't Go}}$. The heavy curve is the graph of the maximum expected payoff — this curve gives the child's optimal strategy for each value of q . Either there are two optimal behaviours possible, as in the left plot of Figure 1, or there are three, as in the right. To distinguish between these situations, one finds that

the graphs of P_{Go} and $P_{Half-Go}$ intersect at (q_c, P_c) where $q_c = (s - t)/(1 - h + s - t)$ and $P_c = (sh - t)/(1 - h + s - t)$. If $h < t/s$ then $P_c < 0$ and there are only two possible optimal strategies: whatever the value of q , $P_{Half-Go}$ is always less than either P_{Go} or $P_{Don't Go}$. If $h > t/s$ then $P_c > 0$ and there is an interval of q values for which the “Half-Go” strategy is optimal. The balance between h and t/s reflects the balance between the decrease of comfort received when a guarded request is attended to ($h/1$) and the decrease in stress caused when a guarded request is ignored (t/s).

Here is a way to view the condition for viability of the “Half-Go” strategy. Consider a mixed strategy of “Go” and “Don’t Go” for the child, which we shall call “Random-Go”, designed to offer the same average level of comfort to the child as does “Half-Go” *in those cases when the mother attends*. That is, the child chooses “Go” with probability h and chooses “Don’t Go” with probability $1 - h$. When the mother attends, the payoff to the child is $1 \cdot h + 0 \cdot (1 - h) = h$, which is the same as for “Half-Go”. How does “Random-Go” compare overall with “Half-Go”? When the mother ignores, the child’s payoff under “Random-Go” is $-s \cdot h + 0 \cdot (1 - h)$, which equals $-sh$. On the one hand, if $-sh$ is better than the payoff under “Half-Go”, $-t$, then it can be seen that “Random-Go” dominates “Half-Go”. That is, if $-sh > -t$ (equivalently, if $h < t/s$), then the child will never want to use the “Half-Go” strategy. On the other hand, if $h > t/s$, then “Half-Go” dominates “Random-Go”; indeed, it turns out that for some values of q , “Half-Go” is better than any mixed strategy that combines “Go” and “Don’t Go”. If “Random-Go” had been designed to offer the same average level of comfort to the child as does “Half-Go” in those cases when the mother ignores, then one would find that the child would choose “Go” with probability t/s and one would come to the same conclusion about $h < t/s$ and $h > t/s$.

In Section 2.1.1, we analyzed the game in terms of the child’s stress response, s , relative to a critical stress level, $s_{crit} = q/(1 - q)$. In doing this, we had taken the parenting strategy, q , as fixed. We also took as fixed the child’s stress reduction when she sought attention and her mother attended to her. This was a little less obvious because it was reflected in the 1 in the payoff matrix of Table 1. In fact, this was originally a free parameter that became 1 when it was used to normalize the entire payoff matrix.

If the child has three options, there are five parameters: q (the parenting strategy), 1 and h (the stress reductions when attended to), and s and t (the increases in stress when requests for comfort are ignored). In Figure 2 we hold q , 1, and h fixed and find that the threshold behaviours for s and t are determined by s_{crit} and hs_{crit} . In the plot to the left, we have taken $h = 1/3$, but we get the same qualitative picture as long as $0 < h < 1$. In this case, the region $0 < t < s$ is divided into three regions, with one strategy being optimal in each region. To better understand the situation, we consider the extremal cases of $h = 0$ and $h = 1$. As h decreases to 0, the points A and B converge to the point $(s_{crit}, 0)$ and “Half-Go” is no longer an optimal strategy. The resulting $h = 0$ plot is shown in the top right of Figure 2. The reason for the disappearance of “Half-Go” is apparent if one looks at the left plot of Figure 1: as $h \rightarrow 0$, the point $(1, h)$ moves down to $(1, 0)$ and $P_{Half-Go}$ will always be less than $P_{Don't Go}$, whatever the values of s and t . (This can also be seen directly from the payoff matrix.) At the other extreme, as h increases to 1, the points A and B converge to the points $(0, 0)$ and (s_{crit}, s_{crit}) respectively and “Go” is no longer an optimal strategy. The resulting $h = 1$ plot is shown in the bottom right of Figure 2. One can either understand this by taking $h \rightarrow 1$ in the right plot of Figure 1 or by noting that if $h = 1$ in the payoff matrix in Table 2 then the “Half-Go” strategy dominates the “Go” strategy, whatever the values of s and t (with $s > t$).

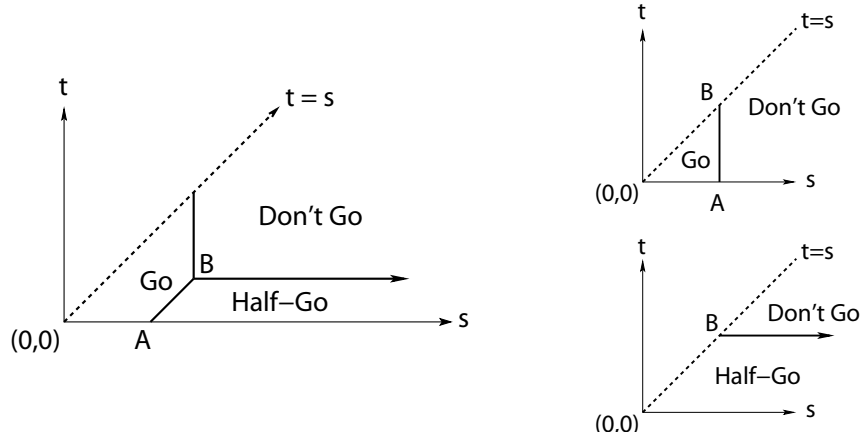


Figure 2 In all three plots, the dashed line reflects the bound $t < s$. The points A and B are $((1 - h)s_{\text{crit}}, 0)$ and $(s_{\text{crit}}, hs_{\text{crit}})$ respectively. Left: $h = 1/3$. There are three regions, with one strategy being optimal in each region. Right: There are only two possible optimal strategies. Top: $h = 0$. Bottom: $h = 1$.

2.2 A Two-Person Game. In using our one-person game as a model, we took the mother’s parenting strategy as fixed and known to the child. We now take into account that attending to the child is at a cost to the mother and that she might choose her strategy in a way that reflects both this cost and what she thinks her child might do. To do this, we use a two-person game with two payoff matrices, one for the child and one for the mother. It should be noted that notions like “optimality” may not be appropriate in multiplayer games where dominating strategies can cycle (see [18] for a broad overview and discussion). For instance, strategy A may dominate B meaning that A will always yield a payoff greater than strategy B . But, C may dominate A and B may dominate C . As we shall see, some situations in the game model yield dominant strategies for both players, and some will not.

As in Section 2.1, the mother executes her options, “Attend” and “Ignore”, with the strategy $\vec{q} = (q, 1 - q)$ where $0 \leq q \leq 1$. If $q = 0$ or 1 then \vec{q} is called a “pure” strategy and otherwise is called “mixed”. Similarly, the child executes her options, “Go” and “Don’t Go”, with the strategy $\vec{p} = (p, 1 - p)$. Whether or not the child seeks comfort from her mother in a particular instantiation of the game is determined by the flip of a p -weighted coin.

		Mother’s action	
		Attend	Ignore
Child’s action	Go	p	$(1, 1 - c)$
	Don’t Go	$1 - p$	$(0, -c)$

Table 3 The payoff matrices for the two-person nonzero-sum game. For each combination of choices, the payoff is represented as an ordered pair. The child’s payoff is the left element of the ordered pair and the mother’s payoff is the right element. For instance, if the child goes to the mother and the mother attends, the child’s payoff is 1 and the mother’s is $1 - c$.

Table 3 gives the payoff matrices for the child and her mother. The child's payoff matrix is the same as in Section 2.1.1. The mother's payoff matrix reflects two things. First, whatever increase or decrease there is in the child's stress levels is also a gain or a loss for the mother, hence the 1 and the $-s$ in the mother's payoff matrix. In other words, we assume the mother accurately interprets the child's responses to attention and develops her strategy accordingly. In addition, attending to her child takes energy and takes time away from some other activity she might prefer doing, hence the $-c$ in the payoff matrix.

To analyze the game, we use concepts from the non-cooperative theory of nonzero-sum games. The mother-child game is considered non-cooperative because the players are unable to make a binding agreement on a joint choice of strategy. Using Table 3, we can construct the individual payoff matrices for the players. Each entry of the matrix is an ordered pair. The child's payoff is the first element of each ordered pair, and the mother's payoff is the second element. We denote the child's payoff matrix by A and the mother's payoff matrix by B , so

$$A = \begin{bmatrix} 1 & -s \\ 0 & 0 \end{bmatrix}, \quad B = \begin{bmatrix} 1-c & -s \\ -c & 0 \end{bmatrix}. \quad (2.3)$$

If the players play the strategies \vec{p} and \vec{q} then the child's payoff is $\vec{p}^T A \vec{q}$ and the mother's payoff $\vec{p}^T B \vec{q}$. This is not a zero-sum game where "money" into one player's pocket comes out of the other player's pocket: $A \neq -B$. Our discussion will focus on the payoffs for Nash equilibria, which are pairs of strategies where a unilateral change in strategy will not improve the player's payoff *even if the player knows the opponent's strategy*. One interesting difference between zero-sum games and nonzero-sum games is that in a zero-sum game, if there are two Nash equilibria (\vec{p}, \vec{q}) and (\vec{p}^*, \vec{q}^*) then their payoffs are the same: $\vec{p}^T A \vec{q} = \vec{p}^{*T} A \vec{q}^*$. We will see below that because the mother-child game is nonzero-sum, one can have two pairs of Nash equilibria which have different payoffs.

To simplify the game further, we can reduce the payoffs into broad categories where we replace the values of the payoff with an integer from best (4) to worst (1) denoting the relative size of the payoff to either the mother or the child. For instance, if $-s < 0$, the ordinal representation for the child's payoff is always $\begin{bmatrix} 4 & 2 \\ 3 & 3 \end{bmatrix}$. The same information could

be presented as $\begin{bmatrix} 3 & 1 \\ 2 & 2 \end{bmatrix}$ because decisions are based on the relative payoffs; the relative order of the elements is the critical feature. We classify all possible outcomes using a binary tree representation where each branch corresponds to a comparison between entries. In the case where s is negative, we assume that $-s < 1$ because should the child approach her mother, it would only make sense for the payoff to be greater if the mother pays attention than if she did not. Type I and II is distinguished by whether $0 < -s < 1$, branching left, and $0 > -s$, branching right. Similarly, subtypes A and B are distinguished by $1 - c < -s$, branching left and $1 - c > -s$, branching right. Sub-types 1 and 2 are distinguished by $1 - c < 0$ and $1 - c > 0$, branching left and right, respectively. Finally, sub-sub-types "a" and "b" are distinguished by $-c < -s$ and $-c > -s$, branching left and right, respectively. The full classification is shown in Figure 3. In some cases, the ordinal representation is the same for all sub-subtypes. In these cases, "Type I B" refers to all subordinate "Type I B 1 a," "Type I B 1 b," etc...

We show all eight payoff configurations in Figure 4 grouped into four broad categories by the positions of the Nash equilibria.

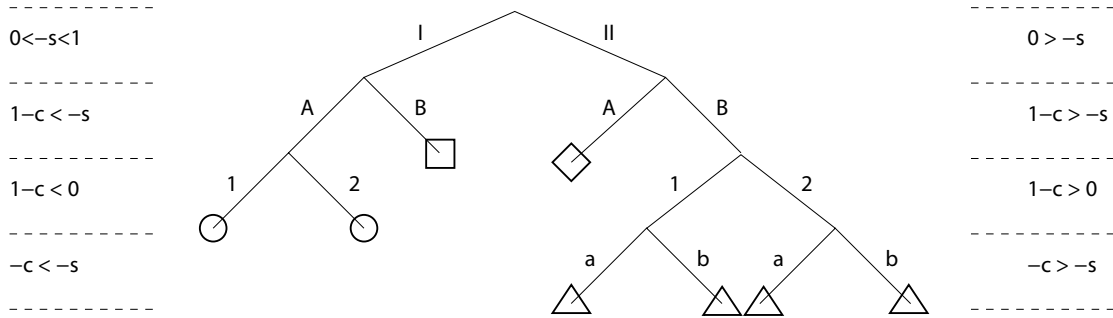


Figure 3 A diagram of possible parameter configurations for the payoff matrix given in Table 3. Every terminal node is a distinct configuration. Terminal nodes are coloured by groups listed in Figure 4: Group 1 (circles), Group 2 (square), Group 3 (diamond) and Group 4 (triangle).

Group 1:

(4,2)	(3,4)	(4,3)	(3,4)
(2,1)	(2,3)	(2,1)	(2,2)
Type I A 1		Type I A 2	

Group 2:

(4,4)	(3,3)
(2,1)	(2,2)
Type I B	

Group 3:

(4,2)	(2,3)
(3,1)	(3,4)
Type II A	

Group 4:

(4,3)	(2,2)	(4,3)	(2,1)	(4,4)	(2,2)	(4,4)	(2,1)
(3,1)	(3,4)	(3,2)	(3,4)	(3,1)	(3,3)	(3,2)	(3,3)
Type II B 1 a		Type II B 1 b		Type II B 2 a		Type II B 2 b	

Figure 4 The payoff matrices in Table 3 can be reduced to four general categories. Nash equilibria are indicated in bold.

For all Type I scenarios where $0 \leq -s \leq 1$, the first row of the child’s payoff matrix is greater than the second row. Thus, the “Go” strategy dominates the “Don’t Go” strategy and the child should always play “Go”. The mother should choose whichever option is better for her, “Ignore” or “Attend”. In the first grouping in Figure 4, it is better for her to “Ignore” and in the second group it is better for her to “Attend”. In the third group, the mother’s “Ignore” strategy is dominant for Type II A scenarios. Given this situation, the child is always better off with “Don’t Go”. The remainder of our discussion focuses on the Type II B configurations. This famous game is often referred to as The Battle of the Sexes

(see [3] for example, for a discussion of many interpretations). In fact, Bernard applies this game to marriage counselling in [4] in a context very similar to attachment.

A pair of strategies, (\vec{p}^*, \vec{q}^*) , is called a Nash equilibrium if neither player can obtain a higher payoff by unilaterally changing her strategy — if she knew her opponent’s strategy and her opponent could not change her strategy, would she then change her own strategy? Nash equilibria occur when,

$$\begin{aligned} \vec{p}^{*\text{T}} A \vec{q}^* &\geq \vec{p}^{\text{T}} A \vec{q}^* && \text{for all probability vectors } \vec{p}, \\ \vec{p}^{*\text{T}} B \vec{q}^* &\geq \vec{p}^{*\text{T}} B \vec{q} && \text{for all probability vectors } \vec{q}. \end{aligned}$$

Because neither player would switch her strategy unilaterally, the players can move away from a Nash equilibrium only through some form of cooperation or intervention.

It is easy to find all Nash equilibria that are pure strategies. If $A_{i_0 j_0}$ is greater than or equal to all other entries in the j_0 column of A and if $B_{i_0 j_0}$ is greater than or equal to all other entries in the i_0 row of B then the pure strategies (\vec{p}^*, \vec{q}^*) with $p_{i_0} = 1$ and $q_{j_0} = 1$ are Nash equilibria. Doing this, we find that our two-person game has two Nash equilibria. First, there is $p = 0$ and $q = 0$ (“Don’t Go” and “Ignore”) where the payoff to each player is 0. Second, there is $p = 1$ and $q = 1$ (“Go” and “Attend”) where the payoff to the child is 1 and the payoff to the mother is $1 - c$.

There is another Nash equilibrium that is easy to find: (\vec{p}^*, \vec{q}^*) where both \vec{p}^* and \vec{q}^* are “equalizing” strategies. An equalizing strategy is one that gives the same expected payoff to your opponent, no matter what your opponent does. (Note that you need to know your opponent’s payoff matrix in order to find your equalizing strategy.) The child seeks a strategy \vec{p}^* such that

$$(\vec{p}^{*\text{T}} B)_1 = (\vec{p}^{*\text{T}} B)_2 \implies p^* - c = -sp^*,$$

and the mother seeks a strategy \vec{q}^* such that

$$(A \vec{q}^*)_1 = (A \vec{q}^*)_2 \implies (1 + s)q^* - s = 0.$$

The child’s equalizing strategy is $p = c/(1 + s)$ and the mother’s is $q = s/(1 + s)$. (This Nash equilibrium only applies to Group 4 scenarios because p and q are probabilities having a range of $[0, 1]$.) The child’s expected payoff is 0 and the mother’s expected payoff is $-cs/(1 + s)$. If $c > 0$ or $s > 0$ this Nash equilibrium is a pair of mixed strategies and is therefore distinct from the two Nash equilibria corresponding to pure strategies.

It is not hard to check that these three are the only Nash equilibria in this game, but dominating strategies, strategies maximizing the payoffs for the individual players, vary depending upon parameter values.

Now, we can summarize the behaviours that would result from the four types of games in the two-player model shown in Figure 4.

- Group 1:** There is only one Nash equilibrium, the pure strategy pair “Go” - “Ignore”. This would appear as a secure relationship because the mother regulates the child’s stress, even though the mother is ignoring the child.
- Group 2:** There is only one Nash equilibrium, the pure strategy pair “Go” - “Attend”. This would appear as a secure relationship as well.
- Group 3:** There is only one Nash equilibrium, the pure strategy “Don’t Go” - “Ignore”. This is an avoidant relationship.

Group 4: There are three Nash equilibria, two pure pairs “Go” - “Attend” and “Don’t go” - “Ignore” as well as the mixed, equalizing strategy. The first two correspond to secure and avoidant relationships just as in the scenarios in Groups 1-3. Unlike the other scenarios, one of the players receives the best possible payoff and the other player receives a payoff that is less than the best possible payoff. This could lead to resentment if the players are non-myopic, meaning the mother and child are capable of understanding the outcomes of other combinations of decisions. The mixed, equalizing strategy has the qualities of an ambivalent relationship. The probability that the child seeks comfort is proportional to c so the more it costs the mother to attend, the clingier the child will be. Likewise, the probability that the mother attends to the child is proportional to s . The more stress the child experiences by rejection, the more likely the mother is to provide comfort.

We have identified equilibrium configurations in the two-player model for mother-child interactions. We have not gone further to hypothesize how mother and child move from one strategy to another because such speculations would go well beyond anything we could defend for two reasons. One, we have no psychological data on how the subjects formulate or adjust their strategies. Two, the mathematical theory of determining equilibria in game theory is quite simple when compared to what is known about formulating strategies based on these equilibria. For instance, on page 359, McKinsey points to a payoff matrix qualitatively equivalent to our Group 4 scenarios, and points out that “It must be remarked that Nash’s theory ... has serious inadequacies and certainly cannot be regarded as a definitive solution of the conceptual problems in this domain... The theory of Nash seems to throw little light on the question of how to play a game having such a pair of payoff matrices” [16]. Certainly, one can argue that pure strategies explain the existence of secure and avoidant relationships, and that once these strategies are employed, it would be irrational for either the mother or child to change unilaterally in certain parameter regimes in Groups 1-3 regimes. The dynamics underlying situations like Group 4 are the subject of continued investigation and deliberation. For instance, Steven Brams offers one model for negotiated solutions in ordinal games called the Theory of Moves to find non-myopic equilibria that avoid cycling or to determine a unique resolution for both players [6, 7, 8, 13]. In our model, the mixed strategy has features resembling an ambivalent relationship. While the process by which the strategies of the mother and child evolve over time remains fertile ground for investigation, we see that this simple two-player, non-cooperative game with two simple parameters yields a rich mathematical structure that recovers three principal attachment behaviours observed in clinical experiments.

3 A dynamical systems approach

The “strange situation” experiment was designed to help examine a child’s relationship with her mother under some stressful conditions. In particular, the experiment can be used to examine the mother’s ability to down-regulate the anxiety of her child. The source of the anxiety in the experiment is due to the mother leaving the room. The child’s reaction to the mother’s return to the room is very telling of the child’s type of attachment to her mother, and how much comfort and security she derives from her mother. In particular, children’s response to this situation correlates well to their general modes of behaviour, described in Section 1.

To attempt to mathematically model and distinguish these behaviours we must consider some measurable quantity available from the data of the experiment. One such quantity is the physical distance between the mother and the child. However, physical distance is not necessarily a sufficient indicator of the child's ability or need to derive comfort from her mother, because, for instance, visual contact may serve the same purpose. Thus, we consider instead "emotional distance". This concept along with a deterministic model that gives the time evolution of this quantity, will be described in detail in Section 3.2. Another measurable quantity of interest is the child's level of anxiety. In the following section, we consider a simplified model that temporarily ignores the distance to focus on the child's anxiety level as a function of time, $A(t)$.

3.1 The anxiety equation. In this section we derive an equation giving the evolution of the anxiety A . Details of the definition of anxiety are left open as some aspects may be specific to different situations, but generally an increase in anxiety will imply a decrease in comfort and feelings of well-being. The anxiety level may be measured using some externally visible measure of the child's comfort or emotional state, although this may be difficult, or, perhaps more quantitatively, via physiological variables such as heart rate or the level of cortisol in the child's saliva. The base-line of anxiety may be determined by considering the child in a familiar situation, say at home with the mother.

As a first version for the equation describing the evolution of anxiety, we write

$$m \frac{d^2 A}{dt^2} + b \frac{dA}{dt} + \frac{1}{r} (A - \bar{A}) = S(t), \quad A(t=0) = \bar{A}, \quad A'(0) > 0. \quad (3.1)$$

Here $S(t) \geq 0$ is a function describing the externally imposed stress on the child; in particular we take it to be an indicator function of the times when the mother is absent, see Figure 5(left). The initial anxiety is assumed to be the baseline level with a tendency for increasing anxiety (positive slope) due to entering an unfamiliar environment.

The parameter m is a measure of the maturity or emotional stability of the child. The parameters r and b determine how the child recovers to her baseline emotional state after a temporary stressful situation. The parameter b is related to the insensitivity of the mother to the child's needs, while the parameter r corresponds to a notion of mother-child distance. The parameter r is in fact related to the ability of the mother to down-regulate the child's anxiety, and is likely to change depending on the immediate situation, and thus, in Section 3.2, we will consider it as a variable and derive an equation to model its time evolution. These parameters and their interpretation are discussed further in the following sections.

This model is analogous to a mechanical system describing a damped-driven harmonic oscillator, a classic problem considered in basic control theory [11]. In such a system, m is the mass, b is a damping coefficient, $1/r$ is a spring constant for a linear restoring force and $S(t)$ is an external driving force. The motivation for this model is that for some parameter values, the anxiety following the stress-event can be sustained (with slow decay) near the peak induced anxiety, while for other values, the anxiety can rapidly decay. This is in agreement with the observed behaviours for insecure (ambivalent and avoidant) and secure infants respectively.

The fact that (3.1) is a linear equation is also convenient because an analytic solution is possible:

$$A(t) = c_1 e^{\lambda_1 t} + c_2 e^{\lambda_2 t} + A_p(t), \quad (3.2)$$

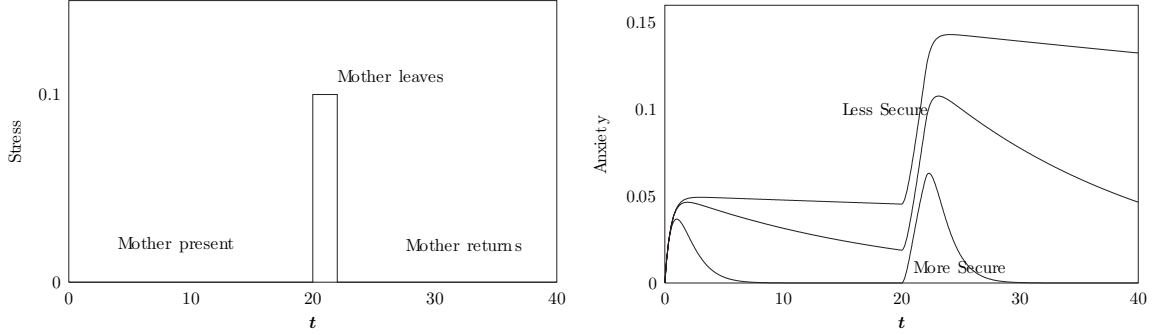


Figure 5 (Left) Stress generated by the temporary absence (3 minutes) of the mother, (Right) Anxiety response generated by (3.1) with m, b fixed for different values of r (the rate of anxiety decay is inversely related to r). An increase in r corresponds to an increasingly less secure anxiety response.

where c_1 and c_2 are constants that depend on the initial conditions, the eigenvalues λ_i are given by

$$\lambda_{1,2} = \frac{-b}{2m} \left[1 \pm \sqrt{1 - \frac{4m}{rb^2}} \right], \quad (3.3)$$

and $A_p(t) = r\bar{S} + \bar{A}$ is a particular solution that must be included when an imposed stress is present (i.e. when the equation is inhomogeneous; see, e.g., [5]). A mathematical artifact of (3.1) that is inappropriate for a model of anxiety is that oscillatory solutions are possible if the parameters are in the “under-damped” regime [5]. To exclude this possibility, we must be in the “over-damped” regime, and thus we require that the parameters satisfy

$$rb^2 > 4m. \quad (3.4)$$

That is, our model is valid when m is small, i.e. when the child has little ability to self-regulate her anxiety, which is expected to valid for children of the ages that are considered.

Given the assumption (3.4), if $b, r > 0$, unforced solutions will exhibit only exponentially decaying modes, dominated by the slowest decaying mode:

$$\lambda_2 = -\frac{b}{2m} \left[1 - \sqrt{1 - \frac{4m}{rb^2}} \right] \sim \begin{cases} -1/br & \text{if } rb^2 \gg 4m \\ -b/(2m) & \text{if } rb^2 \sim 4m \end{cases} \quad (3.5)$$

In Figure 5(right), we present a simulation of (3.1), for a stress profile, given on the left hand side of the figure, that mimics that of the strange situation. That is, the induced stress is zero before the mother leaves the room, jumps to a high constant value while the mother is absent, and again drops to zero when the mother returns. The different anxiety profiles are produced by varying the parameter r while the other parameters are held fixed. As r is increased, it can be seen that (1) the steady state of anxiety increases, and (2) that the rate of decay of anxiety decreases, in particular, the rate decay is inversely related to r .

We conclude this section with a nonlinear generalization of (3.1),

$$\frac{d}{dt} \left(m \frac{dA}{dt} \right) + [\rho^2 A^2 + b] \frac{dA}{dt} + \frac{1}{r} [(A - \bar{A})_+]^\beta = S(t). \quad (3.6)$$

The changes in this model allow for possible effects not considered in (3.1):

- The damping term (i.e., the second term on the left hand side) has been generalized to be of van der Pol type for $\rho > 0$. In this case the damping will increase with increasing anxiety, and thus the larger the child’s anxiety becomes the more difficulty the child will have in recuperating.
- Finally, the restoring force (i.e. the third term on the left hand side) has been generalized to describe a nonlinear stress-anxiety (emotional strain) response parametrized by the exponent β . Three regimes are

$$\begin{cases} 0 < \beta < 1 & \text{“Hard case”}: \text{a child with a higher tolerance for stress} \\ \beta = 1 & \text{“Linear”}: \text{direct proportional response to stress} \\ \beta > 1 & \text{“Soft case”}: \text{a child more likely to develop high anxiety} \end{cases} \quad (3.7)$$

A series of simulations indicating these three cases is shown in Figure 6. In order for these cases to hold, we require $A < 1$, i.e., that the anxiety variable A is scaled by its maximum value. Also note the use of the “one-sided spring model”

$$(A - \bar{A})_+ = \begin{cases} A - \bar{A} & \text{if } A > \bar{A} \\ 0 & \text{else} \end{cases} \quad (3.8)$$

This describes the situation that if a child’s anxiety somehow falls below \bar{A} , then the restoring force would not work to drive it up (back to \bar{A}).

A simulation of (3.6) with $r > 0$ and $\rho = 0$ is shown in Figure 7. Here the imposed stress $S(t)$ describes the mother leaving and returning twice, first at $t = 20$, then again at $t = 40$. Parameter values are selected to yield “secure” behaviour for $\beta = 1$; anxiety rises when the room is entered ($t = 0$) and then the mother leaves, but in all cases it rapidly decays. For comparison, a “soft” child, with $\beta > 1$ but other parameters unchanged, exhibits a much slower decay of anxiety with some accumulation being evident, as in the case of insecure children. Conversely, a “hardened” child ($\beta < 1$) exhibits more rapid dissipation of anxiety than the linear case. Even more strikingly, their anxiety can go *below* their baseline level; for capturing this behaviour and avoiding spurious oscillations the use of (3.8) is essential.

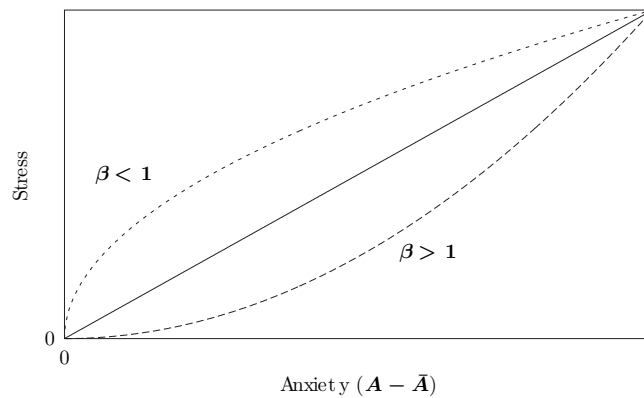


Figure 6 β -dependence of the stress-anxiety response.

At a phenomenological level, these second order differential equations seem to give a reasonable description of the anxiety response to imposed stresses in the experiment. As the parameters of the model described in this section are varied, the solutions describing

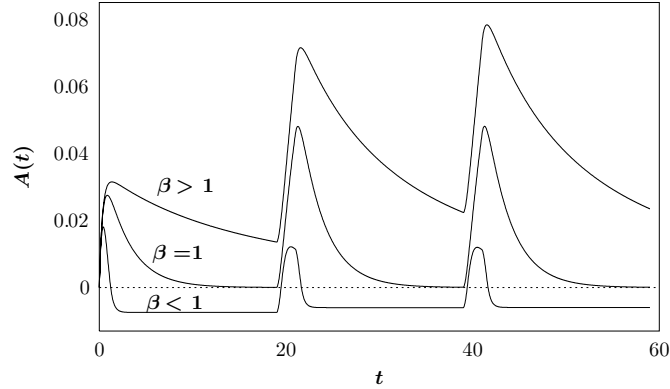


Figure 7 The influence of changing β in (3.6) for a linearly-secure child subjected to successive stresses.

the response to the imposed stress is similar to the responses of a secure or insecure child. However, the model cannot distinguish between ambivalent and avoidant children as their anxiety response should be somewhat similar. In this section, the parameters are assumed to be constant; this is a convenient simplification, but in general, they may exhibit both gradual evolution on long timescales as well as dynamics on shorter time intervals. In particular, there is expected to be short-term variation of r . It is this that we model in the next section. The variety of responses of r to the remaining parameters will distinguish between all attachment types.

The essential element in describing the nature of attachment is relating these parameters of the child's behaviour to properties of the mother's parenting behaviours. This will be the focus of Sections 3.2 and 3.3.

3.2 The mother-child distance equation. The previous section describes an equation for the time evolution of a child's anxiety in a mother-child relationship. The coefficient of the "force" in (3.1) and its nonlinear extension (3.6) is written in terms of a "distance" variable r . This notion of distance is closely related to the actual physical distance between the mother and the child. However, we introduce instead a concept of "emotional distance" between the mother and the child. This concept is more flexible and includes long range interactions between a mother and her child. For instance, visual and verbal contacts between the mother and the child can be effective means by which a mother can aid in the regulation of her child's anxiety, even when the child is not physically close to the mother.

We derive an equation for the child's distance to the mother in terms of the mother's parenting style. The main parenting parameters to be used are

- a =inconsistency of the mother's response to the child's need, and
- b =maternal insensitivity,

where the maternal insensitivity parameter b has already been used in the damping coefficient of (3.1). The emotional distance is described by the variable $r = r(t)$. We will assume that the equation for the time evolution of emotional distance is given by the differential equation

$$\frac{dr}{dt} = \frac{b}{r} - aAr + \frac{c}{1 + A - \bar{A}}, \quad (3.9)$$

where $A = A(t)$ is anxiety, \bar{A} is again the baseline anxiety of the child and c is the intrinsic curiosity of the child at baseline anxiety.

The first term on the right hand side of (3.9) describes the attraction/repulsion the child feels depending on the parenting style of the mother. For high b values (high maternal insensitivity), this term represents a strong impetus to increase emotional distance r when r is not large. However, the effect of this term decreases rapidly as r increases, indicating that a child will still look to her mother to help her regulate her anxiety, in particular in situations of high anxiety. For b close to zero, the effect of this term only becomes important for values of r close to zero. We take $b > 0$, which ensures that if $r > 0$ initially, then it will be so for all time. A mother will have a high value of b if she does not respond to her child's demands during times of anxiety, e.g. the mother is dismissive, responds grudgingly, or ignores the child. A yet higher value of b will result if a mother's response to the child's demands leads to increased anxiety, e.g. a mother becomes angry at the child for demanding attention, and shouts at the child, or in extreme cases, physically harms the child. A low value of b is associated with a parenting style in which the demands of the child are met with sensitivity from the mother.

The second term on the right hand side of (3.9) describes the decrease of the child's emotional distance r as a factor of both anxiety A and the current emotional distance. Thus, we assume there is a natural tendency for the emotional distance to decay exponentially with rate constant aA . The larger the anxiety, the parameter a , or the emotional distance, the faster the decay will be. The parameter a depends on the parenting style of the mother. This parameter will be larger if the mother's response to the child's demands during a time of anxiety is inconsistent, i.e. sometimes the mother responds positively, and sometimes the mother responds grudgingly, dismissively, or ignores the child. In this situation, the emotional distance will tend to decrease relatively quickly even in situations of moderate anxiety, i.e. the child will tend to seek anxiety regulation even when anxiety is not high, because of the uncertainty associated with acquiring the regulation. In the case when a parent provides either consistently positive or consistently negative response, the value of the parameter a will be lower, and the emotional distance will decrease less rapidly for a given value of A . This reflects that for a given level of anxiety, the child will be less likely to seek comfort, either because she knows she will obtain comfort when she needs it, or because she knows that she will not obtain comfort when she seeks it. However, regardless of the value of a , i.e. for all children, this term will represent a large impetus to reduce emotional distance r when anxiety A is high.

Finally, the last term on the right hand side of (3.9) describes the child's impetus to explore. This term will be small when the anxiety is large, i.e. the child will tend to explore only in low anxiety situations.

In Figure 8, we plot the right hand side of (3.9) as a function of r , for various values of the parameters a and b , with anxiety A fixed at its baseline \bar{A} . The values of r at which the graph crosses the horizontal axis correspond to values for which $dr/dt = 0$, and thus represent equilibrium solutions of (3.9). Figure 8 shows the smallest such solution; a second equilibrium exists for a larger value of r . However, we do not try to find an interpretation for this second solution at this stage. We see that children with comparatively low a and b values and children with similar low a value but with a higher b value reach close equilibria. However, if both a and b are raised, the curve crosses the r axis at a significantly lower value. To further elucidate the effect of the parameters on the equilibrium solution we set $dr/dt = 0$ in (3.9), and solve for r to obtain the equilibrium surface $r = \phi(a, b)$. See

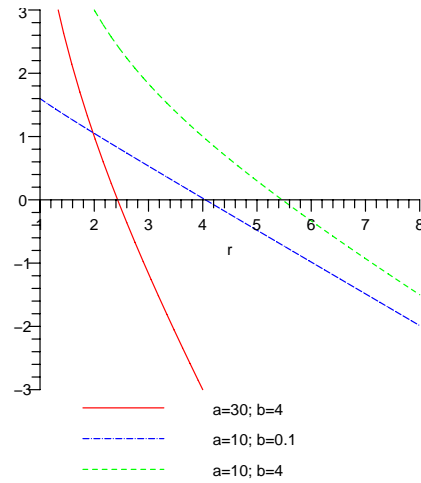


Figure 8 The right hand side of (3.9) is plotted as a function of r , for various values of a and b with A held fixed at baseline ($A = \bar{A} = 0.05$).

Figure 9. It is clear from Figure 9 that the location of equilibrium solutions for (8) depend

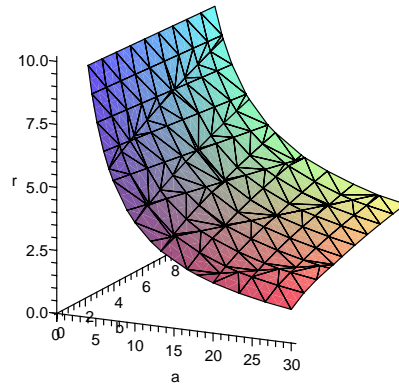


Figure 9 Equilibrium solutions of (3.9) plotted as a function of a and b .

almost exclusively on the parameter a . That is, the child's preferred emotional distance at a time of low anxiety is determined to a large extent by the inconsistency of the mother, while the maternal insensitivity has relatively little effect. Thus, the child of an inconsistent mother (high a) will gravitate to a low emotional distance even at a time of low anxiety.

3.3 The Complete Model. We now turn to the analysis of the full model incorporating anxiety and emotional distance. In the case in which we consider the linear anxiety

equation (3.1), we have

$$\begin{aligned}
 m \frac{d^2 A}{dt^2} + b \frac{dA}{dt} + \frac{1}{r} (A - \bar{A}) &= P \tanh(r) + S(t), \\
 \frac{dr}{dt} &= \frac{b}{r} - aAr + \frac{c}{1 + A - \bar{A}},
 \end{aligned}
 \tag{3.10}$$

where we have added a term $P \tanh(r)$ in the anxiety equation which corresponds to the increase of anxiety that is induced as the emotional distance is increased, where $P > 0$ is a constant. The function $\tanh(r)$ is used to model the saturation of imposed stress on the child as the emotional distance r becomes large.

Figure 10 shows numerical simulations of system (3.10) for values of a and b that distinguish between the three types of mother-child attachment: secure, ambivalent, and avoidant. The simulations begin at a time of high stress, e.g., in the strange situation experiment when the mother re-enters the room after being absence for a short time. Unlike in Section 3.1, we assume that the absence of the mother induces the same level of anxiety in all the children, regardless of their type of attachment to their mother. Thus, we take the initial conditions to be the same in all simulations. As is seen in Section 3.1, the effect of the mother's return on the anxiety A distinguishes the secure child from the ambivalent and the avoidant child; the secure child's return to baseline anxiety is very rapid, while the anxiety of an avoidant or ambivalent child shows slower decay. However, the anxiety response is not sufficient to distinguish the avoidant child from the ambivalent child. From the graph of emotional distance r , we see that the dash-dot curve represents an initial decay of r that is much more rapid than that of the dashed curve, and the minimum value of r for the dash-dot curve is significantly smaller than that of the dashed curve. We conclude that the dash-dot curve describes the dynamics of the anxiety A and emotional distance r of an ambivalent child, because we expect such a child to seek out her mother, even though she is only moderately comforted by her. We also conclude that the dashed curves exhibit the dynamics of an avoidant child, because we expect that, in a situation of high anxiety, such a child would not wish to be too far from her mother, although she would still wish to maintain a 'buffer zone' between her and her mother, and we would expect her anxiety to be dissipated relatively slowly. Thus, the secure child is characterized by a mother with a parenting style with low inconsistency a and low insensitivity b , an ambivalent child is characterized by both a higher inconsistency a and higher insensitivity b , while the avoidant child has low inconsistency a , but a higher value of insensitivity b .

3.4 Analysis of the complete model. We now proceed to a linear stability analysis of the equilibrium solution of the complete model (3.10).

3.4.1 *Existence and uniqueness of equilibrium solution.* We suppose that $S(t) \equiv 0$ and find the equilibrium solutions of system (3.10) rewritten as a first-order system:

$$\begin{aligned}
 \frac{dA}{dt} &= B \\
 \frac{dB}{dt} &= \frac{1}{m} \left(-bB - \frac{1}{r} (A - \bar{A}) + P \tanh(r) + S(t) \right) \\
 \frac{dr}{dt} &= \frac{b}{r} - aAr + \frac{c}{1 + A - \bar{A}}.
 \end{aligned}
 \tag{3.11}$$

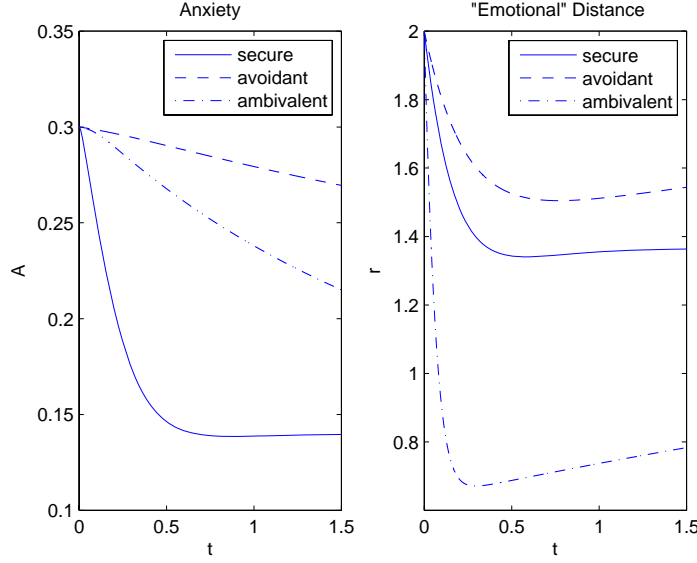


Figure 10 Numerical simulations of the full system as the mother returns to the room. Parameter values are fixed at $c = 2$, $m = 0.001$, $\bar{A} = 0.05$ and $P = 0.075$. Then a and b are varied; ‘secure’: $a = 10$, $b = 0.1$, ‘avoidant’: $a = 10$, $b = 4$, ‘ambivalent’: $a = 30$, $b = 4$.

Set $B = 0$, then the second equation yields

$$A = rP \tanh(r) + \bar{A}.$$

Substituting in the last equation we have

$$G(r) = \frac{b}{r} - a(rP \tanh(r) + \bar{A})r + \frac{c}{1 + rP \tanh(r)} = 0. \quad (3.12)$$

For $b, r > 0$ and all other parameters nonnegative, we have that $\lim_{r \rightarrow 0} G(r) > 0$ and

$$\frac{dG}{dr} = -\frac{b}{r^2} - a(P \tanh(r) + rP(1 - \tanh(r)^2))r - a(rP \tanh(r) + \bar{A}) - \frac{c(P \tanh(r) + rP(1 - \tanh(r)^2))}{(1 + rP \tanh(r))^2}$$

is negative. This guarantees the existence of a unique equilibrium solution for all values of the parameters.

Figure 11 shows $G(r)$ of (3.12) plotted as a function of r for various values of a and b , where, as before, we set the parameter values $c = 2$, $m = 0.001$, $\bar{A} = 0.05$ and $P = 0.075$. The points at which the graph crosses the r -axis represent solutions of (3.12), and thus, equilibrium solutions of the full system (3.10). The dotted curve, for which $a = 30$ and $b = 4$, intersects at $r \approx 1.27$, the solid curve, for which $a = 10$ and $b = 0.1$, crosses at $r \approx 1.36$ and the dashed curve, for which $a = 10$ and $b = 4$, crosses at $r \approx 1.96$. Let $r = r^*$ be the solution to (3.12) and $A^* = r^*P \tanh(r^*) + \bar{A}$. Then, the equilibrium solution is at $(A, B, r) = (A^*, 0, r^*)$.

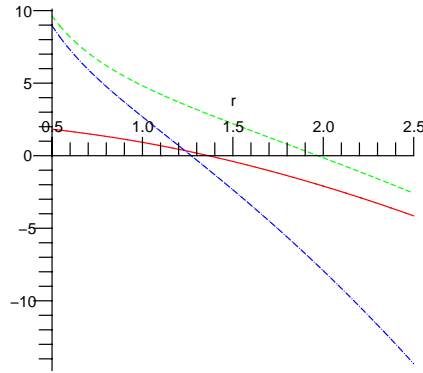


Figure 11 Plot of $G(r)$ indicating the equilibrium solutions of (3.12); dash-dot: $a = 30$, $b = 4$, solid: $a = 10$, $b = 0.1$, and dash $a = 10$, $b = 4$.

3.4.2 Linear stability analysis. We now compute the linear stability at this equilibrium solution. The linearization at $(A^*, 0, r^*)$ is

$$L = \begin{pmatrix} 0 & 1 & 0 \\ -\frac{1}{r^*m} & -\frac{b}{m} & \frac{A^* - \bar{A}}{m(r^*)^2} + P \tanh'(r^*) \\ -ar^* - \frac{c}{(1 + A^* - \bar{A})^2} & 0 & -\frac{b}{(r^*)^2} - aA^* \end{pmatrix}. \quad (3.13)$$

Setting $m = 0.001$, $c = 2$, $\bar{A} = 0.05$ and $P = 0.075$, the characteristic equation for L is

$$p(\lambda) = a_0\lambda^3 + a_1\lambda^2 + a_2\lambda + a_3,$$

where $a_0 = 1$, and

$$a_1 = \frac{aAr^2 + b + 100r^2b}{r^2}$$

$$a_2 = \frac{100(baAr^2 + r + b^2)}{r^2}$$

$$a_3 = \frac{-1}{r^3(A + 0.5)^2} (25b + 100bA + bA^2 + 75rA + 150aA^2r^2 + 375 \tanh(r)r^3 + 125ar^4 \tanh(r) + 5ar^4A^2 \tanh(r) - 12.5ar^2 + 200aA^3r^2 - 37.5r + 50ar^4A \tanh(r)).$$

If $b, r > 0$, one can easily verify that $a_1, a_2 > 0$. The Routh-Hurwitz criterion [12] states that all the eigenvalues of L have negative real parts if and only if

$$a_0 > 0, \quad \Delta_1 = a_1 > 0, \quad \text{and} \quad \Delta_2 = a_1a_2 - a_3 > 0.$$

We verify asymptotic stability for the parameter values of the numerical simulations of Figure 10; the equilibrium solutions have coordinates $(A, 0, r) \approx (0.13, 0, 1.27)$ for $a = 30$,

$b = 4$, $(A, 0, r) \approx (0.14, 0, 1.36)$ for $a = 10$, $b = 0.1$ and $(A, 0, r) \approx (0.19, 0, 1.96)$ for $a = 10$, $b = 4$. Using Maple, it is easy to compute that in all cases Δ_2 is a positive number of the order 10^5 . We see that the equilibrium solution is linearly stable in all these cases. Therefore, after a perturbation (within the stability basin) the dynamics relax back to the equilibrium solution.

These stable equilibrium solutions indicate the long-time behaviour of the model (3.10). That is, they indicate the anxiety A and emotional distance r that we expect the child to have after they recover from the stressful event. If we correlate the different parameter values with the different attachment types as we did for the simulations displayed in Figure 10, we see that, in this case, the ambivalent child has the lowest emotional distance and anxiety, while those of the avoidant child are the highest. This is indeed what we might expect; the increased equilibrium anxiety of the secure child relative to that of the ambivalent child is due to the extra anxiety induced by ‘exploration’, i.e. the increased emotional distance. It should be noted that the equilibrium for the secure child depends significantly on the exploration parameter c , while the equilibrium for the ambivalent child is less sensitive to this parameter. Specifically, an increase in c leads to an increased gap between the emotional distance equilibria of the ambivalent and secure child.

3.5 Slow-time evolution of behavioural parameters. In the previous sections, we find that the different behaviour that is observed in the model (3.10) for different values of the inconsistency parameter a and the insensitivity parameter b are sufficient to distinguish the three different attachment types. We have assumed that the values of these parameters are constant, but in a fuller description, these values will depend on the influence of the environment, and predominantly the actions of the mother toward the child. Some of the fundamental issues in formulating a mathematical model of mother-child attachment centre on understanding how these parameter values are determined and what influences could change them, leading to improvements in the long term development of the child.

Let us assume that while the parameters $(a, b, m, \bar{A}, \dots)$ may be treated as being fixed over the course a short period, e.g. the length of the strange situation experiment, they can change over sufficiently long times, say over the course of a month. Let $\tau = \epsilon t$ represent a slow timescale, where ϵ is a small parameter. If time is measured in minutes, then for example, ϵ could be one over the number of minutes in a month, $\epsilon \approx 1/43,200 \approx 2 \times 10^{-5}$. If we assume that the parameters, e.g., a , vary only over the course of months, then $a = a(\tau)$, where $a(\tau)$ is assumed to be a smooth function, whose value would essentially be unchanged over a short period of time, i.e., $a(\tau + 60 \times 10^{-5}) \approx a(\tau)$. However, given an extended period over which the mother’s response to her child has changed, e.g. due to some intervention, these parameters should evolve in response.

However, it may be useful to assume that the parameter ρ , which appears in the damping term of the nonlinear anxiety model (3.6), varies on intermediate time scales. That is, it can be assumed to be approximately constant on time scales of a single anxious event, e.g. one exit and return of the mother in the strange situation experiment, but that it may vary over the course of several consecutive anxious events, e.g. over the course of the entire experiment. In the strange situation experiment, it has been observed that the mother’s ability to regulate the anxiety of the child decreases as the number of absences of the mother increases. Thus, if we assume that, for instance, the parameter ρ is proportional

to a windowed time-average of the anxiety A over an interval $[t - \delta t, t]$ i.e.,

$$\rho = \rho_s \int_{t-\delta t}^t (A - \bar{A}) dt, \tag{3.14}$$

where ρ_s is a constant, then ρ will increase each time the mother leaves the room. The increase in ρ will lead to a slower decay of anxiety. As this rate of decay increases, the child's responses will appear more and more like those of an ambivalent child. See Figure 12. This is consistent with the observation that given several absences of the mother, all children display characteristics of an ambivalent child.

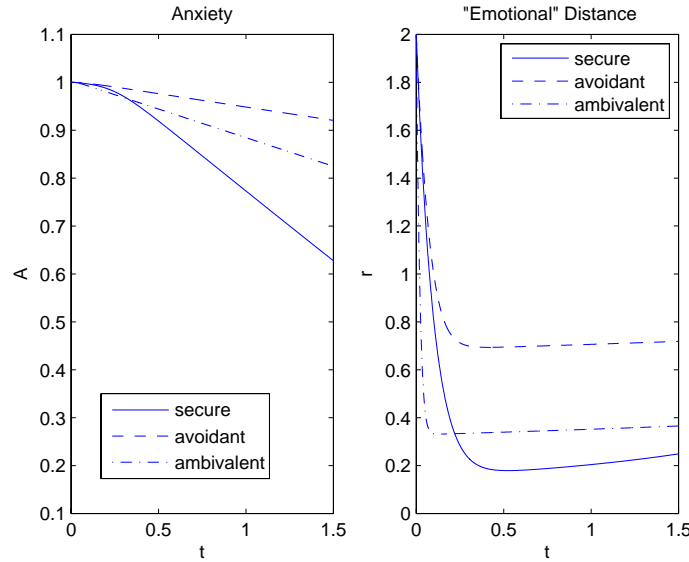


Figure 12 Numerical simulations of the full system with general damping term (i.e. $\rho \neq 0$) as the mother returns to the room. We take $\rho = 20$, while the other parameter values are taken to be the same as those used for Figure 10.

Furthermore, the parameter ρ appears in the damping term multiplied by A^2 . Thus, the damping increases as A increases, leading to the realistic situation that the higher the child's anxiety, the more difficult it is to regulate.

3.6 Discussion. The model presented in Section 3 describes the dynamics observed during the strange situation experiment. In particular, using two variables, anxiety A and emotional distance r , the model has the capacity to distinguish between the three types of mother-child interactions observed in the experiment: secure, ambivalent and avoidant. Moreover, the distinction is achieved by varying only two parameters that are directly linked with the mother's parenting style: the mother's insensitivity b and the inconsistency a in her response to her child's needs. In the construction of the model, we chose reasonable representations of how the characteristics associated with these parameters affect the mother's ability to regulate her child's anxiety. The fact that the variation of these two parameters leads to the qualitative distinction of the attachment types supports the claim that these are indeed the most important factors in the problem.

However, at this stage, the model is only phenomenological. The next stage in the model development will be to incorporate quantitative information. In order to do this, we need

to find reasonable units for the variables and parameters, and we need to approximate the values of the parameters. In some cases it will likely be necessary to design new experiments specifically for this purpose. We also need to acquire quantitative data sets that provide continuous readings of the model variables throughout an experiment. Anxiety A has been measured using levels of cortisol in the child’s saliva. However, existing data sets only include measurements at a few points during an experiment. It may be practical to use heart rate as a measure of anxiety, because it is a quantity that is relatively easy to monitor continuously.

Similarly, data for the emotional distance r is needed. However, before such data can be acquired, it must be determined whether it can be defined in terms of directly measurable quantities such as physical distance, and frequency of visual contact or verbal communication.

The model also contains other parameters, namely “emotional inertia” m , in analogy to Newtonian inertia in the second-order equation describing anxiety, and “curiosity” c , in the equation for emotional distance. At present, we only have a vague concept of the significance of these parameters and it would be interesting to find precise psychological concepts relating to these parameters. This would be particularly significant if those concepts could be quantifiable. By performing various numerical simulations of (3.10), we have found that the qualitative behaviour of the model is not sensitive to these parameters. However, it would be interesting to quantify the model’s dependence on these parameters.

4 Control Theory Approach

(This section contributed by Roger Chau).

In this section, we present an outline of how one might take a control theory approach to the problem of mother-child attachment. In particular, a feedback system is proposed to model the interaction between mother and child during stressful situations. The child’s perception of the mother’s parenting style is modelled using the Preisach model [14], which is commonly used in modelling shape memory alloys (SMAs).

4.1 Feedback System. Consider the feedback system shown in Figure 13. (For background in control theory and feedback systems, please refer to [17]). The system represents the child, whereas the controller, or regulator, models the relationship between the mother and the child. The input disturbance s is the external stress that the child experiences when certain events occur. The reference signal r is the baseline stress level of the child.

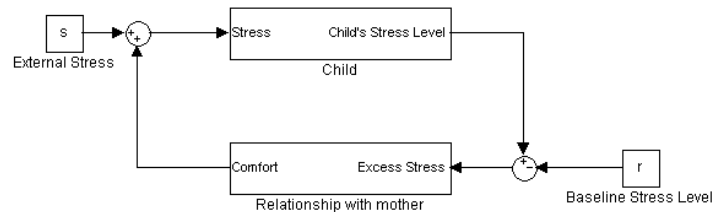


Figure 13 The feedback system

We will first look at the system representing the child; Figure 14 shows the components that make up our *simple child*. We take the input u to the system to be the external stress modulated by the regulator, which represents the relationship of the child with her mother, and we take the output y to be the stress level of the child. In the absence of the mother, the child will amplify the stress received. This is modelled by a gain of k_1 which is the same for every child. In addition, an integrator with gain k_2 is used to model the effect of accumulated stress on the child's stress level.

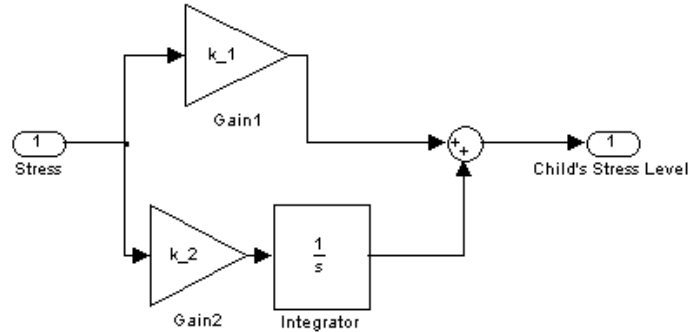


Figure 14 The system representing the child.

The second component of our feedback system is the regulator; see Figure 15. A Proportional-Integral-Differential (PID) controller is used to model the child's relationship with the mother. Note that it takes in the *difference* between the baseline stress level r and the actual stress level of the child y . The regulator's job is to reduce this difference or *error* by changing the input to the system. In essence, the proportional gain k_p deals with the present, the integral gain k_i deals with the past, and the differential gain k_d attempts to predict the future. The proportional gain k_p is assumed to be a random value, because in any given situation, the mother's ability to down-regulate the child's anxiety will vary. The integral gain k_i depends on the 'healthiness' of the child's relationship with the mother. If the mother has a healthy relationship with her child, it is easier for her to reduce accumulated stress. Finally, the differential gain k_d depends on the consistency of the mother's parenting style. This has to do with the child's expectation of the mother's behaviour when a stressful situation occurs. Note that the values of these gains may be positive or negative, depending on the child's experience with the mother.

4.2 Preisach Model. While the implementation of the above model seems to be straightforward, it is not clear how some of the parameter values can be determined. Because we are mainly interested in qualitative results, the values of k_1 and k_2 may be taken as unity, and the baseline stress level may be taken as zero. Two parameters that depend on the mother's parenting style are k_i and k_d . These parameters are similar to those used in the other models in this report, and therefore, it is useful to propose a method to derive them. The following is a description of the Preisach model, which is commonly used to model systems with memory.

In [10], a method for mapping human emotions as a continuous surface is proposed. Here, we will follow a similar approach, this time making use of the Preisach model. Consider

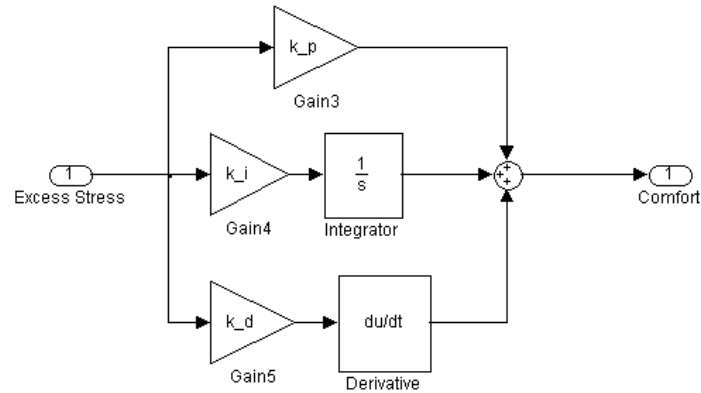


Figure 15 The regulator representing the child's relationship with her mother

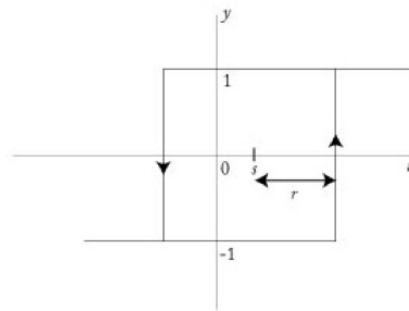


Figure 16 A simple relay

modelling a single emotion with a simple relay as in Figure 16. The input of the relay is the perception or rating of the mother in the child's point of view. The relay has two outputs: +1 corresponding to *good* and -1 corresponding to *bad*. Each relay is categorized by the centre s and the half width $r > 0$.

A relay is used because for a particular emotion to change from one state to another might require different amount of influence. For example, if person A is originally unhappy, then it will take a lot of effort to make A happy; similarly, if A is happy, a lot more *bad influence* is needed to make A unhappy again. Each relay can be uniquely identified by the pair of parameters (r, s) , or as ordered pairs in the plane $\mathbb{R}_+ \times \mathbb{R}$. We can set an arbitrary limit on the maximum magnitude of the input. This is possible due to that fact that after a certain threshold, little effects can be observed if we change the input. This restricted domain is the *Preisach Plane* \mathcal{P} shown in Figure 17.

The goal of using the Preisach model is to find a way to quantify the values of k_i and k_d . The output p of the Preisach model can be used to determine the value of k_i . In order to determine k_d , we can keep track of the number of sign changes of the output y over a fixed period of time. There are several programs written for the Preisach model and the PID controller is trivial to implement using, for example, MATLAB.

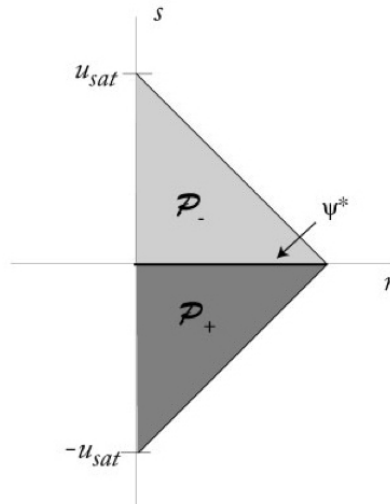


Figure 17 Preisach Plane

5 Summary

In this report, we present three mathematical models relevant to the attachment of a child with her mother. In the first, we approached the problem from a game theory perspective. We find that a simple decision-making process can lead to three distinct attachment types.

In the second model, we present a dynamical system that exhibits various behaviour similar to what might be expected from the three distinct attachment types. We also find that the model parameters that determine the qualitative character of the response are associated with the mother's sensitivity and consistency. In this report, we have only presented qualitative results, and have left some important questions regarding model validation and quantitative predictions unanswered. This will be a subject of future research.

Finally, we present a sketch of a model in control theory. This approach is intriguing, owing to the fact that some of the original results on attachment theory were described in such terms. However, much more work must be done in order to determine whether this model would yield fruitful results.

Acknowledgements

LFR would like to thank Steven Brams for useful discussions and tips on the dynamics of decisions-making processes.

References

- [1] M.D.S. Ainsworth, M.C. Blehar, E. Waters, and S. Wall. *Patterns of attachment: A psychological study of the strange situation*. Lawrence Erlbaum, Hillsdale, NJ, 1978.
- [2] M.D.S. Ainsworth and J. Bowlby. An ethological approach to personality development. *American Psychologist*, 46(4):333–341, 1991.
- [3] David P. Barash. *The survival game*. Henry Holt and Company, 2003.
- [4] Jessie Bernard. Counseling techniques for arriving at optimum compromises: game- and decision theory. *Marriage and family living*, 21(3):264–274, 1959.

- [5] William E. Boyce and Richard C. DiPrima. *Elementary differential equations and boundary value problems*. John Wiley & Sons Inc., New York, 1965.
- [6] Steven J. Brams. *The Theory of Moves*. Cambridge University Press, 1994.
- [7] Steven J. Brams. Game theory and emotion. *Rationality and Society*, 9(1):91–124, 1997.
- [8] Steven J. Brams. Catch-22 and king-of-the-mountain games: Cycling, frustration and power. *Rationality and Society*, 11(2):139–167, 1999.
- [9] I. Bretherton. The origins of attachment: John Bowlby and Mary Ainsworth. *Developmental Psychology*, 28(5):759–775, 1992.
- [10] E.M. Daly, W.J. Lancee, and J. Polivy. A conical model for the taxonomy of emotional experience. *Journal of Personality and Social Psychology*, 45(2):443–457, 1983.
- [11] G. F. Franklin, J. D. Powell, and A. Emami-Naeini. *Feedback control of dynamic systems*. Addison-Wesley, Reading MA, 1988.
- [12] F.R. Gantmacher. *Matrix Theory. Vol. II*. AMS, Chelsea, 2000.
- [13] Arjita Ghosh and Sandip Sen. Theory of moves learners: Towards non-myopic equilibria. In *Proceedings of the fourth international joint conference on Autonomous agents and multiagent systems*, pages 74–80. ACM Press, 2005.
- [14] R.B. Gorbet. *Control of Hysteretic Systems with Preisach Representations*. PhD thesis, University of Waterloo, Ontario, Canada, 1997.
- [15] R. Duncan Luce and Howard Raiffa. *Games and Decisions: Introduction and critical survey*. Dover, 1989.
- [16] J. McKinsey. *Introduction to the Theory of Games*. The Rand Series. McGraw-Hill Book Company, 1952.
- [17] K.A. Morris. *Introduction to Feedback Control*. Harcourt/Academic Press, San Diego, CA, 2001.
- [18] John von Neumann and Oskar Morgenstern. *The Theory of Games and Economic Behavior*. Princeton University Press, 1944.

Normalization and Other Topics in Multi-Objective Optimization

Problem Presenter: Helmut Mausser (Algorithmics Group)

Academic Participants: Yichuan Ding (University of Waterloo), Sandra Gregov (McMaster University), Oleg Grodzevich (University of Waterloo), Itamar Halevy, Zanin Kavazovic (Université de Laval), Oleksandr Romanko (McMaster University), Tamar Seeman (Bar Ilan University), Romy Shioda (University of Waterloo), Fabien Youbissi (Université de Laval)

Report prepared by: Oleg Grodzevich¹, Oleksandr Romanko²

1 Introduction

A *multi-objective optimization* typically arises in various engineering modelling problems, financial applications, and other problems where the decision maker chooses among several competing objectives to satisfy (see, e.g. [5]). In this report we consider a multi-objective optimization problem that comes from the financial sector. However, the analysis is applicable to any problem that retains similar characteristics. In particular, we focus on techniques for the normalization of objective functions. The normalization plays an important role in ensuring the consistency of optimal solutions with the preferences expressed by the decision maker. We also compare several approaches to solve the problem assuming that a linear or a mixed integer programming solver, such as CPLEX, is available. Namely, we consider weighted sum and hierarchical or ε -constraint methods, see also [1, 3, 6].

Although this report tends to provide a general discussion about multi-objective optimization, the proposed analysis and the resulting algorithm are specifically aimed at practical implementation. The reader should keep in mind that different approaches may be more effective should one not be constrained by various factors that are induced by the environment, and that are not discussed within the scope of this paper.

A multi-objective optimization problem can be written in the following form

$$\begin{aligned} \min \quad & \{f_1(x), f_2(x), \dots, f_k(x)\} \\ \text{s.t.} \quad & x \in \Omega, \end{aligned} \tag{1.1}$$

¹ogrodzev@uwaterloo.ca

²romanko@mcmaster.ca

where $f_i : \mathbb{R}^n \rightarrow \mathbb{R}$ are (possibly) conflicting objective functions and $\Omega \subseteq \mathbb{R}^n$ is the feasible region.

For consistency, we transform all the maximization problems of the type $\max f_i$ into equivalent minimization problems $\min(-f_i)$.

The goal of multi-objective optimization is to simultaneously minimize all of the objective functions. In this paper we restrict our attention mainly to the case of convex objectives and convex feasible region. The situation when integrality restrictions are present is also briefly addressed. We further consider only linear or convex quadratic objectives and constraints. In general we distinguish among the following three types of problems:

- linear – with linear objectives and constraints;
- quadratic – with linear and quadratic objectives, but only linear constraints;
- quadratic-quadratic – with both objectives and constraints being either linear or quadratic.

Define the set $Z \subseteq \mathbb{R}^k$ as the mapping of the feasible region into the objective space and denote it as *objective feasible region*:

$$Z = \{z \in \mathbb{R}^k : z = ((f_1(x), f_2(x), \dots, f_m(x))^T \forall x \in \Omega)\}.$$

Since we assume that objective functions compete (or conflict) with each other, it is possible that there is no unique solution that optimizes all objectives simultaneously. Indeed, in most cases there are infinitely many optimal solutions. An optimal solution in the multi-objective optimization context is a solution where there exists no other feasible solution that improves the value of at least one objective function without deteriorating any other objective.

This is the notion of *Pareto optimality* [1, 2, 4, 5, 6]. Specifically, a decision vector $x^* \in \Omega$ is *Pareto optimal* if there exists no another $x \in \Omega$ such that $f_i(x) \leq f_i(x^*) \forall i = 1, \dots, k$ and $f_j(x) < f_j(x^*)$ for at least one index j . The vector of objective function values is Pareto optimal if the corresponding decision vector x is Pareto optimal. The set of Pareto optimal solutions \mathcal{P} forms a Pareto optimal set, which is also known as the *efficient frontier*, see [4].

The definition above refers to global Pareto optimality. In addition, local Pareto optimal solutions can be defined if points in the neighbourhood of an optimal solution are considered (rather than considering all points in the feasible region). Any global Pareto optimal solution is locally Pareto optimal. The converse is true for problems which feature convex Pareto set. More specifically, if the feasible region is convex and objective functions are quasi-convex with at least one strictly quasi-convex function, then locally Pareto optimal solutions are also globally Pareto optimal, see [6].

2 Decision making with multi-objective optimization

From the mathematical point of view, every Pareto optimal solution is equally acceptable as the solution to the multi-objective optimization problem. However, for practical reasons only one solution shall be chosen at the end. Picking a desirable point out of the set of Pareto optimal solutions involves a *decision maker* (DM). The DM is a person who has insights into the problem and who is able to express preference relations between different solutions. In the case of Algorithmics Inc., the DM is the customer running their software.

A process of solving a multi-objective optimization problem typically involves the cooperation between a decision maker and an analyst. The analyst in our situation is represented by a piece of software that is responsible for performing mathematical computations required during the solution process. This analytical software generates information for

the decision maker to consider and assists in the selection of a solution by incorporating preferences expressed by the DM. For example, the DM can assign importance levels, such as "high", "medium", or "low", to each objective or rank objectives in some specific order.

In the context of this report we seek to find a solution that is both Pareto optimal and also satisfies the decision maker. Such a solution, providing one exists, is considered a desired solution to the multi-objective optimization problem and is denoted as a *final solution*.

3 Numerical example

A small portfolio optimization problem is used to test and to illustrate the multi-objective optimization methodology. In portfolio optimization, investors need to determine what fraction of their wealth to invest in which stock in order to maximize the total return and minimize the total risk. In our experiments, the data includes expected returns, return covariances and betas for 8 securities, as well as their weights in the initial portfolio x_0 . If we define our decision variables to be the weights of the securities x then expected return $r^T x$ and beta $\beta^T x$ are linear functions and variance of return $\frac{1}{2}x^T Q x$ is a quadratic function.

We put box constraints on the weights x ($0 \leq x \leq 0.3$) and use three objectives:

- 1) minimize the variance of return;
- 2) maximize the expected return;
- 3) set a target beta of 0.5 and penalize any deviation from this target.

Moreover, we also need to add a constraint that makes the weights sum to 1. The data for the problem is presented in Tables 1 and 2.

Security	x_0	$E(Return)$	Beta
1	0	0.07813636	0.1
2	0.44	0.09290909	0
3	0.18	0.11977273	0.7
4	0	0.12363636	0.5
5	0	0.12131818	0.3
6	0.18	0.09177273	0.25
7	0.13	0.14122727	0.4
8	0.07	0.12895455	-0.1

Table 1 Portfolio data

Security	1	2	3	4	5	6	7	8
1	0.000885	-8.09E-05	9.99E-05	5.80E-05	-0.000306	0.000261	-0.001255	0.000803
2	-8.09E-05	0.022099	0.010816	0.010107	0.011279	0.010949	0.010534	-0.013429
3	9.99E-05	0.010816	0.026997	0.028313	0.031407	0.007148	0.020931	-0.017697
4	5.80E-05	0.010107	0.028313	0.030462	0.035397	0.006782	0.022050	-0.015856
5	-0.000306	0.011279	0.031407	0.035397	0.047733	0.007278	0.023372	-0.015692
6	0.000261	0.010949	0.007148	0.006782	0.007278	0.006194	0.004195	-0.010970
7	-0.001255	0.010534	0.020931	0.022050	0.023372	0.004195	0.052903	-0.013395
8	0.000803	-0.013429	-0.017697	-0.015856	-0.015692	-0.010970	-0.013395	0.121308

Table 2 Return Covariances Matrix

Thus, the multi-objective portfolio optimization problem looks like:

$$\begin{aligned} \min \quad & f_1(x) = -r^T x, f_2(x) = |\beta^T x - 0.5|, f_3(x) = \frac{1}{2}x^T Qx \\ \text{s.t.} \quad & \sum_i x_i = 1, \\ & 0 \leq x_i \leq 0.3 \quad \forall i. \end{aligned}$$

Let us rewrite the beta constraint as $\beta^T x + t_1 - t_2 = 0.5$, in this case $f_2(x) = t_1 + t_2$, $t_1 \geq 0, t_2 \geq 0$. We get the following problem:

$$\begin{aligned} \min_{x,t} \quad & f_1(x, t) = -r^T x, f_2(x, t) = t_1 + t_2, f_3(x, t) = \frac{1}{2}x^T Qx \\ \text{s.t.} \quad & \sum_i x_i = 1, \\ & \beta^T x + t_1 - t_2 = 0.5, \\ & 0 \leq x \leq 0.3, t \geq 0. \end{aligned} \tag{3.1}$$

Suppose that

$$\left(f_1(x^*), f_2(x^*), f_3(x^*) \right) = (-12, 0.1, 26)$$

and

$$\left(f_1(x'), f_2(x'), f_3(x') \right) = (-5, 0.1, 15)$$

are both Pareto optimal solutions. If the DM prefers the first objective over the third, then the DM may prefer solution x' , whereas he may prefer x^* if the opposite scenario holds. The challenge in this multi-objective portfolio optimization problem is to find the Pareto optimal point that meets the DM's given preferences. We propose to focus on two approaches: the weighted sum approach outlined in Section 4 and the hierarchical approach discussed in Section 5.

4 The weighted sum method

The weighted sum method allows the multi-objective optimization problem to be cast as a single-objective mathematical optimization problem. This single objective function is constructed as a sum of objective functions f_i multiplied by weighting coefficients w_i , hence the name. These coefficients can be normalized to 1, while this is not necessary in general.

4.1 Basics of the weighted sum method. In the weighted sum method the problem (1.1) is reformulated as:

$$\begin{aligned} \min \quad & \sum_{i=1}^k w_i f_i(x) \\ \text{s.t.} \quad & x \in \Omega, \end{aligned} \tag{4.1}$$

where $w_i \geq 0, \forall i = 1, \dots, k$ and $\sum_{i=1}^k w_i = 1$.

Under the convexity assumptions, the solution to (4.1) is Pareto optimal if $w_i > 0, \forall i = 1, \dots, k$. The solution is also unique if the problem is strictly convex.

In principle, every Pareto optimal solution can be found as a solution to (4.1), if convexity holds. However, as we will see in Section 4.4, depending on the problem geometry and the solution method some of the Pareto optimal solutions can never be obtained.

4.2 Normalization in the weighted sum method. Ideally, weights of each objective function are assigned by the DM based on the intrinsic knowledge of the problem. However, as different objective functions can have different magnitude, the normalization of objectives is required to get a Pareto optimal solution consistent with the weights assigned by the DM. Hence, the weights are computed as $w_i = u_i\theta_i$, where u_i are the weights assigned by the DM and θ_i are the normalization factors.

Some possible normalization schemas are:

- normalize by the magnitude of the objective function at the initial point x_0 , here $\theta_i = \frac{1}{f_i(x_0)}$;
- normalize by the minimum of the objective functions, $\theta_i = \frac{1}{f_i(x^{[i]})}$, where $x^{[i]}$ solves $\min_x \{f_i(x) : x \in \Omega\}$;
- normalize by the differences of optimal function values in the Nadir and Utopia points that give us the length of the intervals where the optimal objective functions vary within the Pareto optimal set (details are provided below).

The first two schemas have proved to be ineffective and are not practical. The initial point may provide very poor representation of the function behaviour at optimality. Moreover, $f_i(x_0)$ is often equal to zero and can not be used at all. Use of the optimal solutions to individual problems can also lead to very distorted scaling since optimal values by themselves are in no way related to the geometry of the Pareto set.

Let us consider the last normalization schema in more details. It is not difficult to see that ranges of the objective Pareto optimal set provide valuable information for the solution process. The components $z_i^* = f_i(x^{[i]}) \in R$ of the ideal objective vector $z^* \in R^k$ are obtained by minimizing each of the objective functions individually subject to the original constraints, i.e.,

$$z_i^* = f_i(x^{[i]}) \quad \text{where} \quad z_i^* = \operatorname{argmin}_x \{f_i(x) : x \in \Omega\}.$$

The ideal objective vector $z^U = z^*$, called the *Utopia point*, is not normally feasible because of the conflicting nature of the individual objectives. The Utopia point provides the lower bounds of the Pareto optimal set.

The upper bounds of the Pareto optimal set are obtained from the components of a *Nadir point* z^N . These are defined as

$$z_i^N = \max_{1 \leq j \leq k} (f_i(x^{[j]})), \quad \forall i = 1, \dots, k.$$

The normalization schema that uses the differences of optimal function values in the Nadir and Utopia points gives the following values of θ_i ,

$$\theta_i = \frac{1}{z_i^N - z_i^U}.$$

This normalization schema provides the best normalization results as we normalize the objective functions by the true intervals of their variation over the Pareto optimal set. Intuitively, it is not difficult to see that all objective functions after normalization will be bounded by

$$0 \leq \frac{f_i(x) - z_i^U}{z_i^N - z_i^U} \leq 1,$$

that gives the same magnitude to each objective function.

4.3 Computing normalization weights. In order to compute true normalization ranges $z_i^N - z_i^U$ it is necessary to solve k optimization problems of the form $\min_{x \in \Omega} \{f_i(x) : x \in \Omega\}$ to obtain $x^{[i]}$ values.

Knowing $x^{[i]}$ is crucial, as they are required to calculate $z_i^U = f_i(x^{[i]})$ and $z_i^N = \max_j (f_i(x^{[j]}))$.

In practise, it may be computationally expensive to solve k optimization problems if they are mixed integer programming problems or quadratically constrained problems. Even solving k linear or convex quadratic problems can take a significant amount of time if the problem dimensions are large (more than 10,000-100,000 variables/constraints).

On the other hand, it is evident that exact solutions to the individual optimization problems are not required. One can come up with acceptable normalization factors if the estimates of the Utopia and Nadir points are known. For that reason, we propose the following relaxations or modifications to cope with the expensive computational costs.

- Tweak CPLEX parameters to reduce the solution time, i.e. increase one or more of the stopping criteria tolerances, e.g. increase the duality gap in the barrier solver from 10^{-6} to 10^{-3} or 10^{-4} .
- Relax some of or all "difficult" constraints, i.e. relax all quadratic and integer constraints.
- Estimate z_i^U and z_i^N without solving any optimization problem, by relying instead on a random sampling of points x subject to a subset of problem constraints Ω (such as, for example, box-constraints $l_i \leq x_i \leq u_i$). Calculate z_i^U and z_i^N as the minimum and the maximum over the set of sampled points.
- If known, use the initial solution x_0 for normalization when all other methods are still computationally expensive.
- In certain cases, there is a closed form solution for z_i^U . For example, in Problem (3.1), $z_i^U = -0.3(r_{(1)} + r_{(2)} + r_{(3)}) - 0.1r_{(4)}$ where $r_{(i)}$ is the i^{th} order statistic of r_i^2 . The corresponding solution is $x_{(1)} = 0.3, x_{(2)} = 0.3, x_{(3)} = 0.3, x_{(4)} = 0$, and all other $x_i = 0$, which can be used to find z_i^N .

This result is due to the fact that the constraints in the problem define the standard simplex.

Similarly, $z_2^U = 0.5 - \beta_{(1)}$, if $\beta_{(1)} < 0.5$ (and the corresponding optimal solution will be $x_{(1)} = 1$ and $x_i = 0, \forall i \neq (1)$), $z_2^U = \beta_{(8)} - 0.5$, if $\beta_{(8)} > 0.5$ (and the corresponding optimal solution will be $x_{(8)} = 1$ and $x_i = 0, \forall i \neq (8)$), and $z_2^U = 0$ otherwise (in this case, if $\beta_k \leq 0.5 \leq \beta_j$, then $x_j = \frac{0.5 - \beta_k}{\beta_j - \beta_k}$, $x_k = \frac{\beta_j - 0.5}{\beta_j - \beta_k}$ and $x_i = 0, \forall i \neq j, k$.) Clearly, there can be multiple optimal solutions.

4.4 Weaknesses of the weighted sum method. The weighted sum method has a major weakness when objectives are linear and a simplex-type method is used to solve the weighted sum problem. As we noted earlier, the specific Pareto optimal solution can be obtained by the proper choice of weights. However, if the objective Pareto optimal set features a linear face, the simplex method will always pick up a vertex as the possible solution. There does not exist a set of weights that yield points in the interior of the linear face as long as the simplex method is considered. Different solution techniques, such as interior-point methods, may overcome this disadvantage.

²The i^{th} order statistic of r_i is the i^{th} largest value in $\{r_1, \dots, r_n\}$, i.e., $r_{(1)} \geq r_{(2)} \geq \dots \geq r_{(n)}$.

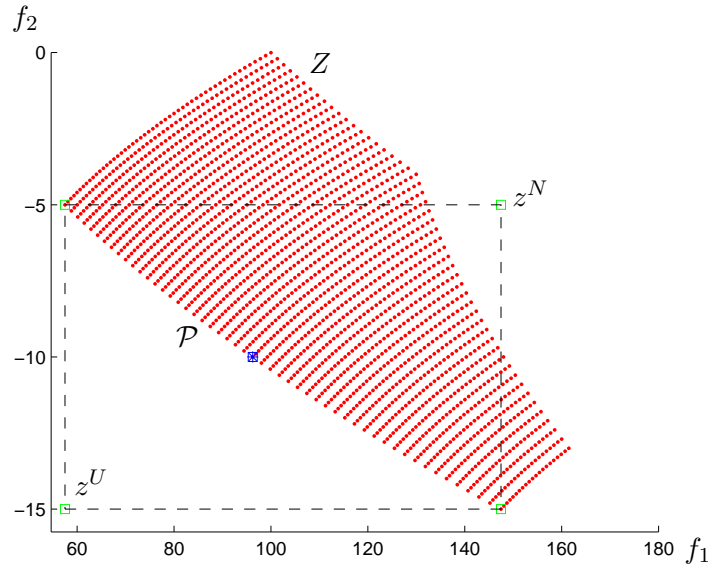


Figure 2 Objective Feasible Region: Non-Linear Case

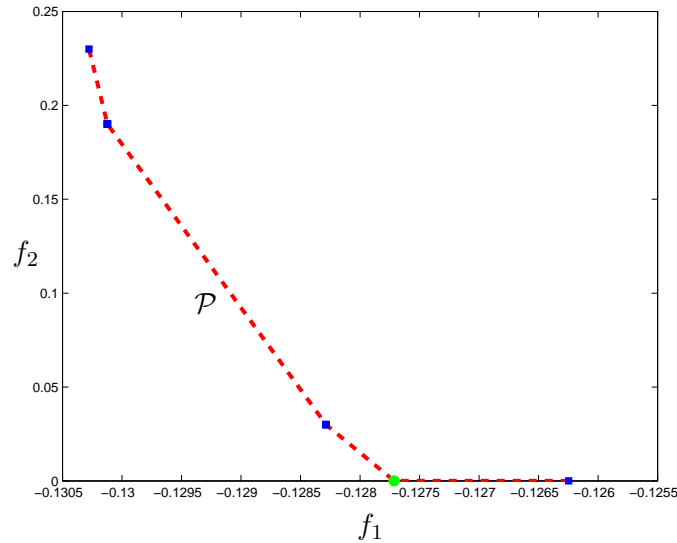


Figure 3 Pareto Optimal Set: Illustrative Portfolio Problem

the illustrative portfolio problem (3.1). In that problem the objective functions f_1 and f_2 are linear, while f_3 is quadratic. Figure 3 shows the Pareto optimal set in the (f_1, f_2) plane. Squares denote the corners of the set, i.e. solutions we can possibly obtain with the weighted sum approach.

We can square the objective function f_2 since

$$\min f_2(x) = \min |\beta^T x - 0.5| = \min f_2^2(x) = \min (\beta^T x - 0.5)^2.$$

Using $f_2^2(x)$ instead of $f_2(x)$ and keeping f_1, f_3 as before, we come up with a more populated Pareto set, as depicted in Figure 4.

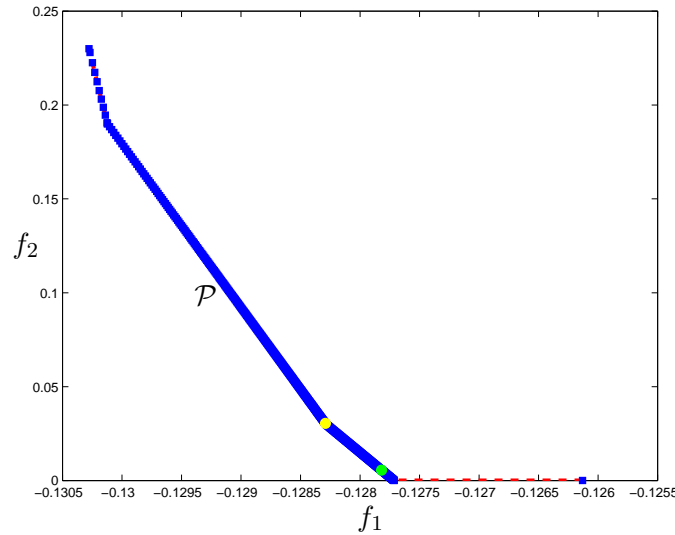


Figure 4 Pareto Optimal Set: Squared Linear Function f_2

Clearly, we cannot square all linear objective functions as squaring some of them may make no sense for the original multi-objective problem formulation. The above discussion illustrates that reformulating the problem may sometimes help in overcoming the weaknesses of the weighted sum method, while keeping the complexity roughly the same.

Another approach that does not suffer from problems experienced by the weighted sum method is the hierarchical (ε -constraint) method, described in the next section.

5 The hierarchical method

This method allows the decision maker to rank the objective functions in a descending order of importance, from 1 to k . Each objective function is then minimized individually subject to a set of additional constraints that do not allow the values of each of the higher ranked functions to exceed a prescribed fraction of their optimal values obtained on the corresponding steps.

In other words, once the optimal value for the specific objective has been obtained, the possible values this objective function can take on the following steps are restricted to a box (or a ball) around this optimal solution. Depending on the size of the restriction this strategy effectively puts more weight on the higher ranked objective functions.

5.1 Basics of the hierarchical method. For illustration purposes, we consider the problem with two objective functions. Suppose that f_2 has higher rank than f_1 . We then solve,

$$\begin{aligned} \min \quad & f_2 \\ \text{s.t.} \quad & x \in \Omega \end{aligned}$$

to find the optimal objective value f_2^* .

Next we solve the problem,

$$\begin{aligned} \min \quad & f_1 \\ \text{s.t.} \quad & x \in \Omega, \\ & f_2(x) \leq f_2^* + \varepsilon. \end{aligned}$$

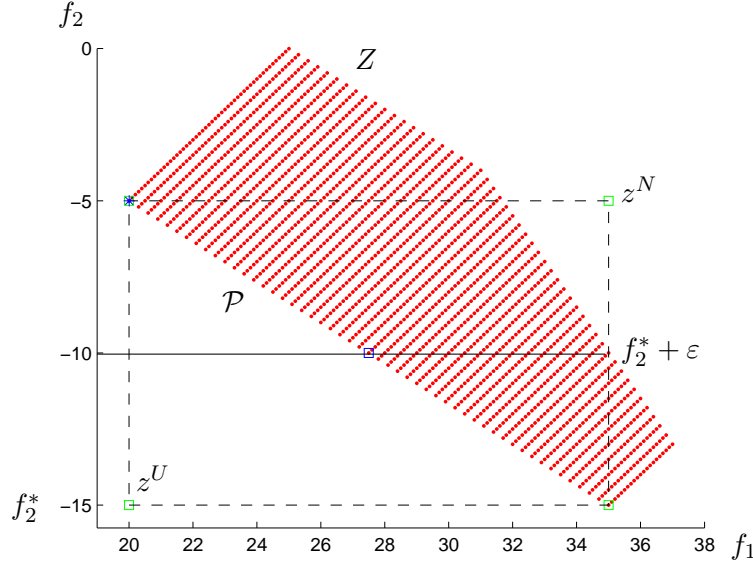


Figure 5 Objective Feasible Region: The Hierarchical Method Cut

Intuitively, the hierarchical method can be thought as saying " f_2 is more important than f_1 and we do not want to sacrifice more than 20% (or 30% or 50%) of the optimal value of f_2 to improve f_1 ."

In the general case of k objective functions and the strict preferential ranking f_1, f_2, \dots, f_k , we start by solving the problem

$$\begin{aligned} \min \quad & f_1 \\ \text{s.t.} \quad & x \in \Omega, \end{aligned}$$

to obtain the optimal solution $x^{[1]}$. Next, for $j = 2, \dots, k$, we find the optimal solution $x^{[j]}$ for the j -th objective function by solving the problem with additional constraints of the following form

$$f_l(x) \leq (1 + \varepsilon_l) f_l(x^{[l]}), \quad \forall l = 1, \dots, j - 1.$$

If both Utopia and Nadir points are known, we can interpret ε_l as the distance from optimality in percents,

$$f_l(x) \leq \left(1 + \varepsilon_l (z_l^N - z_l^U)\right) f_l(x^{[l]}).$$

5.2 Application of the hierarchical method. The hierarchical method provides the decision maker with another way to specify the relative importance of the objective functions: instead of weighting each of them, the DM ranks them and specifies how much of the more important objectives can be traded in order to improve the less important ones.

The hierarchical method avoids the pitfalls of the weighted sum method as it starts with the corner solution and attempts to move away towards the centre of the Pareto set.

Figure 5 shows that the constraint $f_2(x) \leq (1 + \varepsilon_2) f_2(x^{[2]})$ introduces the cut that forces the optimal solution to move out of the corner.

One of the drawbacks of the hierarchical method is the introduction of a quadratic constraint on subsequent steps when the previous problem has a quadratic objective function. Quadratic constraints are generally very hard to deal with and, thus, should be avoided.

However, as we already discussed in Section 4.4, the problem with purely quadratic objectives usually features non-linear efficient frontier and can be tackled by the weighted sum approach. This leads us to the following proposition:

- 1) if linear objective functions are present, rank and apply the hierarchical method to eliminate them from the problem, i.e. replace these functions with the corresponding cuts;
- 2) use the weighted sum method to solve the remaining problem where only quadratic objectives are present.

These ideas are key to the algorithm we present in the next section.

6 The algorithm

We propose the following algorithm to solve the general convex multi-objective optimization problem with linear and quadratic objectives. The algorithm combines both weighted sum and hierarchical approaches and requires only linear or quadratic programs to be solved at each step.

1. Separate linear and quadratic objectives into two index sets \mathcal{L} and \mathcal{Q} , denote linear objectives as f^L and quadratic objectives as f^Q .
2. Rank the linear objective functions in \mathcal{L} from the most important to the least important.
3. Solve (or approximate if possible) each of

$$\min_x \{f_i(x) : x \in \Omega\}.$$

Let x_i^* denote an optimal solution and f_i^* be the optimal objective value. Compute the Nadir vector z^N .

4. Sequentially solve problems

$$\begin{aligned} \min \quad & f_i^L \\ \text{s.t.} \quad & x \in \Omega, \\ & f_l^L(x) \leq f_l^{L*} + \delta_l, l = 1, \dots, i-1, \\ & \delta_l = \varepsilon_l(z_i^N - f_l^{L*}). \end{aligned}$$

One may also consider updating elements of z^N by considering optimal solutions to these problems, as they become available.

5. If no quadratic objectives are present, return the last optimal solution as the final solution; otherwise proceed to the next step.
6. Compute scaling coefficients θ_i for objectives in \mathcal{Q} and set $w_i = u_i\theta_i$, where u_i are the decision maker preferences.
7. Solve for the final solution

$$x^* = \operatorname{argmin}_x \left\{ \sum_{q \in \mathcal{Q}} w_q f_q^Q : x \in \Omega, f_l^L \leq f_l^{L*} + \delta_l, \forall l \in \mathcal{L} \right\}.$$

6.1 Choosing weights based on the geometrical information. In the fourth step of the algorithm, we aim to solve the sequential program $P_i = \{\min f_i^L : x \in \Omega, f_l^L(x) \leq f_l^{L*} + \varepsilon_l(z_i^N - f_l^{L*}), l = 1, \dots, i-1\}$ to get the optimal value f_i^{L*} . Each time we obtain an optimal objective value f_i^{L*} , the constraint

$$f_i^L(x) \leq f_i^{L*} + \varepsilon_i(z_i^N - f_i^{L*})$$

is added in succeeding programs to cut off a portion of the feasible region where the i -th objective can't be well achieved. A challenging problem is to decide the proportion we want to cut off. If we choose a small ε_i , we may overly favour the i -th objective ($\frac{f_i(x^*) - f_i^*}{z_i^U - f_i^*} \leq \varepsilon_i$), while sacrificing subsequent objectives; in contrast, choosing a large ε_i may result in a poor i -th objective, but leaves more space to optimize other objectives. In the multi-objective optimization it is important to develop a fair and systematic methodology to decide on ε_i according to the given information.

The choice of ε_i should depend on the importance of objective f_i^L and the potential conflict between objective f_i^L and other objectives. The importance of f_i^L could be represented by the priority factor u_i , which is scaled to satisfy $\sum_i u_i = 1$. However, there is no explicit indicator measuring the conflicts among different objectives.

We are motivated to measure the conflict based on the geometry of the objective functions. In the second step of the algorithm, we have computed $x_i^* \in \mathbb{R}^n$ for each objective i . Next, a reasonable choice of the centre is the bycentre $x^C = \frac{1}{n} \sum_i x_i^*$. Clearly, there are many choices of the centre, e.g. the analytical centre of the polyhedral feasible set. But the bycentre of $x_i^*, i = 1, 2, \dots, k$ is the easiest to compute.

We propose a metric for the conflict between objectives i and j . Let us call it the *conflict indicator*, denoted by c_{ij} . We first measure the cosine value of the angle θ_{ij} between the vectors from $x_i^* - x^C$ and $x_j^* - x^C$:

$$\cos \theta_{ij} = \frac{\langle x_i^* - x^C, x_j^* - x^C \rangle}{\|x_i^* - x^C\| \|x_j^* - x^C\|}.$$

As discussed above, x^C denotes the point we set to approximate the centre of the feasible set. We define c_{ij} as

$$c_{ij} = \frac{1}{2}(1 - \cos \theta_{ij}).$$

Thus, the larger the angle between the two objectives, the bigger the conflict indicator c_{ij} is. The conflict indicator equals zero when the optimizer of the two objectives coincides; and it is close to one when the two objectives tend to conflict the most. Note that $c_{ii} = 0$.

We propose to set $\varepsilon_i = \alpha \sum_{j=1}^k u_j c_{ij}$, where α is some scalar factor which could be decided by numerical experiment. The weighted sum has two significance: if important objectives conflict with the i -th objective, i.e. they have high priority, then we do not want to impose strict constraints on the achievement of objective f_i^L because it tends to restrict the important objectives, and thus we select big ε . On the other hand, if objectives conflicting with i -th objective are all of low priority, even if there are many conflicts, we can still impose a small ε to the objectives. If i -th objective has a high priority u_i , then the weighted sum of conflict indicators tends to be low.

Writing it mathematically, we denote by u the vector of priority factors:

$$u = \{u_1, u_2, \dots, u_k\}^T,$$

and let $X \in \mathbb{R}^{n,k}$ be

$$X := \{x_1^*, x_2^*, \dots, x_k^*\}.$$

Then, we get a vector $\varepsilon = (E - X^T X)u$, which carries ε_j for each objective j . We could choose to compute ε once in the beginning or update x_j^* after each iteration of the sequential program and use this information to compute ε .

This technique could be generalized to the quadratic constraints, quadratic objective case (QCQP). For this case, if all quadratic constraints are convex, we could linearize the functions by replacing non-negative constraints with positive semi-definite constraints. This will result in a semi-definite programming problem to compute x_j^* , define the bycentre, and then compute conflict indicators c_{ij} . Thus, we can solve the sequential QCQP program and compute ε as one problem.

7 Conclusions and future work

We have reviewed multi-objective optimization problems and normalization methods – weighted sum and hierarchical approaches. Both methods are analyzed and their advantages, as well as disadvantages, are discussed. Based on the analysis, we propose an algorithm to solve convex multi-objective problems with linear and quadratic objectives. A version of the algorithm was implemented in MATLAB and tested on the financial problem discussed in Section 3.

This paper provides a lot of insight on how to attack and what to expect from these kinds of problems. We accept the fact that analysis is rather sketchy, but we feel that the algorithmic approach and, especially, ideas expressed in Section 6.1 may be innovative and of further interest. Since we did not have time to perform an extensive literature review, we should stress that these or related ideas might be already known or better developed elsewhere. We encourage an interested reader to consult numerous publications on multi-objective optimization.

8 Acknowledgements

We thank the organizers of Fields-MITACS Industrial Problem Solving Workshop and the Algorithmics Inc. for giving us the opportunity to work on this problem.

References

- [1] R. Kahraman and M. Sunar (2001), A comparative study of multiobjective optimization methods in structural design. *Turkish Journal of Engineering and Environmental Sciences* 25: 69-78,
- [2] I. Y. Kim and O. De Weck (2005), Adaptive weighted sum method for bi-objective optimization. *Structural and Multidisciplinary Optimization* 29(2):149-158.
- [3] K. Klamroth and J. Tind (2006), Constrained Optimization using Multiple Objective Programming. Technical report. Accepted for publication in *Journal of Global Optimization*.
- [4] P. Korhonen (1998), Multiple objective programming support. Technical Report IR-98-010, International Institute for Applied Systems Analysis, Laxenburg, Austria.
- [5] R. Timothy Marler. *A Study of Multi-Objective Optimization Methods for Engineering Applications*. PhD thesis, The University of Iowa.
- [6] Kaisa Miettinen (2001), Some methods for nonlinear multi-objective optimization. In Proceedings of the First International Conference on Evolutionary Multi-Criterion Optimization (EMO 2001), *Lecture Notes in Computer Science*, 1993:1–20.

List of Participants

Name	Affiliation
Alberti, Lionel	Université de Nice
Arino, Julien	University of Manitoba
Aruliah, Dhavide	University of Ontario Institute of Technology
Baddour, Natalie	University of Ottawa
Bohun, Sean	University of Ontario Institute of Technology
Bowman, Christopher	National Research Council
Beward, Chris	Mathematical Institute, University of Oxford
Buono, Luciano	University of Ontario Institute of Technology
Chau, Roger	University of Waterloo
Cottrell, David	McGill University
Craig, Walter	McMaster University
Cumberbatch, Ellis	Claremont Graduate University
Ding, Yichuan	University of Waterloo
Djounna, George	Université de Laval
ElSheikh, Ahmed	McMaster University
Fan, Guangzhe	University of Waterloo
Ghobeity, Amin	University of Toronto
Gordon, Richard	University of Manitoba
Gregov, Sandra	McMaster University
Grodzevich, Oleg	University of Waterloo
Gumel, Abba	University of Manitoba
Gumel, Abba	University of Manitoba
Halevy, Itamar	
Hazaveh, Kamyar	University of Toronto
Henda, Redhouane	Laurentian University
Huang, Huaxiong	York University
Jaimungal, Sebastian	University of Toronto
Jiang, Xiamei	University of Toronto
Kavazovic, Zanin	GIREF - Université de Laval
Keyfitz, Barbara	The Fields Institute
Khan, Kamran	University of Toronto
King, Andrew	McGill University
Lan, Kunquan	Ryerson University
Langridge, Allan	University of Toronto
Lewis, Gregory	University of Ontario Institute of Technology
Li, Song	University of Saskatchewan
Liu, Jian-Guo	University of Maryland
Liu, Rongsong	York University

Name	Affiliation
Madras, Neal	York University
Melnik, Roderick	Wilfred Laurier University
Minhas, Ravi	University of Toronto
Monifi, Elham	University of Waterloo
Nigam, Nilima	McGill University
Perez Abarca, Juan Manuel	McGill University
Podder, Chandra Nath	University of Manitoba
Pourziaei, Bobby	York University
Pugh, Mary C.	University of Toronto
Raymond, Christopher	New Jersey Institute of Technology
Rodrigues, Hildebrando	Icmc-Universidade de Sao Paulo
Romanko, Oleksandr	McMaster University
Rossi, Louis	University of Delaware
Sabbagh, Mohammad S.	Isfahan University of Tech.
Salisbury, Thomas	The Fields Institute
Seeman, Tamar	Bar Ilan University
Sharomi, Oluwaseun	University of Manitoba
Shioda, Romy	University of Waterloo
Shontz, Suzanne	The Pennsylvania State University
Tritchenko, Olga	McGill University
Vaidya, Naveen	York University
Wang, Steven Xiaogang	York University
Warlow, Scott	Manulife
Williams, JF	Simon Fraser University
Witelski, Thomas P.	Duke University
Wu, Jianhong	York University
Wylie, Jonathan	City University of Hong Kong
Youbissi, Fabien Mesmin	Université Laval
Zhu, Jiaping	McMaster University